2014

Characterization of the hydrodynamic structure of a 3D acoustic fluidized bed

David Roberto Escudero
Iowa State University

Characterization of the hydrodynamic structure of a 3D acoustic fluidized bed

by

David Roberto Escudero Guevara

A dissertation submitted to the graduate faculty
in partial fulfillment of the requirements for the degree of
DOCTOR OF PHILOSOPHY

Major: Mechanical Engineering

Program of Study Committee:
Theodore J. Heindel, Major Professor
Rodney Fox
Song-Charng Kong
Terrence Meyer
Shankar Subramaniam

Iowa State University

Ames, Iowa

2014

TABLE OF CONTENTS

LIST OF FIGURES

LIST OF TABLES

ACKNOWLEDGEMENTS

I would like to dedicate this dissertation to my wife Valeria; thank you for being my support beam, for keeping me on track when I was losing focus. Thank you for always reminding me that the reason I am here today completing my PhD is not because of chance but it is the consequence of hard work and dedication. Finally, thank you for all the love you give me every day.

To my family in Ecuador, thank you all for your support, advice, and more than anything, for all the love you've given me.

I would also like to express immense gratitude to Dr. Ted Heindel, my major professor. Thank you very much for giving me the opportunity to purse my PhD. Thanks to your trust, support and guidance as I successfully completed all my academic goals at Iowa State University.

Special thanks to the members of the committee, Dr. Rodney Fox, Dr. Song-Charng Kong, Dr. Terrence Meyer and Dr. Shankar Subramaniam. Thank you all for the input and feedback on this dissertation.

I would also like to thank everyone in the Experimental Multiphase Flow Laboratory for all their help and assistance in many instances of this research.

The X-ray facility used in this research was funded by the National Science Foundation

ABSTRACT

Multiphase flow systems are used widely in various industrial processes. For example fluidized bed reactors are attractive because they provide uniform temperature distributions, low pressure drops, and high heat/mass transfer rates. Due to the complexity of this gas-solid system, characterizing the hydrodynamics of a fluidized bed has become critical in understanding system behavior.

Minimum fluidization velocity and local gas holdup are important parameters used to characterize the hydrodynamic behavior of a fluidized bed. These characteristics may be modified through the inclusion of sound vibrations.

The hydrodynamic behavior in a 3D fluidized bed filled with glass beads or ground walnut shell, using different particle size ranges, different initial bed heights, and various flow conditions, with and without acoustic intervention, is investigated in this research. X-ray computed tomography (CT) imaging is used to determine time-average local gas holdup. Using the local time-average gas holdup images, qualitative and quantitative information regarding the jetting phenomena near the distributor plate is obtained.

Results show the minimum fluidization velocity is influenced by sound frequency. As the frequency increases, the minimum fluidization velocity decreases until a specific frequency is reached, beyond which the minimum fluidization velocity increases. With increasing sound pressure level, the minimum fluidization velocity decreases because the additional vibration forces imparted to the bed particles helps to loosen the bed, reducing the interparticle forces, which reduces the required energy for particle fluidization. Thus, acoustic fields provide an improvement in the ease of particle fluidization.

Local time-average gas holdup results show that the fluidized bed under the presence of an acoustic field provides a more uniform fluidization; material exhibit less channeling, the acoustic fluidized beds had fewer amounts of active jets than the no acoustic fluidized bed conditions, which allow for a more homogeneous gas holdup region deep into the bed. Thus, an acoustic field affects the hydrodynamic behavior of a fluidized bed.

The acoustic field also influenced the jetting phenomena present near the aeration plate, where it was observed that the jets in the acoustic fluidized bed merged higher in the bed compared to the no acoustic condition.

Finally, the inclusion of acoustic vibrations on the fluidized bed allows larger bubbles to break into smaller ones, increasing the presence of solid particles which decreases the jet momentum dissipation loss allowing the jets to have a higher average jet length compared to the fluidized bed without acoustics vibrations. Moreover, the addition of acoustic vibrations also produced an increase in the expansion angle of the jets.

CHAPTER 1: INTRODUCTION

1.1 Motivation

Fluidization is the phenomenon of imparting the properties of a fluid to a bed of particulate solids by passing a fluid (liquid or gas) through the material. Fluidized beds are reactors in which fluidization of particulate solids takes place. Fluidized beds are used in several industrial processes because of their uniform temperature distributions, low pressure drops, and high heat/mass transfer rates.

In industrial applications, fluidized bed can be used as combustors, as catalytic reactors, and also for drying purposes. Understanding the mixing and jetting phenomena that occurs above the distributor plate is of extreme importance for the overall performance of the fluidized bed. A poor distribution between the fluidizing media and the solid particulate in a combustor can produce low rate of heat transfer, which can cause sintering and defluidization of the particulate matter. In other applications and equipment, jetting can produce surface attrition of heat exchanger tubes.

Characterizing the hydrodynamics of a fluidized bed is important to gain a better understand of the behavior of these multiphase flow systems. Acoustic fluidized beds are the focus of this study to determine the effects produced by an acoustic field on the fluidization behavior and quality. Two different particle types are used in this study. Glass beads, provide a well-characterized particle, whereas biomass particles (ground walnut shell), are irregular in size, shape, and density.

Minimum fluidization velocity is one of the most important parameters when characterizing the hydrodynamics in a fluidized bed (Ramos Caicedo et al., 2002). The minimum fluidization velocity (U_{mf}) is defined as the superficial gas velocity where solid particles start to be suspended

in the fluidizing medium. In general, U_{mf} is a function of particle properties/geometry, fluid properties, and bed geometry. Gas holdup or void fraction is another very important parameter that characterizes the fluidization quality, mixing, and process efficiency in a fluidization system, and is defined as the volume fraction of gas present within the bed. In addition to these parameters, characterizing the phenomena known as jetting, which can be produced either by the addition of nozzles inside the fluidized bed or can be produced by the distributor plate of the fluidized bed, is of great importance to improve the characteristics of a fluidized bed, such as mixing and heat and mass transfer rates.

Noninvasive measurement techniques are valuable because they provide insight into the flow behavior and general hydrodynamic characteristics of multiphase flow and opaque systems (Yates et al., 2002). Noninvasive X-ray techniques such as X-ray computed tomography (XCT) can generate a 3D image of the object of interest. X-rays pass through the object and the intensity values are recorded at several projections by an imaging device. X-ray computed tomography can provide a high spatial resolution of the time-average void fraction; this characteristic can be used to measure the time-average local gas holdup in a very efficient way and can be used to quantify the flow hydrodynamics.

Most of the studies on acoustic fluidized beds available in the literature used both invasive and noninvasive measurement techniques to obtain the hydrodynamic characteristics of the bed. Fiber optic systems, visual observations, pressure analysis or camcorder systems are some of the example of the techniques used. However, non-invasive techniques such as X-ray computed tomography have not been used in sound assisted fluidized bed to determine qualitative and quantitative hydrodynamic characteristics; this will be done in the following study.

1.2 Objectives

The goal of this study is to obtain better mixing and uniformity in the gas-solid distribution of a fluidized bed by determining and characterizing the different effects that acoustic vibrations have on the minimum fluidization velocity, time-average gas holdup, and jetting phenomena near the distributor plate in a cylindrical fluidized bed using X-ray CT imaging, while improving the understanding of the hydrodynamics of fluidized bed. To accomplish this goal, this research will complete the following objectives.

1. Review the literature regarding fluidization, bed height, and acoustic field effects on fluidized beds hydrodynamics, and noninvasive X-ray techniques for visualization of multiphase flow systems.
2. Determine the effects of frequency and sound pressure level on the minimum fluidization velocity.
3. Acquire X-ray CT images and determine time-average local gas holdup information for the fluidized bed.
4. Evaluate the effects of the acoustic field on the time-average local gas holdup.
5. Using the time-average local gas holdup images to determine qualitatively and quantitatively characteristics of the jetting phenomena produced by the distributor plate.
6. Compare results between an acoustic and no acoustic fluidized bed.

1.3 Overview

The following document presents the research performed to accomplish the objectives listed in the previous section. Chapter 2 reviews selected literature on fluidized beds and techniques to characterize fluidized beds hydrodynamics. Chapter 3 describes the experimental procedures, equipment, and methods used to collect data for the analysis of the fluidized bed hydrodynamic

behavior. Chapter 4 presents the results of the analysis for minimum fluidization velocity. Chapter 5 presents the results of the analysis on the time-average local gas holdup distribution. Chapter 6 describes the results of the jetting analysis. Chapter 7 describes a simple one dimensional model used to characterize the acoustic sound wave inside the fluidized bed. Finally, Chapter 8 provides the conclusions of this study and recommendations for future work.

CHAPTER 2: LITERATURE REVIEW

This chapter provides a review of two topics necessary to understand the concepts applied in this research. Section 2.1 will overview fluidization concepts like fluidization regimes, fluidized beds, fluidized bed hydrodynamic parameters such as minimum fluidization velocity, gas holdup, and jetting phenomena, as well as vibration effects (mechanical and acoustic) on the hydrodynamics of the bed. Section 2.2 will provide a summary of the noninvasive X-ray techniques used to characterize fluidized bed hydrodynamics, specifically, X-ray computed tomography. Finally, section 2.3 will provide a brief summary of this review.

2.1 Fluidization

This section provides an overview of the important principles and characteristics related to fluidization and is divided into four subsections. The first describes important features, as well as different types of fluidized beds. The next subsection provides a description of the different fluidization regimes. The third subsection briefly explains gas holdup, minimum fluidization velocity and jetting phenomena. Finally, a discussion on vibration effects on fluidized beds is explained in subsection four.

2.1.1 Fluidized Beds

Fluidized beds are reactors in which fluidization of particulate solids takes place. There are several types and geometries of fluidized beds, but most of them have some key components: a plenum, a distributor, a bed region, and a freeboard region. The plenum is where the fluid enters the bed. Fluid next passes through a distributor or aeration plate, which uniformly distributes the fluid at the base of the bed. The particulate solid is located above the distributor in the bed region. Finally, located above the bed chamber is the freeboard region, which contains particles that may be ejected from the bed. Figure 2.1 shows a schematic of a typical fluidized bed.

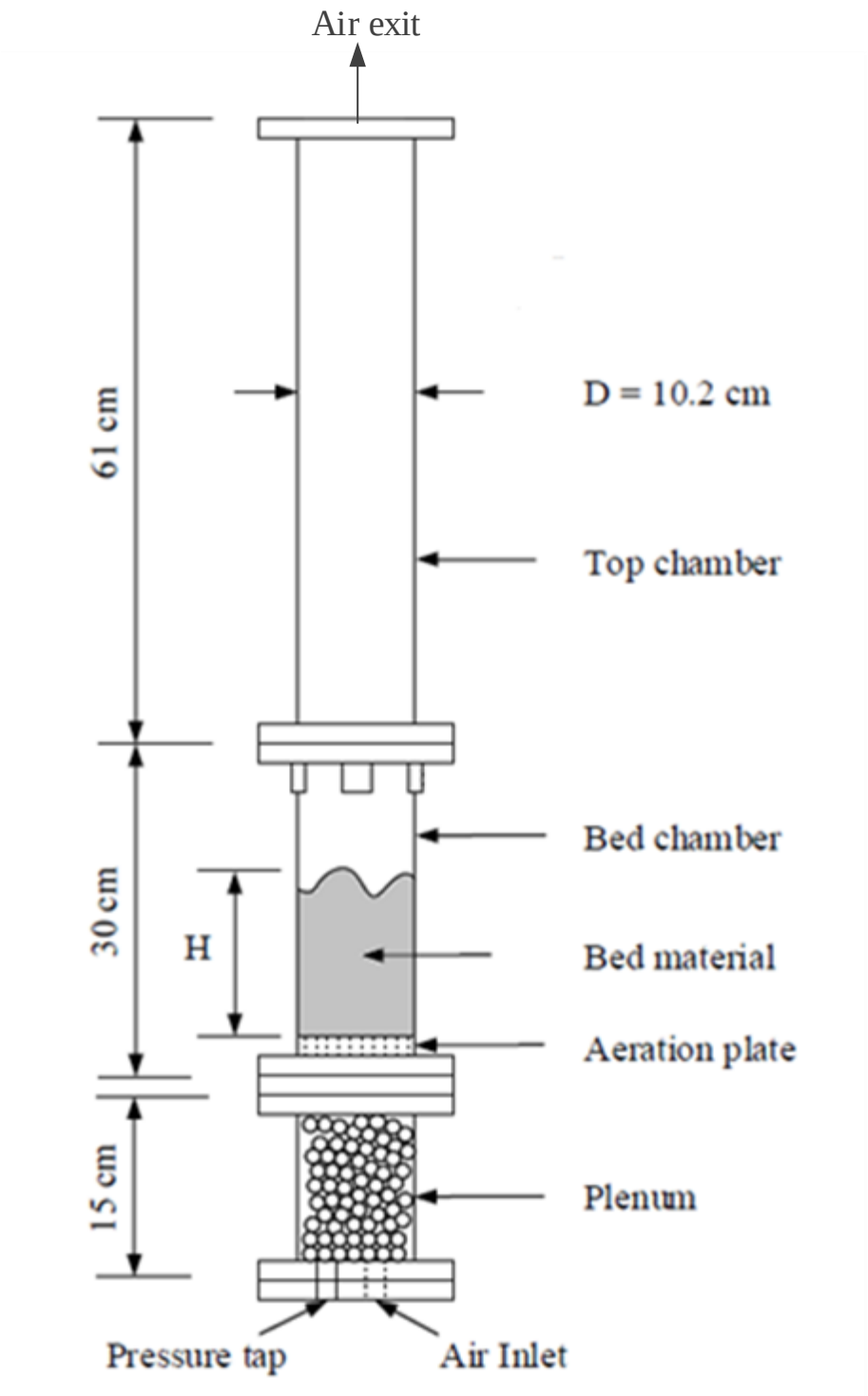

Figure 2.1: Fluidized bed schematic.

Fluidized beds as chemical reactors present several advantages that include a high rate of heat and mass transfer, low pressure drop, and uniform temperature distribution. As stated before, there are several types of fluidized beds; the most common types are the Stationary Fluidized Bed (SFB) or Fixed Fluidized Bed (FFB) and Circulating Fluidized Bed (CFB). SFB or FFB refers to fluidized beds where the particles stay within the bed region. Whereas CFB refer to fluidized beds where, due to the high velocity of the fluid, most of the particles are entrained in the fluid flow and transported out of the bed to be recirculated back into the bed. Moreover, there are special types of fluidized beds like the spouted bed. In a spouted bed, gas (or liquid) is injected from the bottom through a central nozzle into the bottom of a normally cylindrical vessel to form a high velocity up-flow stream of gas (or liquid). The up-flowing gas carries particles in the central region (the spout) that are returned to the central bed region by a slow downward moving layer of particles between the central spout and the wall (the annulus) (Crowe, 2006).

Fluidized beds have several industrial applications depending on the type of reaction that takes place in the reactor. For a gas-solid system, which is of interested in this study, the applications can be divided into four categories described by (Crowe, 2006). The first category is the gas catalytic reaction. In this type of application, the reactants and products are in the same phase; however, the reactions take place on the surface of a solid catalyst. Fluid Catalytic Cracking (FCC) is one example of this type of reaction. FCC converts low value heavy components of crude oil into a variety of high value lighter products (Yang, 2003) . The second category is the gas-phase reaction using solids as heat carriers. In this reaction both the reactants and products are in the same phase (gaseous) but solids are required to produce or carry the heat needed for the reaction. The third category is the gas-solid reaction, where reactants and products

are gases and solids, with the option of being gases or a combination of gas and solids. Combustion and gasification are examples of processes using this type of reaction. Finally, the last category is where no chemical reactions occur. Fluidized bed drying applications are an example of this type and are used due to the fluidized bed high drying rates, high thermal efficiency and lower costs; they are commonly used among the chemical, food, ceramic, and pharmaceutical industries.

2.1.2 Fluidization Regimes

Fluidization is the phenomenon of imparting the properties of a fluid to a bed of particulate solids by passing a fluid (liquid or gas) through the latter at a velocity which brings the fixed or stationary bed to its loosest possible state just before its transformation into a fluid-like bed (Gupta and Sathiyamoorthy, 1999). A fluid-like behavior is attained when the drag and buoyant forces surpasses the gravitational forces of the solid particles, allowing relative motion between them. Fluidization can be obtained using liquid, gas, or a liquid-gas combination, as the fluid passes through the solid material. Liquid-solid and gas-liquid-solid systems are important for several industries, but they are not of interest in this research, which is primarily focused on gas-solid systems.

Yang (Yang 2003) considered at least six different fluidization regimes for gas-solid fluidized beds: fixed bed, bubbling fluidization, slugging fluidization, turbulent fluidization, fast fluidization, and pneumatic conveying. Figure 2.2 shows a schematic of these six fluidization regimes in as gas-solid fluidized bed (Crowe, 2006). In the fixed bed regime, the air flowing across the particle does not have enough velocity to move the particles. Increasing the superficial gas velocity (U_g), defined as the volumetric gas flow rate divided by the cross-sectional area, the system reaches the bubbling fluidization regime. In this regime, bubbles start to form and

coalesce causing solid mixing; the velocity at which bubbles appeared is known as the minimum bubbling velocity (U_{mb}). Yang (Yang 2003) considered that the slugging regime appears in beds where the bed height (H) over the bed diameter (D) is larger than 2. This requirement ensures that bubbles have enough time to coalesce in bigger bubbles called slugs, when the bubbles grow to 2/3 of the bed diameter the system enters to a slugging regime.

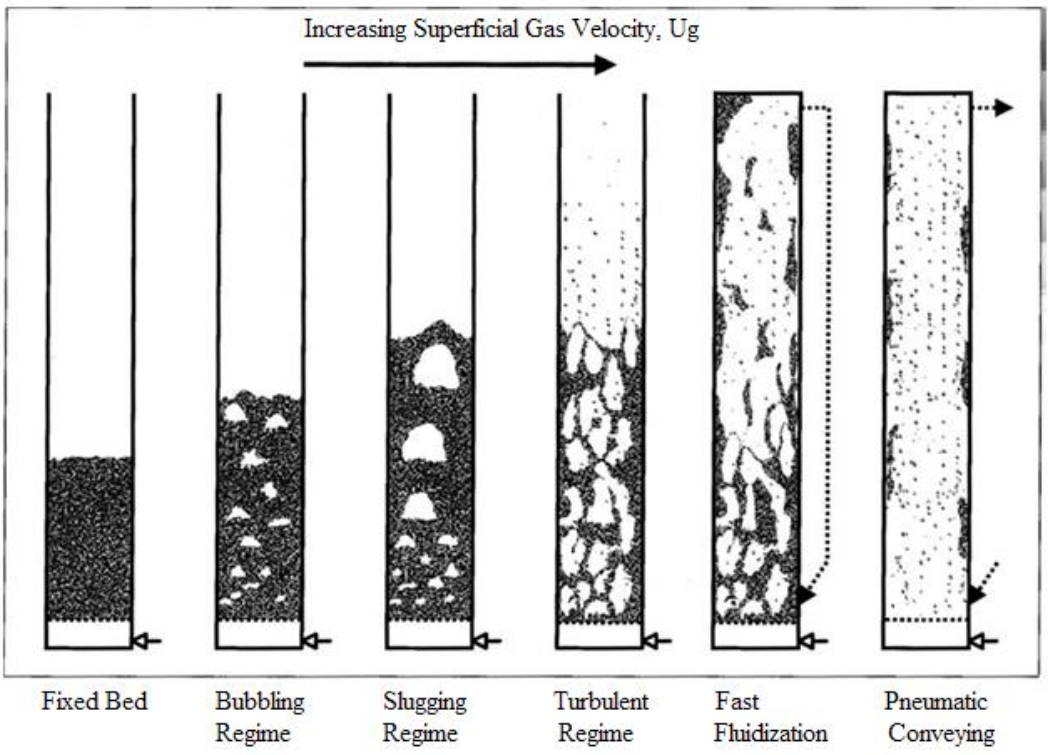

Figure 2.2: Fluidization regimes in a gas-solid fluidized bed (Crowe, 2006)

Furthermore, Crowe (Crowe 2006) said that turbulent fluidization occurs when, as U_g is increased, a point is reached where the bubbles or slugs, begin to break down instead of continuing to grow. The "critical velocity" U_c, which demarcates the onset of the turbulent fluidization flow regime, is usually determined experimentally as the superficial gas velocity at which the standard deviation of pressure fluctuations reaches a maximum. If U_g increases beyond a velocity known as the transport velocity U_{tr}, a fast fluidization regime is reached. In the fast

fluidization regime, solid particles are thrown outside of the bed, which makes the bed surface indistinguishable. Finally, the pneumatic conveying regime is reached when the superficial gas velocity is much higher than the transport velocity; this regime is characterized by the particle being transported out of the bed in a dilute phase.

2.1.3 Fluidized Bed Hydrodynamics

Fluidized bed hydrodynamic behavior is very complex and must be understood to improve fluidized bed operations. Characterizing the hydrodynamics of a fluidized bed is important to gain a better understand of the behavior of these multiphase flow systems. There are several parameters that are important to characterize fluidized bed conditions, including the minimum fluidization velocity, gas holdup, and jetting phenomena.

2.1.3.1 Minimum Fluidization Velocity

The minimum fluidization velocity (U_{mf}) is the superficial gas velocity at which solid particles are just suspended in the fluidizing medium. Minimum fluidization velocity is one of the most important normalized parameters when characterizing the hydrodynamics in a fluidized bed (Ramos Caicedo et al., 2002). Usually, the minimum fluidization velocity is obtained experimentally, and there are several techniques reported in the literature to determine the minimum fluidization velocity in a multiphase flow system. Gupta and Sathiyamoorthy (Gupta and Sathiyamoorthy, 1999) described three different methods to measure U_{mf}: (i) the pressure drop method, (ii) the voidage method, and (iii) the heat transfer method. The first method measures the pressure drop across the bed as a function of the superficial gas velocity. The point of transition between a fixed bed regime and a bubbling regime is denoted by a constant pressure line in a plot of pressure vs. superficial gas velocity; this point marks the minimum fluidization velocity. In the voidage method, the minimum fluidization velocity is determined when the

voidage inside the bed starts to increase due to bed expansion as the superficial gas velocity is increased. However, this method is not commonly used because it is much more complicated to locate the point where bed expansion starts. Finally, in the heat transfer method, the variation of the wall heat transfer coefficient is measured as the gas velocity increases. The point where the heat transfer coefficient increases drastically is the onset of fluidization or the minimum fluidization velocity point. This method, however, is too expensive and requires a good experimental setup to measure the heat transfer data under steady-state conditions.

Zhou (Zhou et al., 2008) used the pressure drop method to find and compare the minimum fluidization velocity of a three phase system (gas-liquid-solid) between a conical and a cylindrical fluidized bed. They compared the experimental results of the minimum fluidization velocity with minimum fluidization results obtained using reported theoretical correlations, like the Ergun equation, as well as other models developed by other researchers. Results agreed when using both theoretical models and experimental procedures to obtain the minimum fluidization velocity.

The minimum fluidization velocity depends on the material properties, the bed geometry, and the fluid properties. Sau et al. (Sau et al., 2007) determined the minimum fluidization velocity for a gas-solid system in a tapered fluidized bed (conical fluidized bed) and studied the effects that bed geometry, specifically the tapered angle, had on the minimum fluidization velocity. They used three different angles (4.61, 7.47, and 9.52 degrees) to observe their effects on minimum fluidization velocity. Results showed that as the tapered angle increased, U_{mf} also increased, which implied a dependence of the minimum fluidization velocity on the geometry of the fluidized bed. Moreover, Hilal et al. (Hilal et al., 2001) analyzed the effects of bed diameter, distributor, and inserts on minimum fluidization velocity. It was shown that both the bed

diameter and the type and geometry of the distributor affected U_{mf}. Minimum fluidization velocity values increased with an increase in the number of holes in the distributor plate. Furthermore, with an increase in the bed diameter, there was a decrease in the minimum fluidization velocity. Finally, insertion of tubes along the fluidized bed reduced the cross-sectional area available for fluid flow, which produced a high interstitial gas velocity causing a decrease in U_{mf}.

The influence of bed height on minimum fluidization velocity has been studied using different types of fluidized beds. Zhong et al. (Zhong et al., 2006) completed minimum fluidization experiments in spouted fluidized beds. In a spouted fluidized bed, the bed chamber is tapered like a funnel, which creates different hydrodynamics, and the fluidization air is typically injected through a single orifice. Filling the bed with different materials (Geldart type D) to different heights (300-550 mm), they determined that the minimum spouting fluidization velocity, which is analogous to the minimum fluidization velocity in a bubbling fluidized bed, was influenced by the change in bed height; increasing the bed height increased the spouting velocity.

Sau et al. (Sau et al., 2007) used a gas-solid conical tapered fluidized bed to find the minimum fluidization velocity and the pressure drop across the bed. They concluded that bed height for this type of bed did not have a significant effect on the minimum fluidization velocity, i.e., U_{mf} was independent of bed height for this type of conical tapered fluidized bed.

Ramos Caicedo et al. (Ramos Caicedo et al., 2002) studied the minimum fluidization velocity for gas-solid 2D fluidized beds. Their results revealed that as the static bed height increased, U_{mf} increased.

Gunn and Hilal (Gunn and Hilal, 1997) and Cranfield and Geldart (Cranfield and Geldart, 1974) studied gas-solid 3D fluidized beds using glass beads as the bed material and four different bed heights. The results for minimum fluidization velocity in both studies showed that for all the material and experimental conditions used in these studies, there was no significant change in the minimum fluidization velocity when the bed height was increased. Therefore, U_{mf} was independent of bed height. Similar results showing independence between minimum fluidization velocity and bed height were concluded by Escudero and Heindel (Escudero and Heindel, 2011) using different Geldart type B particles (glass beads, ground walnut shell and ground corncob) in the size range of 500-600 μm.

2.1.3.2 Gas Holdup

Fluidized bed hydrodynamics are important to understand how fluidization behaves inside the fluidized bed. Gas holdup or void fraction is one very important parameter that characterizes the fluidization quality, homogenous mixing, and process efficiency in a fluidization system, and is defined as the volume fraction of gas present within the bed material. Using an optical probe, Zhu et al. (Zhu et al., 2008) determined the solid concentration (the inverse of gas holdup) in a gas-solid system for bubbling and turbulent fluidization regimes. Results show that solids concentration in the turbulent regime is not uniform in the axial and radial direction, showing a nonuniformity of the flow structure. In the bubbling regime, the nonuniformity increases as the superficial gas velocity increases. Moreover, Zhu et al. (Zhu et al., 2008) studied the effects that changing the static bed height have on the solid concentration. Results showed that increasing the static bed height produced an increase in the solid concentrations mainly in the central region of the bed, while the wall region had no significant change. This phenomenon is attributed to the increased presence of bubbles in the material as the bed height increased.

Escudero and Heindel (Escudero and Heindel, 2011) calculated the local time-average gas holdup using X-ray computed tomography imaging for three different materials (glass beads, ground walnut shell and ground corncob) in the size range of 500-600 µm, and found that as bed height increased, the bed hydrodynamics were similar at low superficial gas velocities for the same material. However, as superficial gas velocity increased and material density changed, differences were observed between bed heights due to localized mixing and packing effects.

Du et al. (Du et al., 2003) measured the solid concentration for a turbulent fluidized bed. Results show that at high gas velocities, especially in the turbulent regime, the cross-sectional solids holdup exhibits a radially symmetric distribution, while this is not the case for the bubbling regime. At low gas velocities in the bubbling regime, dispersed bubbles yield a lower solids concentration in the center of the bed. The asymmetric distribution of solids concentration was attributed to the spiral motion of bubbles in the bed.

2.1.3.3 Jetting Phenomena

Jetting phenomena at the distributor plate is of interest for gas-solids mixing, heat and mass transfer, and erosion on any bed internals, which can all affect the performance of the fluidized bed. Moreover, in industrial-scale reactors, much of the gas–solids contacting may occur in the region near the distributor where the bubbles are still small. Higher in the bed, the small bubbles coalesce forming large, fast-moving bubbles leading to gas bypassing and poor contacting. The design of the distributor influences the size and shape of the bubbles formed and is therefore a major factor in determining gas–solids mixing in gas–solid fluidized beds. Secondly, the velocity of the gas through the orifices in multi-hole distributors can be an order of magnitude higher than the superficial velocity of gas in the bed, leading to the formation of jets in which the particles are travelling at a high velocity relative to the rest of the bed. This can result in the erosion of

walls, or bed internals, such as cooling tubes, within the region affected by the jets. Finally, dead zones can be found on distributors between the orifices where the material is poorly fluidized (Pore et al., 2010). Thus, studying the hydrodynamics created by jetting near the distributor plate is of great importance to increase fluidized bed process efficiencies.

Jetting has been studied extensively in the literature; see for example Yang and Keairns (Yang and Keairns, 1987), Ettehadieh et al. (Ettehadieh et al., 1988), Guo et al. (Guo et al., 2001, Guo et al., 2001), Chen et al. (Chen et al., 2008), or Müller et al. (Müller et al., 2009). However, most of the studies focused on jetting produced by using a central nozzle or focused on jetting produced by a horizontal nozzle; there is limited information available for the studies of jetting produced by the distributor plate of a fluidized bed, even though the hydrodynamics that are produced around this area are of extreme importance for the performance of the fluidized bed.

Yang (Yang, 1998) made a comparison of the vertical jetting phenomena between a 30 cm and a 3 m diameter fluidized bed. He studied the momentum dissipation, the jet penetration depth and the jet velocity profile by visual observation. Also, he proposed several correlations for the parameters studied above.

Wang et al. (Wang et al., 2010) calculated the volumetric solids holdup (inverse of gas holdup) of a bubbling gas-solid fluidized bed with a horizontal gas jet using electrical capacitance volume tomography (ECVT). They concluded that the solids holdup in the region of the gas-solid mixture jet is higher than that in the gas jet. Also, the penetration length of the horizontal gas solid mixture jet was larger than the gas jet.

Jet structure in a 3D fluidized bed was studied by Pore et al. (Pore et al., 2010) using nonintrusive techniques such as magnetic resonance imaging in a 0.64 cm diameter bed. They used different distributor plate configurations to study the jet-jet interactions, and the jet-wall

interactions. They obtained maps of solid concentrations to investigate the jet stability under the different distributor configurations. They concluded that depending on the design of the distributor plate, jets migrate in preferential directions. For example, the jets that are closer to each other are attracted to one another, while jets that are near the wall have a tendency to bend out towards the wall.

Guo et al. (Guo et al., 2010) studied the flow characteristics in a fluidized bed with jetting produced by a horizontal nozzle under acoustic assistance. They investigated the jet penetration depth and the particle concentration using an optical probe. They concluded that the jet penetration depth increased when an acoustic field of a certain sound pressure level and frequency is applied to the fluidized bed; also they concluded that sound waves have a different effect on particle concentration depending on the region of the bed.

2.1.4 Vibration Effects on Fluidized Bed Hydrodynamics

Intrusive and nonintrusive methods have been study in the literature to improve the fluidization quality of granular material. These methods may produce changes in the hydrodynamic behavior of the fluidized material. In industrial applications, vibrations have been used together with fluidization in order to overcome cohesion problems. Vibrations, in fact, are able to interact directly with structures of the dispersed phase determined by cohesive forces such as aggregates and channels (Barletta et al., 2013). These vibrations can be applied to the fluidized bed in the form of mechanical vibrations or acoustic vibrations. The following subsections summarize studies made first using mechanical vibrations and then studies that focus on the use of acoustic vibrations.

2.1.4.1 Mechanical Vibrations

Mechanical vibrations are being used to ease fluidization in materials that present poor fluidization quality. Zhang et al. (Zhang et al., 2012) studied the fluidization characteristics of fly ash in a fluidized bed subjected to mechanical vibrations. They found that the minimum fluidization velocity decreased due to the vibrations, implying that fly ash can be fluidized at a lower superficial gas velocity. Marring et al. (Marring et al., 1994) studied the effect of vibration on the fluidization behavior of glass beads and potato starch. Glass beads falling in the Geldart type A category had a decrease in the minimum fluidization velocity and bed voidage when the vibration frequency was keep constant and the amplitude was increased. Moreover, for a more cohesive powder like potato starch, which presents a poor fluidization quality without vibration, the use of vibration allowed the bed to fluidize well with different conditions of cohesiveness, thus showing vibration helped to improve the fluidization quality for cohesive powders.

Barletta et al. (Barletta et al., 2008) also studied the effects of mechanical vibration on the fluidization of a fine aeratable FCC powder. Changing the parameters of peak acceleration and frequency, they determined the effects on bed expansion, voidage, and fluidization. They found that bed packing degree reached without gas flow when the bed was vibrated was always higher than that reached without vibration. Also, the pressure drop in the fully fluidized bed may be equal to or smaller than, sometimes significantly, those obtained without vibration. The bed started to expand when the gas pressure drop was consistently smaller than what was necessary for fluidization. The largest bed expansion of the vibrated bed was always smaller than that attained without vibration. If the discrepancies between vibrated and not vibrated fluidization was assumed as a measure of the significance of the effect of vibration, these were generally larger at low frequencies and tended to become less important at high frequencies; these effects

were also apparent under full fluidization conditions. Similar and more recent studies were performed by Barletta and Poletto (Barletta and Poletto, 2012) and Barletta et al. (Barletta et al., 2013)

Finally, Levy and Celeste (Levy and Celeste, 2006) studied the combined effects of mechanical and acoustic vibrations on the fluidization of cohesive powders. In their experiment, they used powder ranging in size from 0.012 to 15 μm, using both acoustic vibration and horizontal mechanical vibrations to produce fluidization of these powders. They found that when the fluidized bed was subjected to both types of vibrations, the agglomerate size and the minimum fluidization velocities were reduced for all the powders tested; however, the vertical acoustic vibrations were found to be more effective than the horizontal mechanical vibrations, even when the relative accelerations caused by the mechanical vibrations were of the same magnitude as those caused by the acoustics.

2.1.4.2 Acoustic Vibrations

Acoustic vibrations can also be used to enhance particle fluidization. Acoustic fluidized beds have been studied for different Geldart type particles (Geldart type A-C) to understand the effects produced by the acoustic field on the fluidization behavior and quality. This is an attractive option because no internal changes are made to the bed and there is no limitation to the particle type that can be fluidized.

Leu et al. (Leu et al., 1997) studied the fluidization of Geldart type B particles in an acoustic fluidized bed. They determined the influence of speaker power, sound frequency, particle loading, and distance between the speaker and bed surface on the hydrodynamic properties of a fluidized bed filled with 194 μm sand. They found that when an acoustic field was applied, a different particle loading height created a different minimum fluidization velocity, making

minimum fluidization velocity dependent on bed height. They also showed that the standard deviation of the pressure fluctuations and the bubble rise velocity was reduced in the presence of an acoustic field.

Guo et al. (Guo et al., 2006) investigated the behavior of ultrafine (Geldart type C) particles under the influence of sound waves. They studied both nanometer and micrometer size particles, and found that as frequency increased, the minimum fluidization velocity decreased. After a specified frequency (40-50 Hz), the minimum fluidization velocity then increased. When the sound pressure level was changed (100 dB - 103.4 dB) and the sound frequency remained fixed, the minimum fluidization velocity decreased for all particles, thus improving the fluidization quality of the particles. The same trends were found by Kaliyaperumal et al. (Kaliyaperumal et al., 2011) and Levy et al. (Levy et al., 1997).

Herrera et al. (Herrera et al., 2002) used visual observations as well as invasive techniques such as fiber optic probes to measure the bubbling characteristic of a Geldart type A fluidized bed. Using these techniques they determined that high values of the sound pressure level affected the fluidization behavior of the bed, and had a large impact on the bubble characteristics, such as size and frequency.

Moreover, Guo et al. (Guo et al., 2011) analyzed the effects of the acoustic field on a fluidized bed at different temperatures for quartz sand (74 μm, 2650 kg/m^3) and SiO_2 particles (0.5 μm, 2560 kg/m^3) using pressure transducer and pressure fluctuations analysis as a measurement technique. The results obtained in that study showed that minimum fluidization velocity decreased with increasing temperature with, as well as without, acoustic assistance. In the same way, at a fixed sound pressure level (120 dB), the minimum fluidization velocity

decreased when the frequency was increased from 50-200 Hz, and then the minimum fluidization velocity increased with frequency from 200-400 Hz.

Si and Guo (Si and Guo, 2008) studied how an acoustic fluidized bed improved the fluidization of two different biomass particles, sawdust and wheat stalks, alone or mixed with quartz sand. They compared the fluidization behavior of the biomass without and with the acoustic field to determine if there was any improvement due to the acoustic field. Additionally, they determined the effects that the sound pressure level (SPL) had on the minimum fluidization velocity. Initially, they found that the biomass by itself fluidized poorly with and without the presence of the acoustic field. They then added quartz sand to aid fluidization and maintained the biomass mass fraction at 60%. They observed that below a SPL of 90 dB, plugging and channeling occurred in the fluidized bed. Increasing the SPL diminished the effects of channeling and improved the quality of fluidization. By varying the sound frequency between 50 to 400 Hz, they determined that the minimum fluidization velocity decreased with increasing frequency until it reached a minimum value and then increased with increasing frequency. Similar results were found by Escudero and Heindel (Escudero and Heindel, 2012) using glass bead particles.

Si and Guo (Si and Guo, 2008) also fixed the sound frequency at 150 Hz and varied the sound pressure level between 90 and 120 dB. Using these conditions, they determined the effects on the minimum fluidization velocity. They found that when the sound pressure level was above 100 dB, the fluidization quality improved, and they observed that the biomass mixture fluidized smoothly without any obvious slugging or channeling. All of their conclusions were obtained using visual observations.

2.2 Fluidized Bed Hydrodynamics: Measurement Techniques

This section summarizes several techniques used to visualize and characterize hydrodynamics of opaque multiphase flow systems, emphasizing noninvasive X-ray techniques used in this study such as X-ray computed tomography. The first subsection describes general noninvasive measurement techniques commonly used to visualize and characterize multiphase flow systems. The second subsection provides a deeper explanation of the X-ray computed tomography technique used in this study.

2.2.1 Noninvasive Measurement Techniques

Noninvasive imaging techniques are valuable because they provide insight into the flow behavior and general hydrodynamic characteristics of multiphase flow and opaque systems (Yates et al., 2002). There are several noninvasive techniques used to measure gas/liquid holdup, pressure drop, flow regime, bubble size and distribution, and gas and liquid velocity. Contrary to the invasive techniques, noninvasive techniques are able to measure several of the characteristics listed above. According to Chaouki et al. (Chaouki et al., 1997), noninvasive techniques can be classified into tomography and radiography techniques and velocimetry techniques. Tomographic and radiographic techniques are divided into two categories: nuclear based imaging techniques like gamma-ray computed tomography (GRT), X-ray computed tomography (XCT), positron emission tomography (PET), X-ray diffraction tomography (XDT), X-ray and neutron transmission radiography, nuclear magnetic resonance imaging (MRI or NMRI), and non-nuclear based techniques like electrical capacitance tomography (ECT), optical tomography, and ultrasonic tomography. On the other hand, positron emission particle tracking (PEPT), radioactive particle tracking (CARPT or RPT), cinematography, laser Doppler anemometry (LDA), and particle image velocimetry (PIV or PTV) are forms of velocimetry techniques.

Even though there are several techniques for visualization and measurement of multiphase flow systems, not all the techniques are applicable to fluidized beds. Gamma-ray tomography (GRT) uses a gamma-ray source and detector to quantify the gamma-ray attenuation through an object. The attenuation provides a measure of the local mass density distribution along the path traversed by the gamma beam (Chaouki et al., 1997). Patel et al. (Patel et al., 2008) used GRT to determine the gas maldistribution of a gas-solid fluidized bed drier and how the gas maldistribution was affected by various parameters, such as particle size, particle density, and superficial gas velocity. Results showed that GRT was a reliable technique that provided a good estimation of the gas maldistribution with a good spatial resolution (Patel et al., 2008).

Mandal et al. (Mandal et al., 2012) used gamma densitometry to study the void fraction distribution in an unary and packed fluidized bed. They determined that packed beds produced a more homogeneous fluidization than unary fluidized beds. Veera (Parasu Veera, 2001) also used gamma densitometry to study gas holdup profiles in bubble columns and showed how useful this technique can be for understanding different flow behaviors in laboratory or industrial scale bubble columns.

ECT is another tomographic technique used in fluidized beds. The ECT principle uses electrical measurements like capacitance, resistance, or inductance, for imaging the distribution of these parameters within a medium. This technique is safer and faster than nuclear based techniques, it also provides more flexibility to accommodate large or small vessels. However, the spatial resolution provided is lower than the nuclear based techniques (Chaouki et al., 1997). Du et al. (Du et al., 2003) used the ECT technique to study the dynamic behavior of a turbulent gas-solid fluidized bed. From the ECT images, they quantified the dynamic characteristics of the bubble/void phase and the emulsion phase of the system. Results showed that ECT imaging

provided robust and reliable measurements and showed similar results compared with other techniques like optical probes. Finally, Du et al. (Du et al., 2005) used electrical capacitance tomography to investigate local void fraction distributions in various fluidized beds; they showed that radial symmetry was observed when the bed was operated in the turbulent fluidization regime.

X-rays have been used to study gas-solid fluidized beds as well as two and three phase fluidized systems for more than 50 years (Yates et al., 2002). They are commonly employed in noninvasive techniques because they are safer than other nuclear based techniques which cannot be turned on and off at will, have high resolution, and can be controlled by varying the voltage or current to improve penetration or contrast (Heindel, 2011). X-rays are produced by accelerated electrons emitted from a heated cathode; the electrons hit an anode producing a deceleration of the electrons and an emission of electromagnetic radiation. The interaction between X-rays and the materials through which they pass cause a decrease in the X-ray intensity (Grassler and Wirth, 2000).

Heindel et al. (Heindel et al., 2008) developed an X-ray visualization facility to study the different characteristics of opaque multiphase flows, from bubble columns to fluidized beds, with good both spatial and temporal resolution depending on the type of X-ray imaging technique used. Their facility is capable of producing three different X-ray imaging techniques: X-ray radiography, X-ray stereography, and X-ray computed tomography.

2.2.2.1 X-Ray Computed Tomography

X-ray computed tomography (XCT) can generate a 3D image of the object of interest. X-rays pass through the object and the intensity values are recorded at several projections by an imaging device. After the images are collected, computer algorithms reconstruct the images to produce a

3D representation of the object. Figure 2.3 shows how XCT images are taken. However, due to the number of projections that must be acquired in order to obtain a whole reconstruction of the object, this technique does not have good temporal resolution. Conversely, having multiple scans from different projections give a high spatial resolution to this technique, a characteristic that can be used to measure the local time-average gas holdup in a very efficient way.

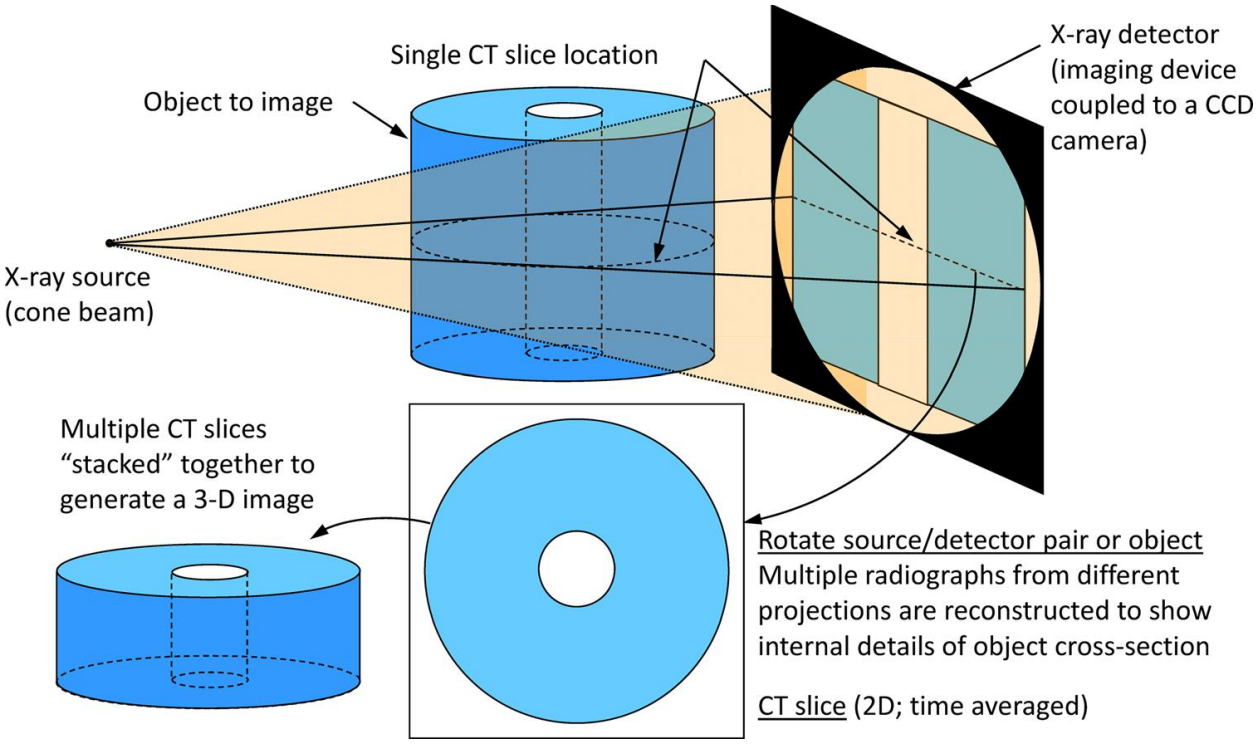

Figure 2.3: X-ray computed tomography schematic (Heindel et al., 2008).

XCT has been widely used in measuring multiphase flow characteristics. Franka et al. (Franka et al., 2007) used XCT in four different materials (glass beads, melamine, ground walnut shell and ground corncob) to visualize and compare the fluidization structure between the materials. Results showed that in terms of fluidization uniformity, glass beads fluidized symmetrically about the center of the bed and maintained a constant uniformity as the gas velocity increased while less dense melamine, ground walnut shell, and ground corncob showed regions where jetting, spouting, and channeling effects appeared and decreased the bed

uniformity. As gas velocity increased, the uniformity of the non-glass materials increased too, obtaining a better gas distribution inside the material. Kantzas et al. (Kantzas et al., 1997) used X-ray computed tomography to analyze channelling in a gas-solid system composed of polyethylene resin at various gas flow rates and bed heights. With the help of CT scans, they determined the voidage distribution along the bed, identifying the regions with high gas holdup as areas of gas channelling. Channelling was dependent on the gas velocity and the bed height. Their results showed that as the gas superficial velocity increased or the bed height decreased, channelling inside the resin increased.

Moreover, XCT data analysis allows for the calculation of time-average local gas holdup or solid holdup. Grassler and Wirth (Grassler and Wirth, 2000) used XCT to determine the solids concentration in a 0.19 m diameter circulating fluidized bed with 50-70 μm glass beads as the bed material. Tests were carried out in two different systems. In the first, solid concentrations were calculated with an up flow system. Results for this system showed that radial solid concentration exhibited a parabolic shape with a maximum concentration close to the wall of the reactor and a minimum concentration in the center of the bed. For the second, the solid concentration was calculated with a down flow system. For this case, the solid concentration distribution was much more complex and depended upon the gas-solid distributor operating conditions. Results showed various solid concentration distributions from a homogeneous distribution with a parabolic profile to concentrated strands in the center of the bed. Finally, the study also showed that the solids concentration was accurately calculated within 5% error for concentrations up to 20 vol% with a minimum resolution of 0.2 mm.

Franka and Heindel (Franka and Heindel, 2009) studied the effects of side air injection, superficial gas velocity, and bed material on the local time-average gas holdup of a 10.2 cm

fluidized bed, using X-ray computed tomography. Using different materials (glass beads, ground corncob, and ground walnut shell), superficial gas velocities (U_g), and side air injection flow rates (Q_{side}), they determined the variations on the fluidization hydrodynamics of the bed. They found that with side air injection, the side air flow rose near the wall but then expanded into the bed as height and Q_{side} increased. As U_g increased the effects caused by the side air injection were less pronounced, and the overall gas holdup in the system increased. Fluidization in other materials had similar behaviors with some notable differences. Side air injection was less influential on the less dense material and gas holdup was lowest for the denser material. Finally, they demonstrated the usefulness of X-ray computed tomography in visualizing the internal features of fluidized beds (Franka and Heindel, 2009). Similar studies were presented by Drake and Heindel (Drake and Heindel, 2012).

Drake and Heindel (Drake and Heindel, 2011) used the X-ray computed tomography technique to study the repeatability and uniformity of gas holdup measurements in a 15.2 cm fluidized bed. They used two different materials and a range of fluidization conditions. They concluded that the time-average gas holdup data obtained from the CT's is highly repeatable; moreover, they determined that the uniformity of the data was dependent of the bed characteristics and the flow conditions.

Escudero and Heindel (Escudero and Heindel, 2011) studied the effects of bed height, superficial gas velocity, and bed material on the local time-average gas holdup of a 10.2 cm fluidized bed, using X-ray computed tomography. Using different materials (glass beads, ground corncob, and ground walnut shell), superficial gas velocities (U_g), and height-to-diameter ratios (H/D), they determined the variations on the fluidization hydrodynamics of the bed. They found that as superficial gas velocity increased, the overall gas holdup increased for every bed height

studied. Flow behavior was also affected with the increase in superficial gas velocity. Increasing bed height, particularly at the higher gas flow rates, enhanced bubble coalescence creating slugs that rose through the center of the bed, producing regions of low gas holdup near the walls of the fluidized bed. Also, the effects of bed height observed in the time-average local gas holdup varied depending on the bed material tested. Finally, as material density decreased, gas holdup increased. Glass beads had lower gas holdup than both ground walnut shell and ground corncob, while ground corncob exhibited the largest gas holdup of all three materials in this study. Ground corncob also exhibited a better distribution of gas holdup along the entire bed, therefore providing a more uniform fluidization.

2.3 Summary

This chapter reviewed two important topics related to this proposed work. In section 2.1, fluidization was examined. The section described fluidized beds and the different fluidization regimes present in a multiphase flow system, and how important hydrodynamic parameters, such as gas holdup, minimum fluidization velocity and jetting, are influenced by the inclusion of vibrations. In section 2.2, different techniques used for the visualization and characterization of multiphase flow systems were described. This section described noninvasive techniques, with a particular focus on noninvasive X-ray techniques used in this research. Understanding this background will be very important for the subsequent work.

CHAPTER 3: EXPERIMENTAL SETUP

A summary of the basic equipment, techniques, and procedures to be used in this research is provided in this chapter. In section 3.1, a description of the equipment is provided, including the fluidized bed reactor, air system, pressure transducer, flow instrumentation, and sound equipment. Section 3.2 outlines the material selection and preparation procedures. Section 3.3 summarizes the experimental procedures used to determine the minimum fluidization velocity for the respective materials. Section 3.4 further describes the sound wave behavior inside the fluidized bed. Section 3.5 describes the X-ray equipment, X-ray CT imaging procedures, calibration requirements, and how gas holdup is calculated from the CT images. Finally, section 3.6 describes the procedure used to identify and quantify the jetting phenomena inside the fluidized bed.

3.1 Equipment

This section describes the equipment used for this research including the fluidized bed reactor, the air flow system, the instrumentation used to measure pressure and gas flow rates and the equipment used to provide the acoustic field to the bed.

3.1.1 Fluidized Bed Reactor

The reactor used in these experiments is a cold flow fluidized bed reactor. The cylindrical fluidized bed was fabricated from 10.2 cm internal diameter (ID) acrylic tubing with a 0.64 cm wall thickness. As shown in Figure 3.1, the reactor consists of three main chambers: the top chamber or freeboard region, the bed chamber, and the plenum. Fluidization occurs in the bed chamber which is 30.5 cm tall and 10.2 cm ID. Square flanges (16.5×16.5 cm) connect each section.

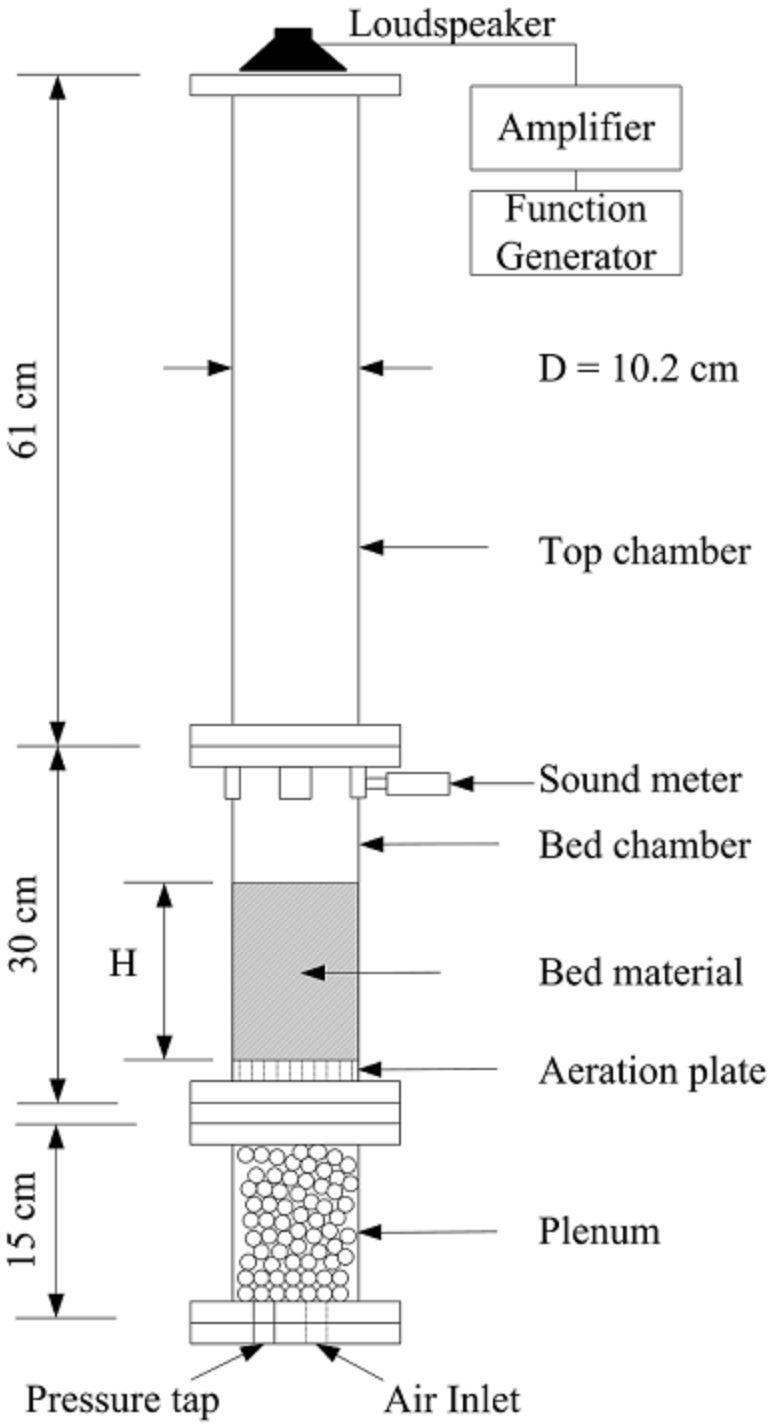

Figure 3.1: Fluidized bed reactor schematic (not to scale). The static bed height is identified by H.

An aeration plate is located immediately below the bed chamber; it is fabricated from a 1.27 cm thick acrylic plate with 62, 1 mm diameter holes spaced approximately 1.27 cm apart in a circular grid for a total open area of 0.60 %.

Filtered compressed air from the building supply is used as the fluidizing gas. The pressure at which the compressed air is delivered inside the laboratory is 620 kPa (90 psi). However, since the flow rates used for fluidization vary depending of the specific conditions of each experiment, an air flow control board with four independent air lines is used to deliver the required air to the fluidized bed.

The fluidized bed air flow is regulated using a stepper motor valve (Aalborg SMV40-SVF2-A). The regulated air flows through a 0-1000 Lpm stainless steel Aalborg GFM771 flow meter. The mass flow meters for this study have an error of 2% of full scale.

Pressure is measured with a Dwyer 0-34.5 kPa (0-5 psig), 4-20 mA output pressure transducer located in the bottom of the plenum. The signals obtained from the pressure transducer and mass flow meter are connected to a computer controlled data acquisition system. Average measurements were necessary due to the highly variable pressure signal caused by the bubbling fluidized bed. In this study, data collection occurred at a rate of 1000 Hz for a time interval of 5 seconds; average pressure and average fluidization gas flow rate were subsequently written to a data file. Pressure readings have an estimated error of 1% to 4%, the larger error corresponding to the smaller pressure drops associated with a fix (static) bed.

As with any other measurement device, the pressure transducer and flow meters are calibrated before starting the experiments. The technique used to calibrate the pressure transducer was to fill up a tube with water, and then measure the hydrostatic pressure at different water level heights. Since the output signal of the transducer is a voltage, the specified pressure

is linearly related to the output voltage, which is then used in a calibration function in the data acquisition software. The mass flow meters are calibrated using a calibration drum. The output voltage of the flow meters is measured as a function of the calculated mass flow that passes through the drum during a specified time period. Afterwards, a linear curve fit is applied and used as the calibration function in the data acquisition software.

3.1.2 Sound Equipment

In order to induce the acoustic vibrations into the fluidized bed, sound equipment is used in this study. A function generator (BK Precision 4011A) is used to produce sine waves, which serve as the acoustic wave source. The frequency of the waves can be adjusted and displayed using this function generator.

A stereo power amplifier (AudioSource Amp 100) allows changing the amplitude of the sinusoidal wave originated by the function generator, by increasing or decreasing the volume in the amplifier.

Finally, the sound is emitted from a Peerless 7.62 cm ID full range woofer speaker located at the top of the fluidized bed. To measure the power of the sound (Sound Pressure Level), which is emitted by the speaker, a pressure sound meter with a maximum pressure level of 130 dB and with an approximate error of less than 1% is located at the top of the bed chamber at a distance of 61 cm from the acoustic source. Refer to Figure 3.1 to see the setup for the entire experiment.

3.2 Bed Material

The bed material is a significant parameter in this study. The following section describes the criteria used to select the material, how it was prepared, and the calculation of important material properties.

3.2.1 Material Selection and Preparation

For this study, two different materials were selected, glass beads (ρ_{glass} = 2500 kg/m^3) and ground walnut shell ($\rho_{walnut\ shell}$ = 1440 kg/m^3) over three different size ranges (212-425 µm, 425-500 µm, and 500-600 µm). The true material densities were measured using a pycnometer. As shown in Figure 3.2, both materials fall within the Geldart Type B classification. Figure 3.3 shows how the materials appear.

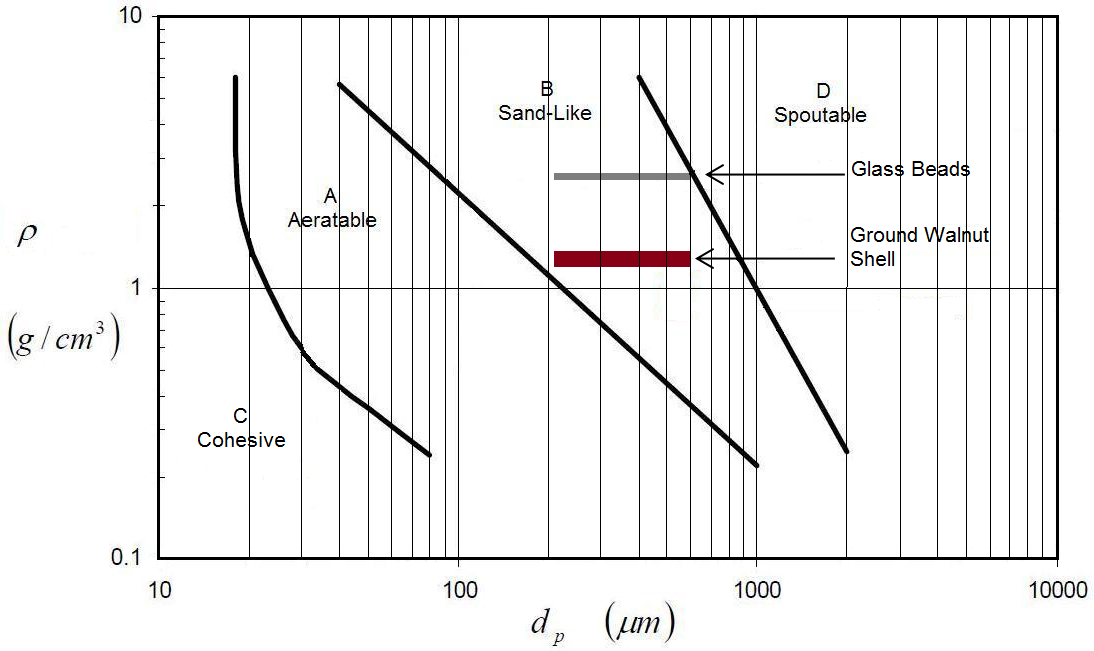

Figure 3.2: Material selection based on Geldart's classification (Geldart, 1973).

The materials are divided into the different size classes by initially filling a 600-800 µm sieve with the desired material. The 500-600 µm, 425-500 µm, and 212-425 µm sieves are then added sequentially to the sieve stack, with a bottom under the smallest sieve. With the help of a mechanical shaker, the sieve stack is vibrated for about 20 minutes; this process is repeated several times to ensure that the desired particle size range is retained in the respective sieve.

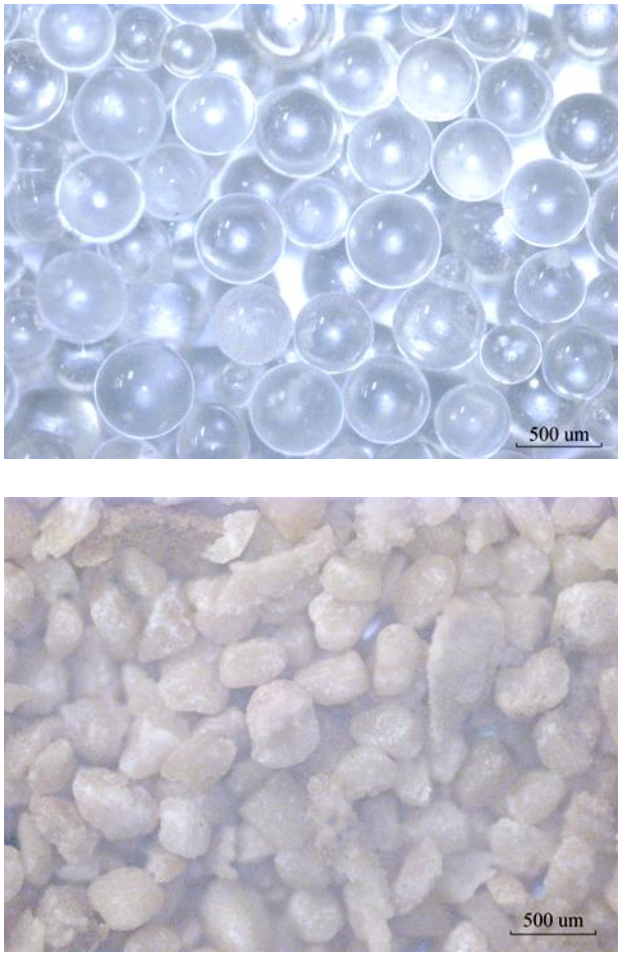

Figure 3.3: Glass beads and ground walnut shell of different particle sizes.

The bed bulk density was determined knowing the material mass and the static bed volume. Bed material was slowly added until the desired static bed height was reached, which corresponded to H/D = 0.5, 1, 1.5, and 2, where H is the static bed height and D is the bed diameter. Before the bed height was measured, the bed was fluidized and then allowed to collapse to avoid any packing effects due to the filling process. The material mass was then measured and the given bed bulk density was calculated. Table 3.1 summarizes the general bed characteristics. Bed height had a small, if any, effect on bulk density. There is no effect of

particle diameter because the overall particle size range (212-600 um) is still relatively narrow. Note that all bulk densities are based on measured bed mass and bed height.

Table 3.1: Summary of bed material characteristics.

	Glass Beads	
H/D	**Bed Mass (g)**	**Bulk density (kg/m^3)**
0.5	620	1505
1	1240	1505
1.5	1860	1505
2	2570	1530
Diameter (μm)	212-425, 425-500, 500-600	
Particle Density (kg/m^3)	2500	
	Ground Walnut Shell	
H/D	**Bed Mass (g)**	**Bulk density (kg/m^3)**
0.5	250	610
1	500	610
1.5	750	610
2	1100	670
Diameter (μm)	212-425, 425-500, 500-600	
Particle Density (kg/m^3)	1440	

3.3 Minimum Fluidization Velocity Procedures

The minimum fluidization velocity is defined as the minimum superficial gas velocity where particle fluidization is achieved. For this study, the minimum fluidization velocity is used as a reference for different bed heights and bed materials with and without acoustic assistance; it is also used as a reference in the X-ray CT imaging work. This section describes the method used to determine the minimum fluidization velocity for each material, for each specific bed height, and for each acoustic condition.

Humidified air is used to reduce the electrostatic effects that may appear during the fluidization process. The air supplied by the building before entering the fluidized bed was passed through a vessel filled with water, creating humidified air at the outlet of the vessel, which then it was supply to the fluidized bed. The relative humidity level of the air measured inside the fluidized bed ranges between 55 to 70% depending of the time of year. This simple solution has been implemented in the laboratory and in several studies found in the literature (Baron et al., 1987, Zhang et al., 2010, Escudero and Heindel, 2011, Escudero and Heindel, 2012)

Minimum fluidization velocity is determined using the following pressure measurement procedure. First, the reactor is filled with the desired material to a specified height. Air at U_g = 40.8 cm/s is passed through the bed for about an hour to condition the system. After the conditioning period, the pressure and flow rate are acquired using the DAQ system. Data are collected at 1000 Hz over a 5 second interval, averaged over this period, and then output to an Excel file. Next, the air flow rate is decreased by 1 cm/s by automatically closing the stepper motor valve. Then, when the flow rate mean, pressure mean, and pressure standard deviation are between specific thresholds, the DAQ system again records the pressure and flow rate and averages them over a 5 second interval. This process is repeated until the flow rate reaches approximately U_g = 0 cm/s; at this point the test is completed. For statistical purposes, each test for every specified condition is repeated 10 times.

Minimum fluidization tests were carried out at a reference state without sound but with a measured average background noise sound pressure level of 60 dB (i.e., the average background noise in the lab), and with sound emitted from a Peerless 7.62 cm ID full range woofer located at the top of the bed. Sine waves at different frequencies (50-200 Hz) are generated by a function

generator and passed through an amplifier (Audio Source AMP100); three different sound pressure levels, which are a logarithmic measure of the effective sound pressure relative to a reference value, are tested (90, 110, and 120 dB), and these values are measured by a sound pressure meter located at the top of the bed chamber, at a distance of 61 cm from the acoustic source (see Fig. 3.1). Table 3.2 summarizes some sound pressure level values encounter daily in industrial applications, to show a comparison with the sound pressure level used in this study.

Table 3.2: Example of typical Sound Pressure Levels (SPLs) (Fahy, 2001)**.**

Source	**Sound Pressure Level (dB)**
Launch noise outside rocket payload bay	160
Heavy artillery at gunners' heads	140
Threshold of pain	130
Large engine jet at 30 m	120
1 m from pneumatic chipping hammer	110
Inside a textile Factory	90
Laboratory background noise	60

After all the bed material data are collected, the same procedure is repeated in an empty reactor. This is done to quantify the pressure drop through the aeration plate and plenum. The empty reactor pressure data are then subtracted from the fluidized bed data at the respective superficial gas velocities. Since the flow rates between the empty reactor and fluidized bed tests do not match exactly, a linear interpolation method is employed to calculate the empty bed pressures corresponding to the fluidized bed flow rates. Finally, the bed pressure drop is plotted as a function of superficial gas velocity and the minimum fluidization velocity is defined as the point in which the pressure drop across the bed remains constant. To determine the value of the minimum fluidization velocity, a point located around the knee of the plot (e.g., Figure 3.4) is identified as a reference point; then two linear trend lines are plotted using the reference point and 10 data points above and 10 data points below the reference point. The minimum fluidization

velocity is then identified as the point where the two trend lines intersect. Figure 3.4 shows a sample plot obtained for glass beads where the static bed height corresponds to H/D = 1 without any acoustic field influence.

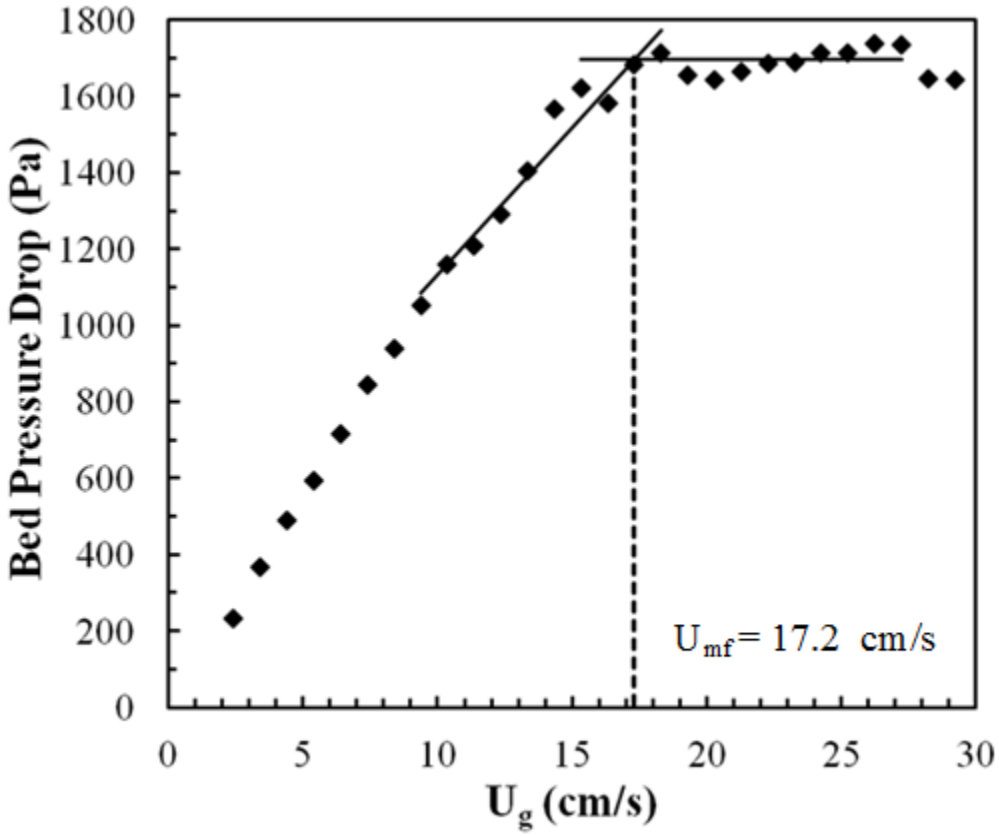

Figure 3.4: Sample minimum fluidization plot for glass beads with H/D = 1 without acoustics.

3.4 Sound Wave Behavior Inside a Fluidized Bed

In order to analyze and understand the effects that the acoustic waves have on the hydrodynamic structures of a fluidized bed, it is important to first describe the behavior that the sound waves exhibit inside the fluidized bed. This section describes first the experiments perform to obtain the behavior of the sound wave produced by the loudspeaker at different

operational conditions, and second, describes a 1D model used to compare and explain the experimental data.

3.4.1 Experimental Procedures

Experimental data on the sound pressure level emitted by the loudspeaker at different operational frequencies (50, 100, 150, 200 Hz), keeping the amplitude of the acoustic wave source constant were obtained to understand the behavior of the sound wave inside the fluidized bed. The goal was to determine the change in the sound pressure level as a function of height between the acoustic source and the sound pressure meter.

An EMM 6 Dayton Audio Measurement Microphone was utilized to measure the sound pressure level produce by the loudspeaker to determine how the sound pressure level changes as a function of height. The microphone was first calibrated using a calibration file for the given microphone and the Room Equalizer Wizard audio analysis software. Once the microphone was calibrated, it was located at different axial positions inside the fluidized bed. In each axial position, the function generator which serves as the acoustic source was set to an initial frequency of 50 Hz and the amplifier was set to specified amplitude. The sound pressure level measurement that came from the microphone was recorded using the audio analysis software. Once the sound pressure level was recorded, the frequency was changed and again the sound pressure level was recorded. This procedure was repeated for the four operational frequencies described above at every axial position of the microphone.

This procedure was performed first without any material inside the fluidized bed and then with both materials (glass beads and ground walnut shell) inside the fluidized bed. In both situations, different superficial gas velocities (U_g = 0 U_{mf}, 1.5 U_{mf} and 3U_{mf}) were tested in order to determine if the presence of fluidizing gas inside the fluidized bed affected the reading of the

microphone; and thus, the behavior of the sound wave. The minimum fluidization values used were the ones determined by the procedure in Section 3.3.

Once all the measurements for all the conditions were obtained, the sound pressure level data were plotted as a function of microphone axial location relative to the distributor plate. This provided information on how the sound pressure level varied within the fluidized bed, and is used to further understand the effects of the acoustic waves on the minimum fluidization velocity, local gas holdup distribution, and finally the effects on jetting produced by the distributor plate.

3.4.2 One Dimensional Acoustic Model

When a sound wave is confined in a fluidized bed, where two single-phase (gas and solid) elements are presented, the transmission of the sound wave occurs in the following way: the incident wave pressure from the acoustic source (P_i) first travels through air, when P_i reaches the interface between air and the fluidizing material, part of the energy of P_i is reflected P_r and the rest of the energy is transmitted downward through the material (P_t). Once the incident wave P_{i1} reaches the distributor plate, another reflected wave P_{r1} appears. These waves have an additive effect creating what is called in acoustics engineering a standing wave. Figure 3.5 shows a schematic of the wave propagation inside the fluidized bed.

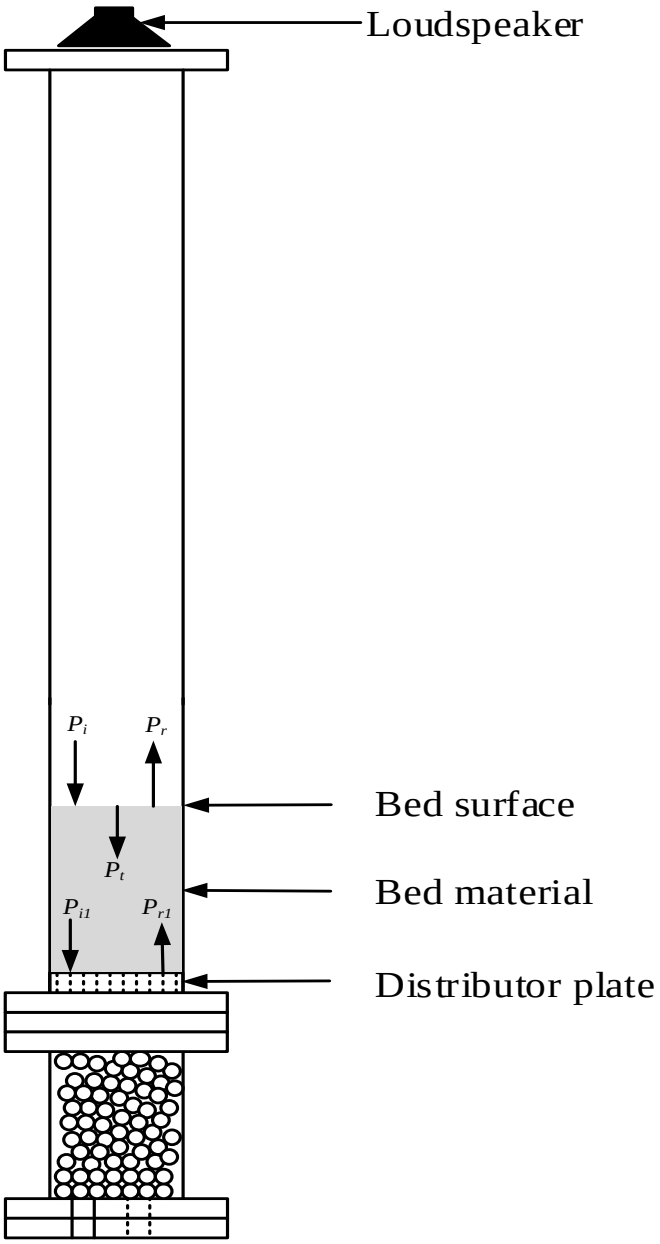

Figure 3.5: Schematic of the sound wave transmission in a fluidized bed.

Using the theory of a standing wave, a simple 1D model of the propagation of the sound wave inside the fluidized bed can be developed. For this particular study, the model equations were developed using Matlab and is based on the model previously developed by Herrera et.al (Herrera et al., 2002).

The sound pressure distribution can be described by:

$$p(x,t)=P_{fs}\sqrt{\frac{\cos^2 kx}{\cos^2 kh}}\cos\omega t \tag{3.1}$$

where P_{fs} is the source amplitude in dB, k is the wave number which can be expressed as $k = 2\pi f/c$ (f is the frequency and c is the speed of sound) , x is the distance from the distributor plate, h is the height of the static bed material inside the fluidized bed, and ω is the angular velocity ($2\pi f$). Since only positive values are used in this model, the maximum amplitude of Eq. (3.1) is:

$$|p(x,t)|=P_{fs}\sqrt{\frac{\cos^2 kx}{\cos^2 kh}} \tag{3.2}$$

When bed material is present, the pressure distribution of the sound wave changes due to the fact there is an attenuation of the wave caused by the attenuation coefficient α, which is an acoustic property of the material; therefore the amplitude of the sound pressure distribution with attenuation is described by:

$$|p(x,t)|=2P_{fs}\sqrt{\cosh^2\alpha x\cos^2 kx+\sinh^2\alpha x\sin^2 kx} \tag{3.3}$$

Using these equations in Matlab, the model was developed and validated with the experimental data obtained using the procedures explained in the previous subsection.

3.5 X-ray Facility

The X-ray equipment available for the study of multiphase flow systems in the X-ray Flow Visualization (XFloViz) facility at Iowa State University is described in this section. The first subsection describes the different components of the X-ray facility, followed by a description of the X-ray computed tomography imaging procedures as well as calibration techniques. Finally, the last subsection explains how gas holdup data are obtained using the CT images of the object of interest.

3.5.1 X-ray Equipment

The X-ray equipment used in this research is the same as that described by Heindel et al. (Heindel et al., 2008); only a summary is provided here. The equipment consists of two LORAD LPX200 portable X-ray sources. X-rays are emitted from the beryllium window on the tubehead in a 60° horizontal, 40° vertical conical beam. The beam spot size of each source is 1.5 mm. Current and voltage can be adjusted from 0.1 to 10.0 mA and 10 to 200 kV, respectively, with a maximum total power of 900 W. The X-ray tubes are liquid-cooled with two LORAD pump systems. X-ray energy is limited by a collimator surrounding the source. Copper and aluminum filters may be placed in front of the source to reduce the low energy radiation. Filters are used according to the attenuation characteristics of the object being visualized.

An X-ray detector/CCD camera pair is located opposite each X-ray source. The XFloViz facility has two image intensifier/CCD camera detectors which are used primarily for radiographic and stereographic imaging due to their relatively high temporal resolution and good spatial resolution. A second detector/camera pair is primarily used for CT imaging because of its high spatial resolution. In addition, individual radiographs may be captured. For this system, incident X-ray energy is transformed into visible light by a square 44×44 cm cesium-iodide (CsI) scintillator screen. A 50 mm Nikon lens captures images which are digitized by an Apogee Alta U9 system. This system has 3072×2048 active pixels and is thermoelectrically cooled to allow long exposure times with low noise conditions. One difficulty in using the CsI scintillator screen is in the response of the scintillation crystals at the beginning of an X-ray test. If the detector is used without previously exciting the crystals, the detector's response will change throughout a test, causing inaccurate data. To overcome this problem, the scintillator is excited with X-rays

for approximately 20 minutes before data collection. Additionally, the scintillator requires about 5 minutes without incident X-rays to completely return to an unexcited state.

The detectors and sources are mounted on extension arms from a 1.0 m ID rotation ring that can rotate 360º around the fluidized bed. The rotation ring is controlled by a stepper motor to allow for different visualization orientations. The facility also features a vertical lift which is located under the imaging region to adjust the vertical location of an object. The lift is controlled by a 910 kg winch to provide 2.75 m of vertical travel. The data are acquired using software developed at Iowa State University. The software allows control of both detectors and provides motion control for the rotation ring.

3.5.2 X-ray Computed Tomography

X-ray computed tomography (CT) scans are captured with and without acoustic intervention at different H/D ratios (0.5, 1, 1.5) and different superficial gas velocities U_g = 1.5 and 3 U_{mf}, where U_{mf} is the minimum fluidization velocity. CT images allow for quantitative analysis of the time-average local gas holdup, and identified the effects that acoustic vibrations have on the hydrodynamic behavior in a fluidized bed.

3.5.2.1 Experimental Procedures

The following procedure is used for each acquired CT scan in this study. Custom X-ray imaging software captures the CT images, controls the camera settings, and controls the rotation ring motion. First, the X-ray source that is located opposite the CT detector is warmed up at the same time the thermoelectric cooler on the camera is simultaneously cooled to 0°C to reduce noise and allow for long CT scans. After completing the warm-up process, the X-ray voltage and current, as well as the camera exposure time and binning options are adjusted. For this study, the power settings are constant at a voltage of 150 keV and a current of 3 mA for glass beads, for

ground walnut shell the voltage is equal to 130 keV and a current of 3 mA, and the exposure time is set to 1 second and the binning is set to 4×4. Next, the fluidized bed is placed in the imaging region and the scintillation crystals in the detector are excited with X-rays for about 20 minutes.

After the CT's are generated the files are transferred to a cluster at CNDE (Center for Nondestructive Evaluation) for reconstruction using standard algorithms (Heindel, 2011). Volume files are reconstructed and analyzed using custom software that allows selecting the region of interest (ROI) in the image and generating 2-D images of different planes. For this study, three viewing axes are selected (Figure 3.6) that include images in the x-y plane at different heights, and images in the x-z plane and y-z plane passing through the center of the bed. These planes are also referred as a z-slice, y-slice, and x-slice, respectively. A false color scale is then applied to each image to provide a better appreciation for the flow structure.

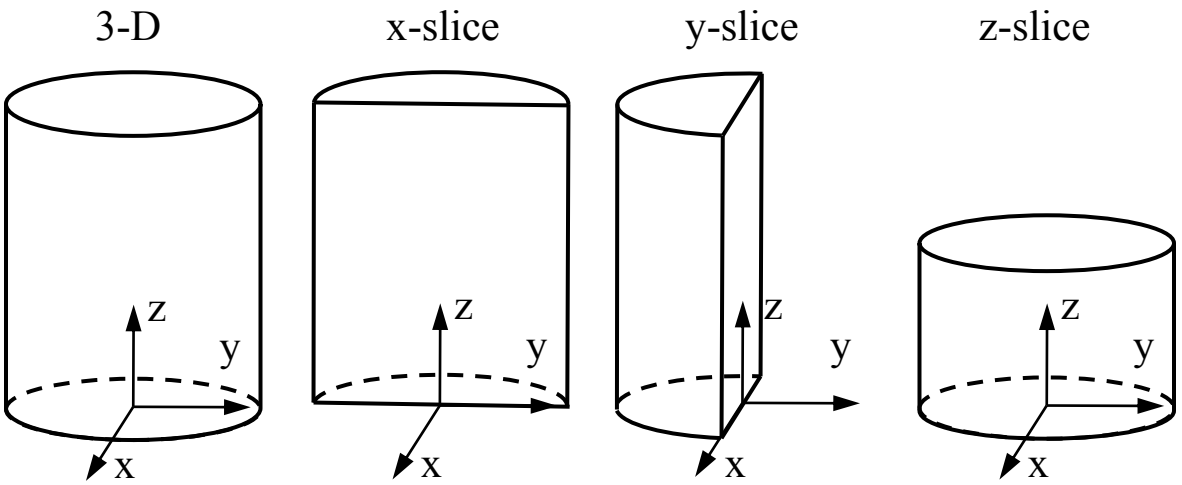

Figure 3.6: CT imaging slices (Escudero, 2010)

3.5.2.2 Determining Gas Holdup from CT Data

Time-average local gas holdup information is calculated using the data obtained from the CT reconstruction volume files. Gas holdup or void fraction, as mentioned in Chapter 2, is the amount of gas present in the solid material, and is useful to characterize the hydrodynamic

behavior of the multiphase flow system. Quantifying the local time-average gas holdup, ε_g, using the XRIP program, which is a software that was developed in the laboratory, requires the CT intensity of the empty reactor (I_g), a CT intensity of the reactor filled with a fixed bed of the bulk material (I_b), and a CT intensity of the reactor under specified fluidization conditions (I_f). To ensure the same response for each condition from the detector system, each CT is taken with the same X-ray source power settings for the respective conditions.

The local time-average gas holdup is then determined from the two reference CT images and the flow CT image using XRIP (Escudero and Heindel, 2011):

$$\varepsilon_g = \frac{I_f - I_b + (I_g - I_f)\varepsilon_{g,b}}{I_g - I_b} \tag{3.4}$$

where the bulk void fraction, $\varepsilon_{g,b}$, is defined as:

$$\varepsilon_{g,b} = 1 - \frac{\rho_b}{\rho_p} \tag{3.5}$$

where ρ_b and ρ_p are the measured bulk and particle densities, respectively. The method used to calculate gas holdup uses a smoothing process of the gas and bulk volume files, then calculates the gas holdup with the intensity values of the gas, bulk and flow files, and finally passes the resulting 3D file through another smoothing process to minimized noise. Further details of the data processing techniques are found elsewhere (Escudero, 2010).

3.6 Jetting identification and quantification

Jetting produced by the aeration plate is an important phenomenon to understand the distribution of particulate matter and fluidizing gas inside a fluidized bed, as well as the heat and mass transfer rates between the materials. Gas holdup images previously obtained using the X-ray computed tomography technique are used to identify and quantify the jets present in the fluidized bed under different operating conditions. This section first describes the method used to

extract and identify the jets that are created by the distributor plate. Then, the method to define individual jets and eliminate noise is described. Finally, the procedure used to calculate jet characteristics such as jet length and expansion angle, is summarized.

3.6.1 Jet identification

Once the X-ray CT images have been obtained and processed, local time average gas holdup information is calculated and volume files for several operational conditions are generated. Using image analysis software, each of the volumetric pixels (voxels) in the gas holdup volume file are analyzed to determine the edge of each jet present inside the fluidized bed. To identify the jets, first, the voxel of interest is determined to be located inside the fluidized bed. Then, the center of the fluidized bed is located in the xy-plane. Once the center is located, the radius of the fluidized bed is determined (for this study the radius of the fluidized bed is equal to 86 voxels). Once the radius is determined, the next step is to ensure that the distance from the center of the bed to the voxel of interest is less than or equal to the radius of the bed.

To identify a jet, the gas holdup in a voxel of interest is compared to the neighboring local average gas holdup values. The local average gas holdup is determined by averaging the neighboring voxel gas holdup found in the same xy-plane and within a specified radius of the voxel of interest, making sure that only voxels that are within the fluidized bed are used in the average. The local average contains only voxels located in a single xy-plane because the vertically changing interface between the jet and the rest of the bed would otherwise skew the average. The average is localized so that sharp differences, such as that between a jet and the rest of the bed, are more clearly defined.

A circular area for the local average value is used because the jets are assumed to be roughly circular, and the bed is circular. The optimal radius for the local average area is approximately

the distance from the center of a jet to the next closest jet. This is done to minimize the effect of the surrounding jets. If surrounding jets are included in the averaging region, a higher value of gas holdup can be obtained, skewing the average producing unfavorable results. Figure 3.7 demonstrates this principle; for this study the optimal radius is 18 voxels. The area inside the black circle is the region included in the average of the gas holdup values.

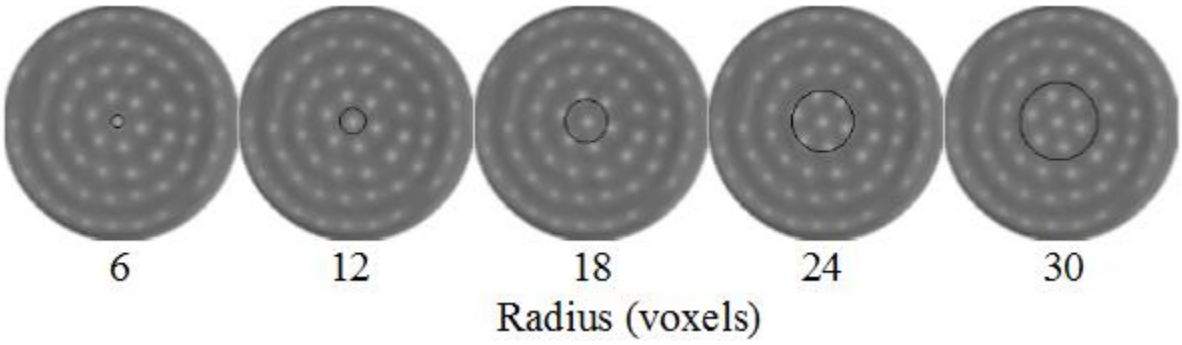

Figure 3.7: Different radius averaging regions for jet identification. The lighter regions indicate a higher gas holdup, indicating a jet location.

Finally, if the gas holdup value in the voxel of interest is a specified threshold (10%) greater than the local average, it is marked as likely being located within a jet. Otherwise, it is left unmarked. Figure 3.8 shows y-slice planes at different thresholds for glass bead volume files. The threshold of 10% is chosen based on the number of voxels marked as a jet. Beyond the 10% threshold, the number of voxels marked as jets decrease, so there is no improvement in the identification of jets after this threshold.

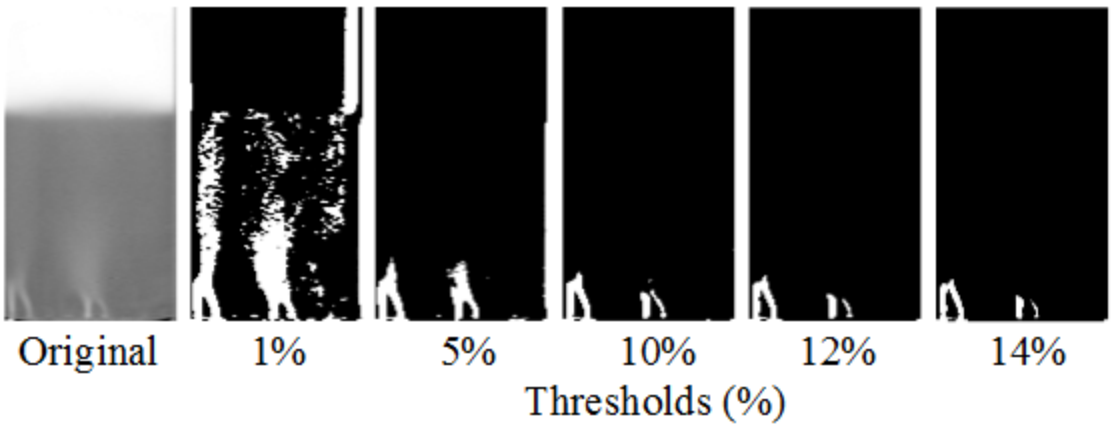

Figure 3.8: Different threshold percentages for glass beads.

3.6.2 Defining individual jets

To define individual jets, the image of the fluidized bed is assumed to be located in a 3D space such that the aeration plate is located at z-slice = 0 and all voxels have positive, integer values for all x, y, and z locations within the bed. The image is analyzed by looking at all the local voxel gas holdup values, compared to the local voxel average, in one xy-plane and then continuing to the next xy-plane.

Each jet is defined in a grouping of voxels that are determined to have a local gas holdup higher than the local average by a given threshold. For each voxel defined to be in a jet, it is first checked to see if the voxel of interest, labeled as (x, y, z), is adjacent to a voxel already found in a jet grouping. If so, the voxel is added to the jet grouping. If not, a new jet group is defined starting with the voxel of interest.

Eventually, jets merge and lose their individual identities but are still strong enough to be considered jets. Therefore, the merged jets are divided so that a more accurate description of the jets can be given. In order to do this, the jets are assumed to have an approximate circular cross-section, and the center of each jet is calculated in each xy-plane. If an area of voxels that are marked as within a jet by the initial analysis is determined to be over the centers of more than

one jet, the marked area is divided such that the voxels closest to each jet center are added to that jet's group.

The initial analysis that defines which voxels are within jets will necessarily have some voxels marked as within jets that are not actually part of a jet. This "noise" is eliminated with filtering in the identification of individual jets. One filter through which the data are passed determines if the group of voxels identified as a jet begins at the aerator plate. If it does not, then the group of pixels is not a jet. If the number of identified jets is still higher than the number of aeration holes in the aeration plate, another filter successively removes the groups with the smallest number of voxels identified until the appropriate number of jets is established. It is assumed that the small number of voxels in the group indicates that the group is not a jet and is simply "noise" from the first analysis.

3.6.3 Determining jet geometric features

In order to have a better appreciation of the effects that acoustics have on the jet structure and hydrodynamic behavior above the distributor plate, a quantitative analysis is important to fully understand the implications of having acoustic vibration in the fluidized bed operation.

There are several quantitative characteristics that define the jet geometry, such as jet length (L_j), jet angle (α), and jet diameter. This study will focus on obtaining values for jet length and jet angle, to compare between the acoustic and no acoustic conditions, and also to compare with correlations available in the literature (Figure 3.9).

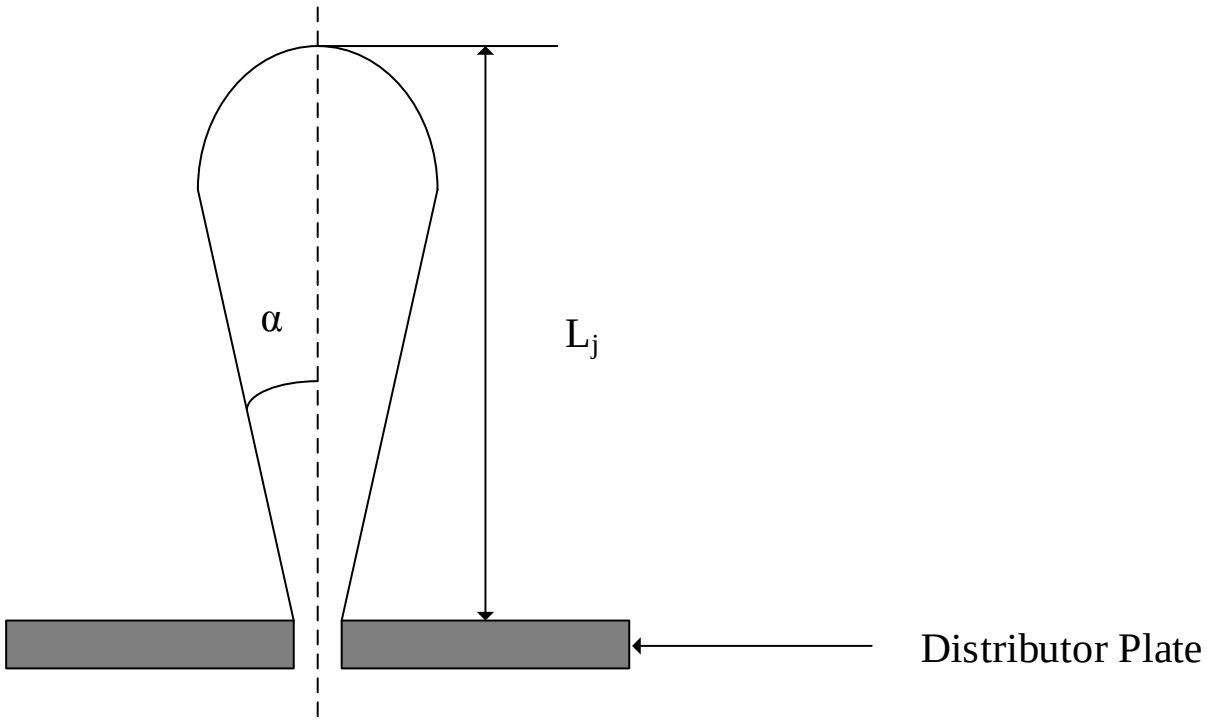

Figure 3.9: Schematic of jet geometric features.

Once the jet identification and definition analysis is performed, the jet length must be identified for each group identified as a jet. In order to do this, the xy-plane in which a jet no longer has any voxels identified as within a jet directly above it is defined as the top of the jet. The number of voxels between the aeration plate and the top of the jet are counted, and the number of voxels is then converted into a physical distance using a conversion factor based on the resolution of the CT images originally obtained using x-rays. This conversion factor amounts to 0.395 mm per voxel.

In order to define a jet expansion angle, the jets are assumed to be approximately conical in shape. Also, the expansion angle is calculated using only voxels located beneath the point at which the jet touches another jet and thereby merges.

The height (L_1) and cross sectional area of the smallest cross section of a jet (A_1) beneath a merged region is recorded as well as the merge height (L_{merge}) and cross sectional area of the largest cross section of a jet (A_2) beneath the merged region. From the areas, the effective radii of the respective cross sectional areas are calculated. Using the distance between the cross sectional areas and their lengths above the aeration plate, the expansion angle (α) (Equation (3.6)) can be calculated via similar triangles (Figure 3.10).

$$\alpha = \tan^{-1}\left(\frac{r_2 - r_1}{L_{merge} - L_1}\right) \tag{3.6}$$

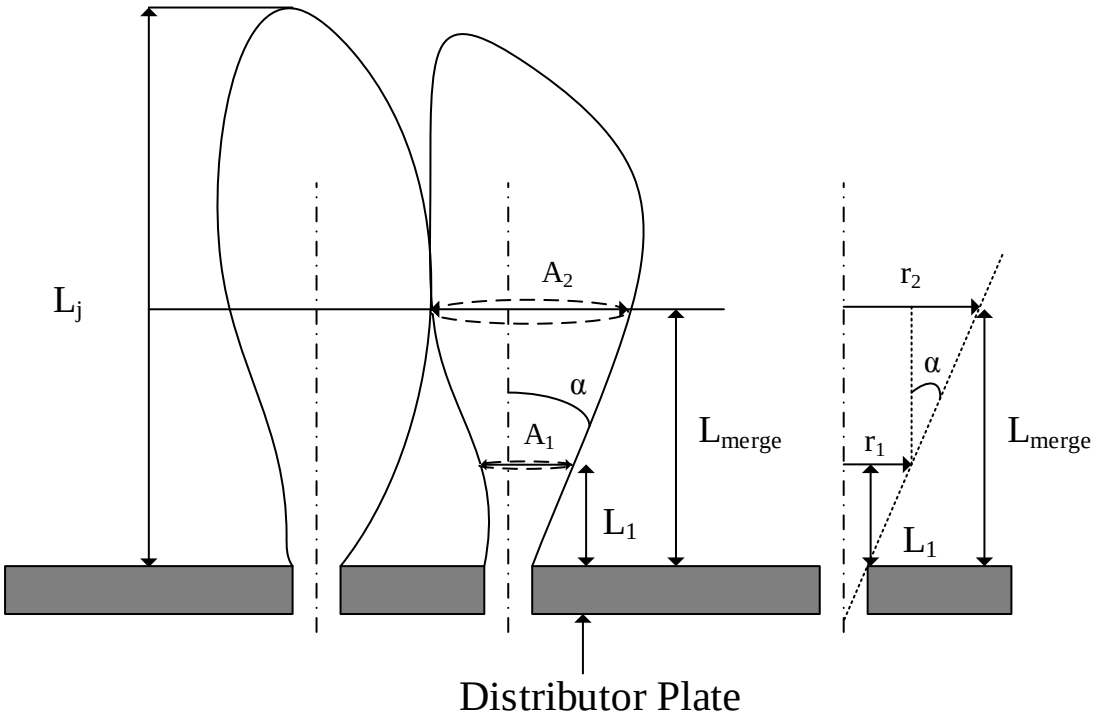

Figure 3.10: Schematic of jet expansion angle calculation.

3.7 Summary

This chapter described the equipment and the experimental procedures used for this research project. The first section described the cold-flow fluidized bed reactor components, the air flow system, the instrumentation, and the acoustic equipment used in this study. The next section

overviewed the procedure used to select and prepared the material for the experiments. Two different Geldart B materials, glass beads and ground walnut shell, allow for comparisons between materials. The process to determine the minimum fluidization velocity at different flow rates and different bed heights with and without acoustic assistance was also explained in this section. Section 3.4 described the experimental and computational methods used to understand the behavior of the acoustic wave inside the fluidized bed.

The XFloViz facility was used to perform the noninvasive analysis of the flow structure behavior in the fluidized bed. The description of the X-ray equipment, as well as the procedure used to take X-ray CT scans was explained in section 3.5. In section 3.6, the procedure to obtain qualitative and quantitative information of the jetting phenomena present in the fluidized bed was explained. The following chapters will discuss all the results obtained for this study; most of the results will be presented as how they were published in or submitted to, peer reviewed journals.

CHAPTER 4: MINIMUM FLUIDIZATION VELOCITY IN A 3D FLUIDIZED BED MODIFIED WITH AN ACOUSTIC FIELD[1]

David Escudero[2] and Theodore J. Heindel

Department of Mechanical Engineering, Iowa State University
Ames, Iowa, 50011, USA
drescude@iastate.edu, theindel@iastate.edu

Abstract

Fluidized beds are used in a variety of process industries because they provide uniform temperature distributions, low pressure drops, and high heat/mass transfer rates. Minimum fluidization velocity is an important factor in understanding the hydrodynamic behavior of fluidized beds, and this characteristic may be modified through high frequency (sound) vibrations. The effects caused by sound wave frequency and sound pressure level on the minimum fluidization velocity in a 3D fluidized bed are investigated in this study. Experiments are carried out in a 10.2 cm ID cold flow fluidized bed filled with either glass beads or ground walnut shell, and particle sizes ranged between 212-600 μm. In this study, four different bed height-to-diameter ratios are examined: H/D = 0.5, 1, 1.5, and 2. Moreover, the sound frequency of the loudspeaker used as the acoustic source ranged between 50-200 Hz, and the sound pressure level ranged 90-120 dB. Results show that the minimum fluidization velocity is influenced by the frequency change. As the frequency increases, the minimum fluidization velocity decreases until a specific frequency is reached, beyond which the minimum fluidization

[1] Originally published as: Escudero, D. and Heindel, T. J. (2013). "Minimum fluidization velocity in a 3D fluidized bed modified with an acoustic field." *Chemical Engineering Journal*. **231**(0): 68-75.
[2] Corresponding author: David Escudero G. (davidrescudero@gmail.com)

velocity increases. With increasing sound pressure level, the minimum fluidization velocity decreases because the additional vibration forces imparted to the bed particles helps to loosen the bed, reducing the interparticle forces, which reduces the required energy for particle fluidization. Thus, acoustic fields provide an improvement in the ease of fluidization of these particles.

Keywords: Acoustic field, bed height, fluidized bed, minimum fluidization velocity

4.1 Introduction

Characterizing the hydrodynamic behavior of a fluidized bed is very complex and must be understood better in order to improve fluidized bed operations. Minimum fluidization velocity is one of the most important parameters when characterizing the hydrodynamics in a fluidized bed (Ramos Caicedo et al., 2002). The minimum fluidization velocity (U_{mf}) is the superficial gas velocity at which solid particles are just suspended in the fluidizing medium. The minimum fluidization velocity depends on the material properties, bed geometry, and fluid properties. Sau et al. (Sau et al., 2007) determined the minimum fluidization velocity for a gas-solid system in a tapered fluidized bed for different Geldart Type B particles and studied the effects that bed geometry, specifically the tapered angle, had on the minimum fluidization velocity. Results showed U_{mf} changed when the geometry of the bed changed.

Moreover, Hilal et al. (Hilal et al., 2001) analyzed the effects of bed diameter, gas distributor, and inserts on minimum fluidization velocity for particles of different diameter and density. It was shown that both the bed diameter and the type and geometry of the distributor affected U_{mf}. For example, U_{mf} increased with an increase in the number of holes in the distributor plate. Furthermore, with an increase in the bed diameter, there was a decrease in U_{mf}. Finally, the

insertion of tubes along the fluidized bed reduced the effective cross-sectional area for fluidization, which produced a higher interstitial gas velocity causing a decrease in U_{mf}.

The influence of bed height on minimum fluidization velocity has been studied using different types of fluidized beds. Zhong et al. (Zhong et al., 2006) completed minimum fluidization experiments in spouted fluidized beds. In a spouted fluidized bed, the bed chamber is tapered like a funnel, which creates different hydrodynamics, and the fluidization air is typically injected through a single orifice. Filling the bed with different materials (Geldart type D) to different heights (300-550 mm), they determined that the minimum spouting fluidization velocity, which is analogous to the minimum fluidization velocity in a bubbling fluidized bed, was influenced by the change in bed height; increasing the bed height increased the spouting velocity.

Sau et al. (Sau et al., 2007) used a gas-solid conical tapered fluidized bed to find the minimum fluidization velocity and the pressure drop across the bed. They concluded that bed height for this type of bed did not have a significant effect on the minimum fluidization velocity, i.e., U_{mf} was independent of bed height for this type of conical tapered fluidized bed.

Ramos Caicedo et al. (Ramos Caicedo et al., 2002) studied the minimum fluidization velocity for gas-solid 2D fluidized beds for Geldart type B glass beads. Their results revealed that as the static bed height increased, U_{mf} increased.

Gunn and Hilal (Gunn and Hilal, 1997) and Cranfield and Geldart (Cranfield and Geldart, 1974) studied gas-solid 3D fluidized beds using glass beads (Geldart type B particle) as the bed material and four different bed heights. The results for minimum fluidization velocity in both studies showed that for all the material and experimental conditions used, there was no significant change in the minimum fluidization velocity when the bed height was increased.

Therefore, U_{mf} was independent of bed height. Similar results showing independence between minimum fluidization velocity and bed height were concluded by Escudero and Heindel (Escudero and Heindel, 2011) using different Geldart type B particles (glass beads, ground walnut shell, and ground corncob) in the size range of 500-600 μm.

Mechanical vibrations are being used to ease fluidization in materials that present poor fluidization quality. Zhang et al. (Zhang et al., 2012) studied the fluidization characteristics of fly ash in a fluidized bed subjected to mechanical vibrations. They found that the minimum fluidization velocity decreased due to the vibrations, implying that fly ash can be fluidized at a lower superficial gas velocity. Marring et al. (Marring et al., 1994) studied the effect of vibration on the fluidization behavior of glass beads and potato starch. Using Geldart type A particles, they found that increasing the frequency and the amplitude of the vibrations decreased the minimum fluidization velocity and the bed voidage. Moreover, for a more cohesive powder like potato starch, which presents a poor fluidization quality without vibration, the use of vibration allowed the bed to fluidize well even with different levels of cohesiveness, thus showing vibration improved the fluidization of cohesive powders.

Barletta et al. (Barletta et al., 2008) also studied the effects of mechanical vibration on the fluidization of a fine aeratable FCC powder. Changing the parameters of peak acceleration and frequency, they determined the effects on bed expansion, voidage, and fluidization. They found that the degree of static (no air flow) bed packing reached by the vibrated bed was always higher than that reached without vibration. Also, the pressure drop in the fully fluidized bed may be equal to or smaller than (sometimes significantly) those obtained without vibration. The bed started to expand when the gas pressure drop was consistently smaller than what was necessary for fluidization. The largest bed expansion of the vibrated bed was always smaller than that

attained without vibration. If the discrepancies between vibrated and not vibrated fluidization was assumed as a measure of the significance of the effect of vibration, these were generally larger at low frequencies and tended to become less important at high frequencies; these effects were also apparent under full fluidization conditions. More recent studies were performed by Barletta and Poletto (Barletta and Poletto, 2012) and Barletta et al. (Barletta et al., 2013) to analyze the effects of mechanical vibrations on the dynamic response of fine and cohesive powders.

Sound-assisted fluidized beds have been studied for different Geldart type particles (Geldart type A-C) to understand the effects produced by the acoustic field on the fluidization behavior and quality (Roy et al., 1990, Herrera and Levy, 2001, Herrera et al., 2002). This is an attractive option because it is a noninvasive technique that could influence the bed hydrodynamic structure without affecting the properties of the bed material.

Leu et al. (Leu et al., 1997) studied the fluidization of Geldart type B particles in an acoustic fluidized bed. They determined the influence of the speaker power, sound frequency, particle loading, and distance between the speaker and bed surface on the hydrodynamic properties of a fluidized bed filled with 194 μm sand. They found that when an acoustic field was applied, a different particle loading height created a different minimum fluidization velocity, making minimum fluidization velocity dependent on bed height. Guo et al. (Guo et al., 2006) investigated the behavior of ultrafine (Geldart type C) particles under the influence of sound waves. They studied both nanometer and micrometer size particles. They found that as frequency increased, the minimum fluidization velocity decreased and then after a specified frequency (40-50 Hz), the minimum fluidization velocity increased. When the sound pressure level was changed (100 dB - 103.4 dB) and the sound frequency fixed, the minimum fluidization velocity

decreased for all particles, thus improving the fluidization quality of the particles. The same trends were found by Kaliyaperumal et al. (Kaliyaperumal et al., 2011) and Levy et al. (Levy et al., 1997).

Moreover, Guo et al. (Guo et al., 2011) analyzed the effects of the acoustic field on a fluidized bed at different temperatures for quartz sand (74 μm, 2650 kg/m^3) and SiO_2 particles (0.5 μm, 2560 kg/m^3). The results obtained in that study showed that minimum fluidization velocity decreased with increasing temperature with, as well as without, acoustic assistance. In the same way, at a fixed sound pressure level (120 dB), the minimum fluidization velocity decreased when the frequency was increased from 50-200 Hz, and then the minimum fluidization velocity increased with frequency from 200-400 Hz.

Si and Guo (Si and Guo, 2008) studied how an acoustic fluidized bed improved the fluidization of two different biomass particles, sawdust and wheat stalks, alone or mixed with quartz sand. They compared the fluidization behavior of the biomass without and with the acoustic field to determine if there was any improvement due to the acoustic field. They also determined the influence of sound pressure level (SPL) on the minimum fluidization velocity. Initially, they found that the biomass by itself fluidized poorly with and without the presence of the acoustic field. They then added quartz sand to aid fluidization and maintained the biomass mass fraction at 60%. They observed that below a SPL of 90 dB, plugging and channeling occurred in the fluidized bed. Increasing the SPL diminished the effects of channeling and improved the fluidization quality. By varying the sound frequency between 50 to 400 Hz, they determined that the minimum fluidization velocity decreased with increasing frequency until it reached a minimum value and then increased with increasing frequency.

Si and Guo (Si and Guo, 2008) also fixed the sound frequency at 150 Hz and varied the sound pressure level between 90 and 120 dB. Using these conditions, they determined the effects on the minimum fluidization velocity. They found that when the sound pressure level was above 100 dB, the fluidization quality improved, and they observed that the biomass mixture fluidized smoothly without any obvious slugging or channeling.

The goal of this paper is to determine the effects caused by an acoustic field on the minimum fluidization velocity of Geldart type B particles in a 3D cylindrical fluidized bed filled to different bed heights.

4.2 Experimental Setup

The reactor used in these experiments is a cold flow fluidized bed reactor. The cylindrical fluidized bed was fabricated with 10.2 cm internal diameter (ID) acrylic with a 0.64 cm wall thickness. As shown in Figure 1, the reactor consists of three main chambers: the top chamber or freeboard region, the bed chamber, and the plenum. Fluidization occurs in the bed chamber which is 30.5 cm tall and 10.2 cm ID. Square flanges (16.5×16.5 cm) connect each section. An aeration plate is located immediately below the bed chamber; it is fabricated from a 1.27 cm thick acrylic plate with 62, 1 mm diameter holes spaced approximately 1.27 cm apart in a circular grid for a total open area of 0.62%.

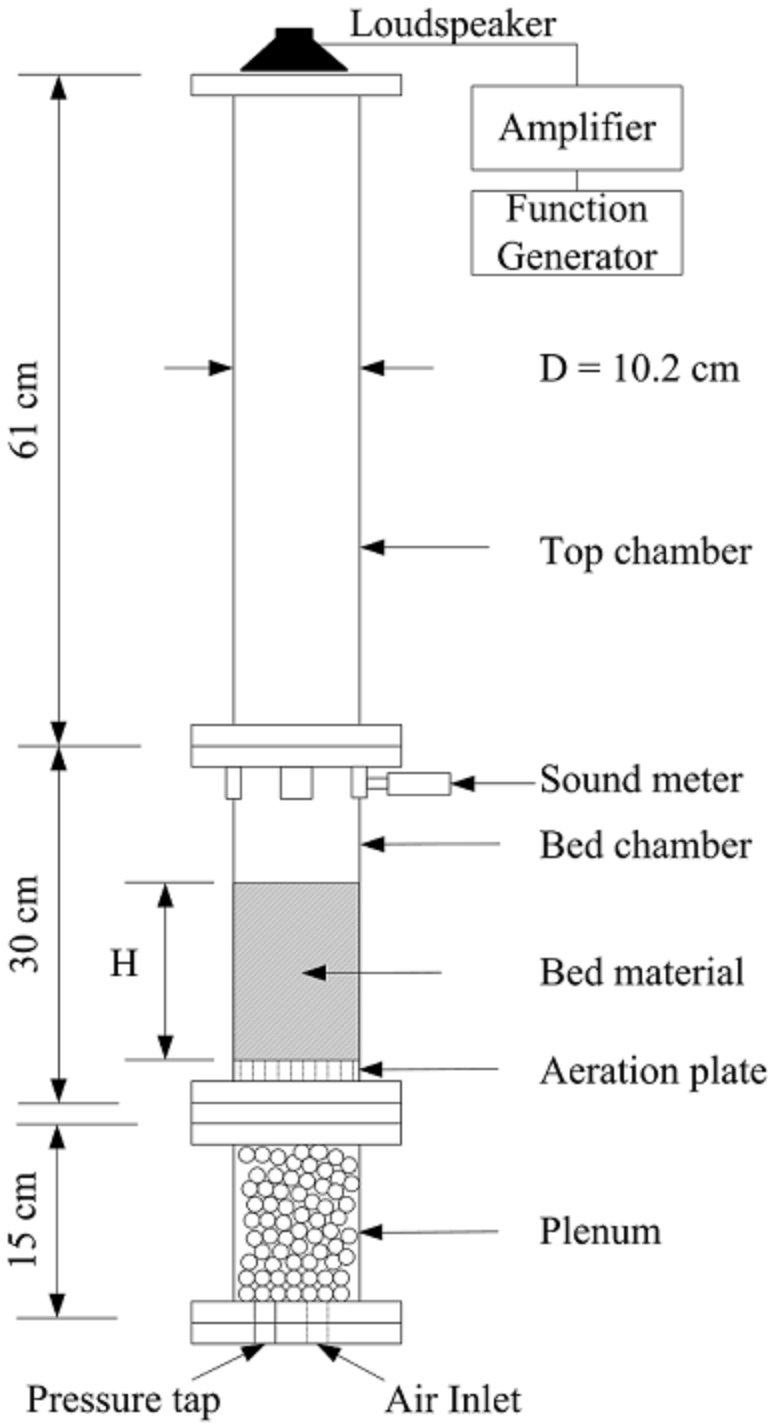

Figure 4.1: Fluidized bed reactor (not to scale). The static bed height is identified by H.

Filtered compressed air from the building supply is used as the fluidizing gas. The pressure at which the compressed air is delivered inside the laboratory is 620 kPa (90 psi). However, since

the flow rates used for fluidization vary depending of the specific conditions of each experiment, an air flow control board with four independent air lines is used to deliver the required air to the fluidized bed.

The fluidized bed air flow is regulated via a stainless steel pressure regulator and attached filter, with a pressure range of 0-862 kPa (0-125 psi) and maximum inlet pressure of 2.07 MPa (300 psi). A stepper motor valve (Aalborg SMV40-SVF2-A) is used to automatically decrease the air flow rate during the minimum fluidization velocity tests, which are described in detail below. The regulated air flows through a 0-1000 Lpm stainless steel Aalborg GFM771 flow meter.

Pressure is measured with a Dwyer 0-34.5 kPa (0-5 psig), 4-20 mA output pressure transducer located in the bottom of the plenum. The signals obtained from the pressure transducer and mass flow meter are connected to a computer controlled data acquisition system. Average measurements were necessary due to the highly variable pressure signal caused by the bubbling fluidized bed. In this study, data collection occurred at a rate of 1000 Hz for a time interval of 5 seconds; average pressure and average fluidization gas flow rate were subsequently written to a data file.

The fluidizing materials used in this study are glass beads (ρ_{glass} = 2500 kg/m^3) and ground walnut shell ($\rho_{walnut\ shell}$ = 1440 kg/m^3) over three different size ranges (212-425 µm, 425-500 µm, and 500-600 µm). To prepare the materials for the fluidization experiments, they are initially sieved to the different size ranges using a series of sieves and a mechanical shaker. This process is repeated several times to ensure that the selected particles are located within the desired size range. The bed bulk density was determined knowing the material mass and the static bed volume. Bed material was slowly added until the desired static bed height was reached, which

corresponded to H/D = 0.5, 1, 1.5, and 2, where H is the static bed height and D is the bed diameter. Before the bed height was measured, the bed was fluidized and then allowed to collapse to avoid any packing effects due to the filling process. The material mass was then measured and the given bed bulk density was calculated. Table 4.1 summarizes the general bed characteristics. Bed height had a small, if any, effect on bulk density. There is no effect of particle diameter because the overall particle size range (212-600 um) is still relatively narrow. Note that all bulk densities are based on measured bed mass and bed height.

Table 4.1: Bed material properties.

	Glass Beads		**Walnut Shell**	
H/D	**Bed Mass (g)**	**Bulk density (kg/m^3)**	**Bed Mass (g)**	**Bulk density (kg/m^3)**
0.5	620	1505	250	610
1	1240	1505	500	610
1.5	1860	1505	750	610
2	2570	1530	1100	670
Diameter (µm)	212-425, 425-500, 500-600		212-425, 425-500, 500-600	
Particle Density (kg/m^3)	2500		1440	

To avoid electrostatic effects that may build up during fluidization, the fluidization air is passed through a humidifier before entering the fluidized bed inlet. Several trials in the laboratory have shown that using this simple solution minimized electrostatic effects.

The minimum fluidization velocity is defined as the minimum superficial gas velocity where particle fluidization is achieved. Minimum fluidization velocity is determined using the following pressure measurement procedure. First, the reactor is filled with the desired material to a specified height. Air at U_g = 40.8 cm/s is passed through the bed for about an hour to condition the system. After the conditioning period, the pressure and flow rate are acquired using the DAQ system. Data are collected at 1000 Hz over a 5 second interval, averaged over this period, and then output to an Excel file. Next, the air flow rate is decreased by 1 cm/s by automatically

closing the stepper motor valve. Then, when the flow rate mean, the pressure mean, and the pressure standard deviation are between specific thresholds, the DAQ system again records the pressure and flow rate and averages them over a 5 second interval. This process is repeated until the flow rate reaches approximately $U_g = 0$ cm/s; at this point the test is completed. For statistical purposes, each test for every specified condition is repeated 10 times.

Minimum fluidization tests were carried out at a reference state without sound but with a measured average background noise sound pressure level of 60 dB (i.e., the average background noise in the lab), and with sound emitted from a Peerless 7.62 cm ID full range woofer located at the top of the bed. Sine waves at different frequencies (50-200 Hz) are generated by a function generator and passed through an amplifier (Audio Source AMP100); three different sound pressure levels, which are a logarithmic measure of the effective sound pressure relative to a reference value, are tested, 90, 110, and 120 dB, and these values are measured by a sound pressure meter located at the top of the bed chamber, at a distance of 61 cm from the acoustic source (see Fig. 4.1).

After all the bed material data are collected, the same procedure is repeated in an empty reactor. This is done to quantify the pressure drop through the aeration plate and plenum. The empty reactor pressure data are then subtracted from the fluidized bed data at the respective superficial gas velocities. Since the flow rates between the empty reactor and fluidized bed tests do not match exactly, a linear interpolation method is employed to calculate the empty bed pressures corresponding to the fluidized bed flow rates. Finally, the bed pressure drop is plotted as a function of superficial gas velocity and the minimum fluidization velocity is defined as the point in which the pressure drop across the bed remains constant. To determine the value of the minimum fluidization velocity, a point located around the knee of the plot (Figure 4.2) is

identified as a reference point; then two linear trend lines are plotted using the reference point and 10 data points above and 10 data points below the reference point. The minimum fluidization velocity is then identified as the point where the two trend lines intersect. Figure 4.2 shows a sample plot obtained for glass beads where the static bed height corresponds to H/D = 1 without any acoustic field influence.

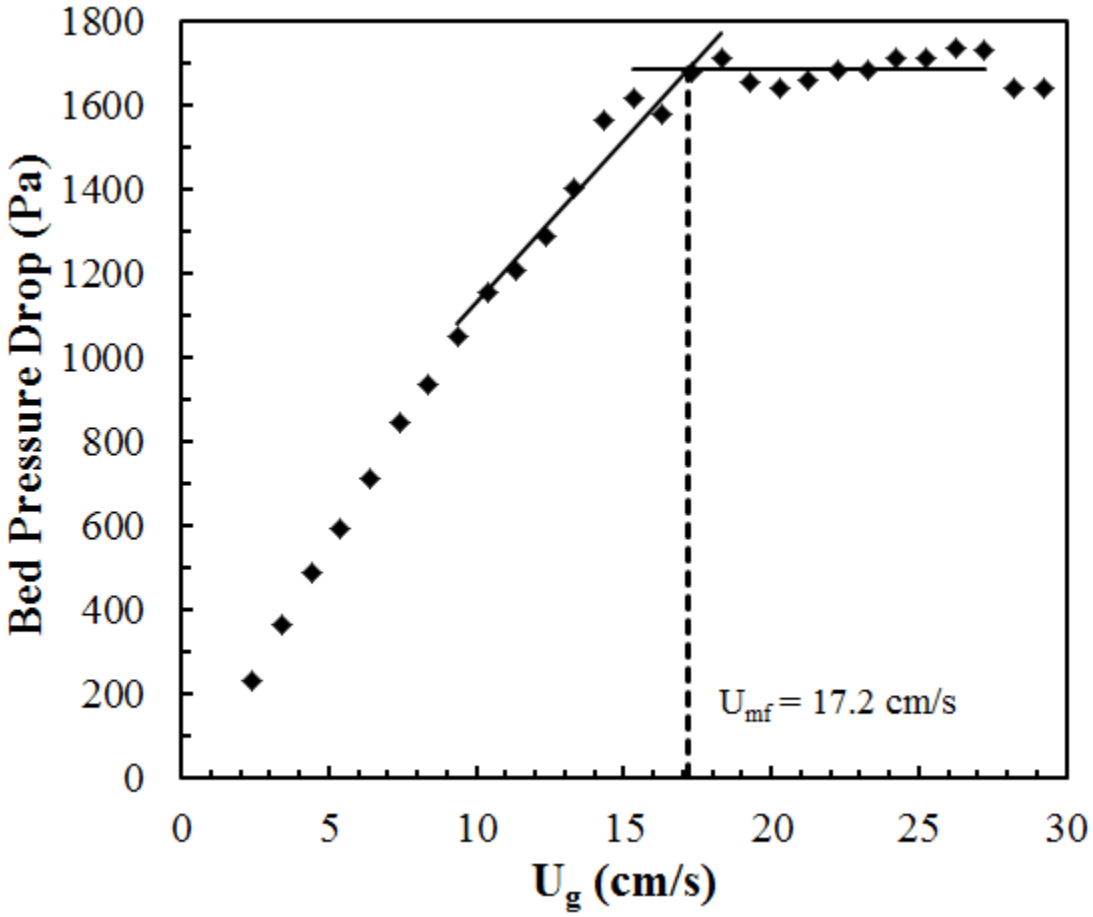

Figure 4.2: Sample minimum fluidization plot for glass beads with H/D = 1 (no acoustic field was applied).

4.3 Results and Discussion

4.3.1 Effect of Frequency on the Minimum Fluidization Velocity

Figure 4.3 shows the bed pressure drop as a function of superficial gas velocity for 500-600 μm glass beads at H/D = 0.5. Bed pressure drop increases as frequency increases, until it reaches

a certain frequency, specifically 150 Hz, after this frequency, the bed pressure drop decreases with a further increase in frequency. Note that the "no acoustic" case in all figures corresponds to the conditions when the loudspeaker was off, but an average background noise level of 60 dB was recorded.

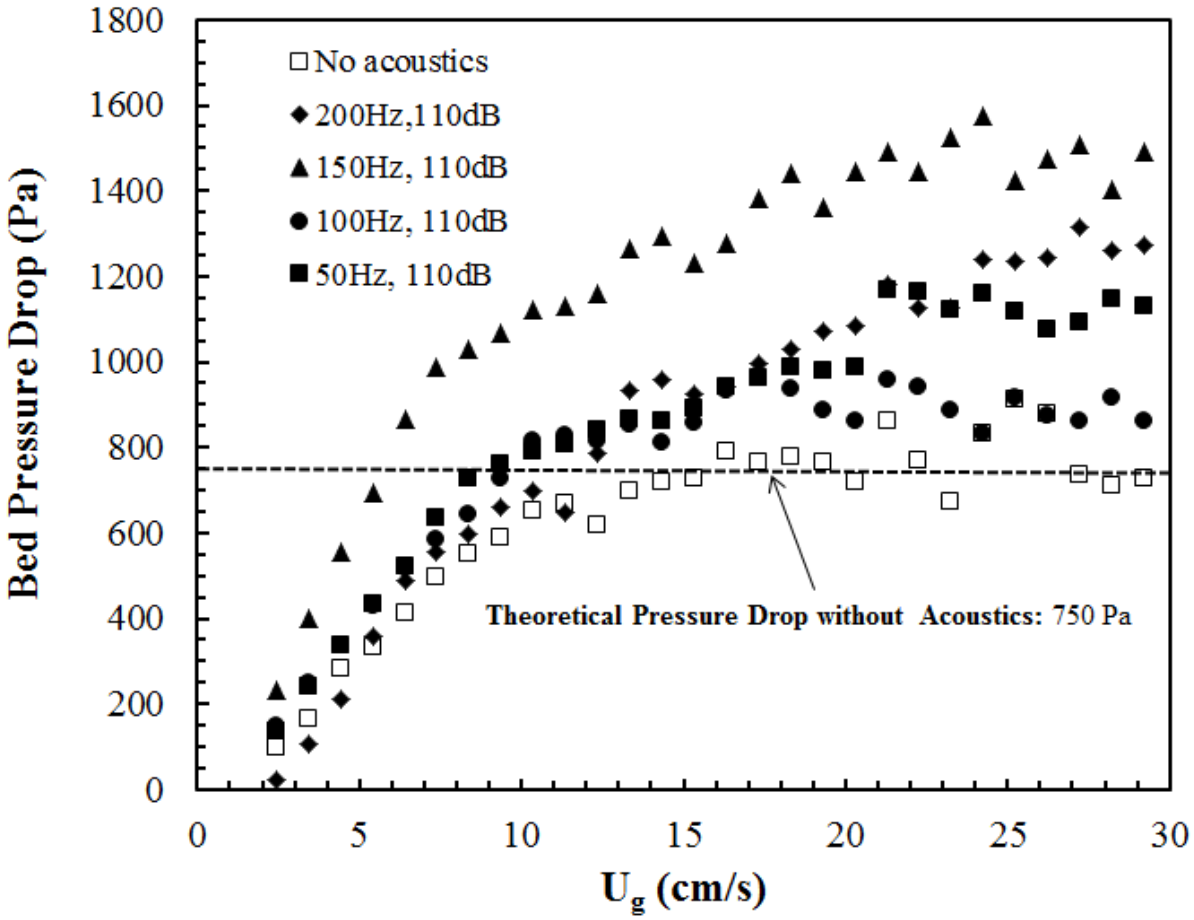

Figure 4.3: Bed pressure drop as a function of superficial gas velocity for 500-600 µm glass beads at H/D = 0.5.

Minimum fluidization velocity, on the other hand, showed a significant change when frequency increased. As shown in Figure 4.4, for glass beads the minimum fluidization decreased until it reached 150 Hz, where a minimum value is attained, after this frequency the minimum fluidization velocity increased again. This phenomenon is repeated for each size range tested,

which indicates that the effect of frequency is independent of material size over the range 212-600 μm. Furthermore, 25 Hz intervals between 0-200 Hz were tested for 500-600 μm glass beads with H/D = 0.5, and it was concluded that the minimum fluidization velocity followed the trends observed for data taken at 50 Hz intervals (Figure 4.4). Moreover, for walnut shell (Figure 4) the frequency that provides the minimum value of U_{mf} in the range of frequencies tested is 200 Hz, the different frequencies for the different materials can be attributed to the natural frequencies of the respective gas-solid systems, which is define as the natural or resonant frequency of the bed oscillation. This natural frequency is a function of density (both gas and solid), as well as bed height (Kaliyaperumal et al., 2011) (Roy et al., 1990). For example, according to the correlation of Roy et al. (Roy et al., 1990), glass beads at a H/D = 0.5 have a natural frequency of 64 Hz, while ground walnut shell particles at a H/D = 0.5 have a natural frequency 83 Hz. Also, the different trends observed between materials can be attributed to the different geometric characteristics of the materials, were glass beads are more spherical and walnut shell particles are more "chunk-like". Different fluidization behavior is also observed between glass beads and walnut shell. Walnut shell has a higher propensity to form channels, which is less likely to occur in glass beads; this chanelling results in the different observed trends between glass beads and walnut shell. Finally, the minimum fluidization velocity values presented in Figure 4.4 are the average of 10 tests for each size range, and the error bars shown in Figure 4.4 represent one standard deviation of the average values. The value of the standard deviation for each of the size ranges varies between 0.2-0.23 cm/s for glass beads, and 0.1-0.12 cm/s for walnut shell, which represents approximately ± 1-2% of the measured U_{mf}. Thus, Figure 4.4 clearly shows that there is a change in the minimum fluidization velocity due to a change in the acoustic frequency. Similar trends were observed for the different H/D ratios tested.

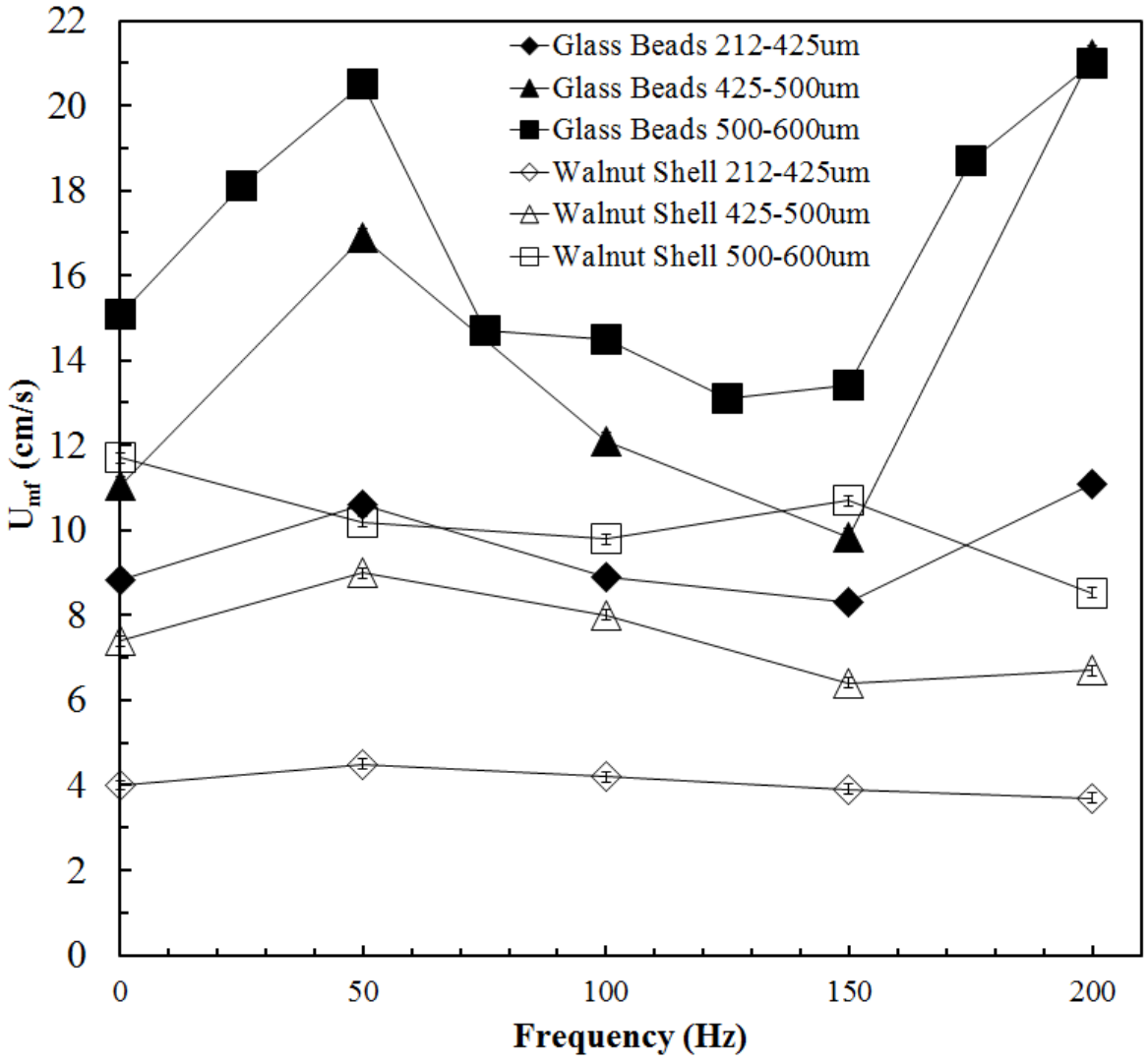

Figure 4.4: Minimum fluidization velocity as a function of frequency for glass beads and walnut shell at H/D = 0.5 and SPL = 110 dB.

Similar results were also found by Guo et al. (Guo et al., 2006) and Russo et al. (Russo et al., 1995). Both studies revealed the same trends shown in Figure 4.4, a reduction in the U_{mf} value until a certain frequency, and then an increase in U_{mf}. The difference between the results found in the literature and those of this study is the frequency value at which a minimum U_{mf} is observed, this difference between frequencies is hypothesized to be due to the natural frequencies of the respective gas-solid fluidized beds, which are a function of the density of the material and the

bed height.

The fluidization index is defined as the bed pressure drop divided by the hydrostatic pressure created by the weight of the bed. Figures 4.5 and 4.6 show the fluidization index as a function of the superficial gas velocity for different sizes of glass beads and different H/D ratios. The sharp "knee" in each plot correlates to U_{mf} and these plots offer a clear picture of the effect of frequency on the minimum fluidization velocity. As frequency increases, less superficial gas velocity is needed to achieve material fluidization.

The fluidization index for all the acoustic cases is greater than the no acoustic cases. It is hypothesized that an acoustic fluidized bed creates a network of vibrating particles, acting like a structural porous media in which a higher pressure drop is maintained while allowing gas to diffuse through it. Hence, the fluidization index in an acoustic fluidized bed is always higher than the no acoustic case. Moreover, at high superficial gas velocities the fluidization index is not constant and may even decrease. This behavior is attributed to the fact that at high velocities, instabilities in the jets that are formed at the aeration plate create voids that, as they rise, coalesce forming large fast-rising bubbles, in which large amounts of interstitial gas and small amounts of bed material are present, producing a decrease in the pressure drop of the fluidized bed. Hence, a decrease in the fluidization index is observed.

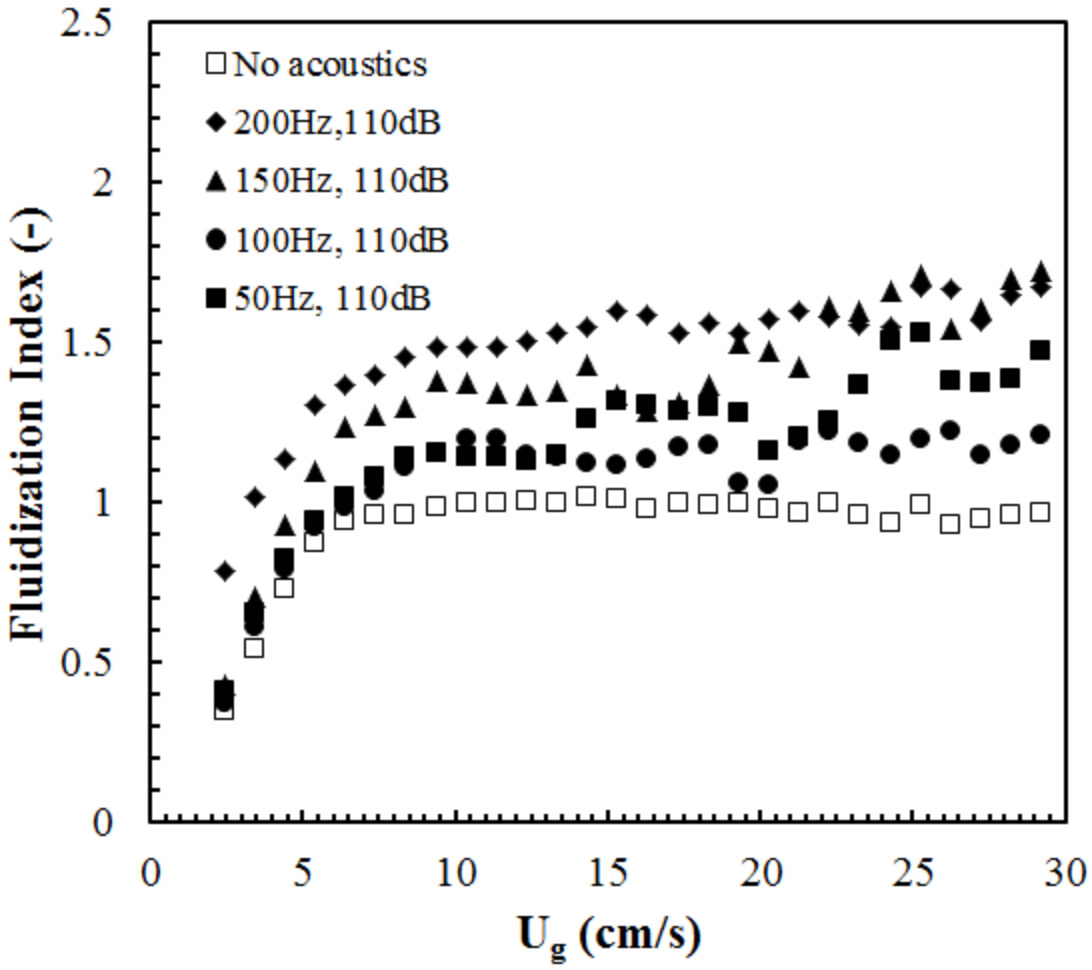

Figure 4.5: Fluidization index as a function of superficial gas velocity for glass beads 212-425 μm at H/D = 0.5.

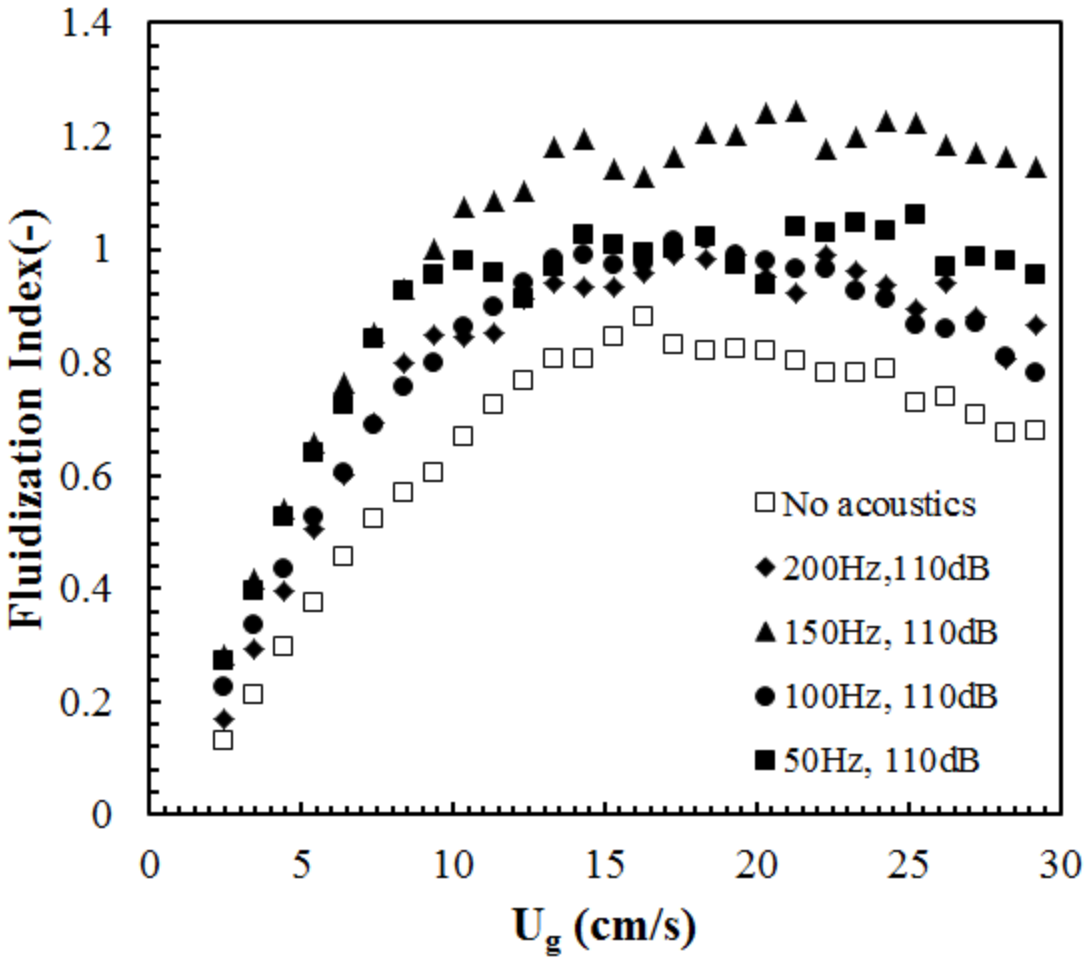

Figure 4.6: Fluidization index as a function of superficial gas velocity for glass beads 500-600 µm at H/D = 1.

4.3.2 Effect of Sound Pressure Level (SPL) on the Minimum Fluidization Velocity

Once the optimal frequency for the minimum value of the minimum fluidization velocity was found for each of the tested materials at each of the H/D ratios, the sound pressure level (SPL) was varied at a fixed frequency to assess its effect on U_{mf}. Figure 4.7 shows that when the frequency is maintain constant at 150 Hz, the minimum fluidization velocity decreased as the SPL increased for all of the glass beads particle sizes tested, corroborating again that the acoustic field effects are observed for all particle size ranges in this study. The increase in the acoustic energy enhances the external forces (drag and inertial forces) acting on the particles; this

additional energy provides a net force that is higher than the interparticle frictional force between the particles and counterbalances the gravity force to achieve fluidization at lower U_{mf} values.

Similar trends are seen for walnut shell (Figure 4.8). The increase in SPL in walnut shell beds produced a decrease in the minimum fluidization velocity. However, for walnut shell particle size has a dependence on the optimal frequency that gives the minimum value of U_{mf}, which is the reason why for 425-500 um particle size, the frequency is different than from the other particles size ranges tested.

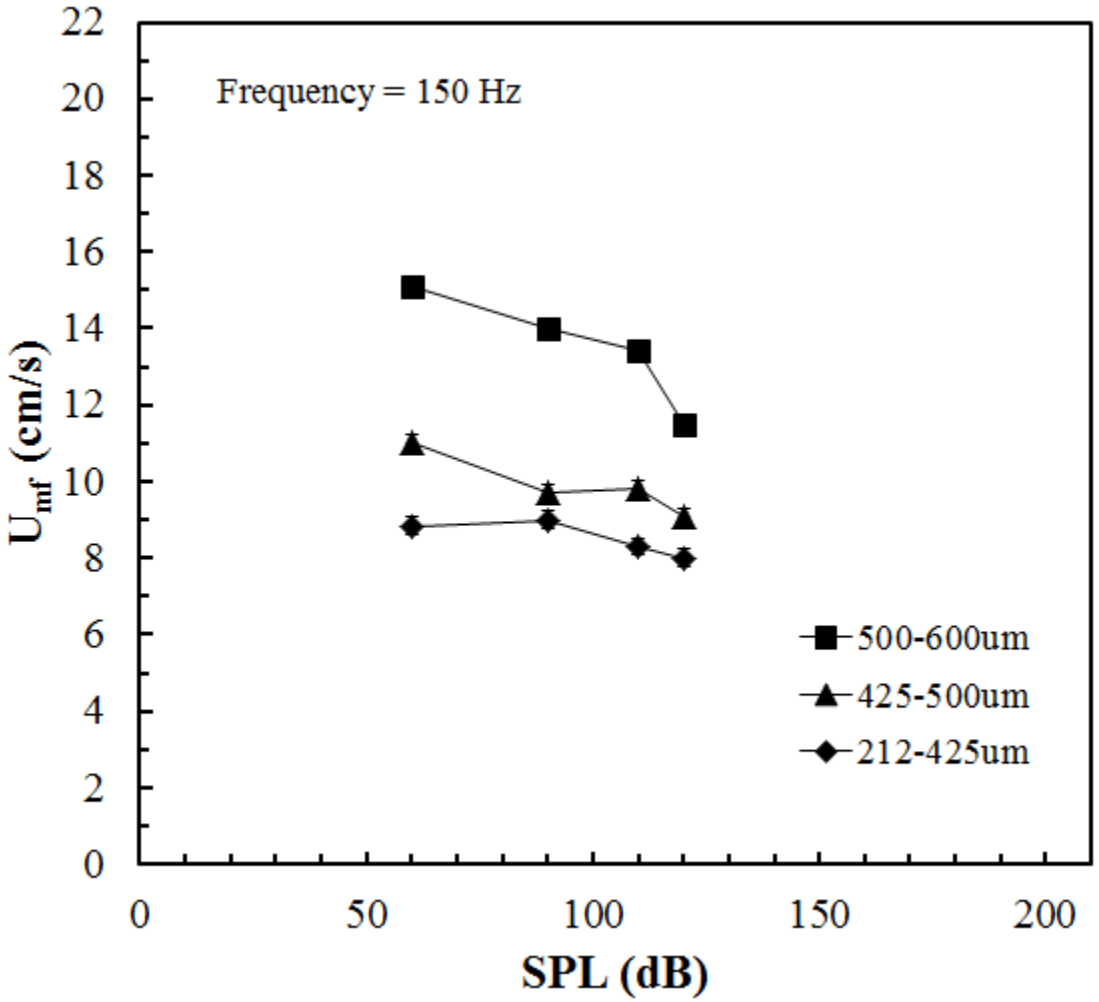

Figure 4.7: Minimum fluidization velocity as a function of sound pressure level (SPL) for glass beads at H/D = 0.5.

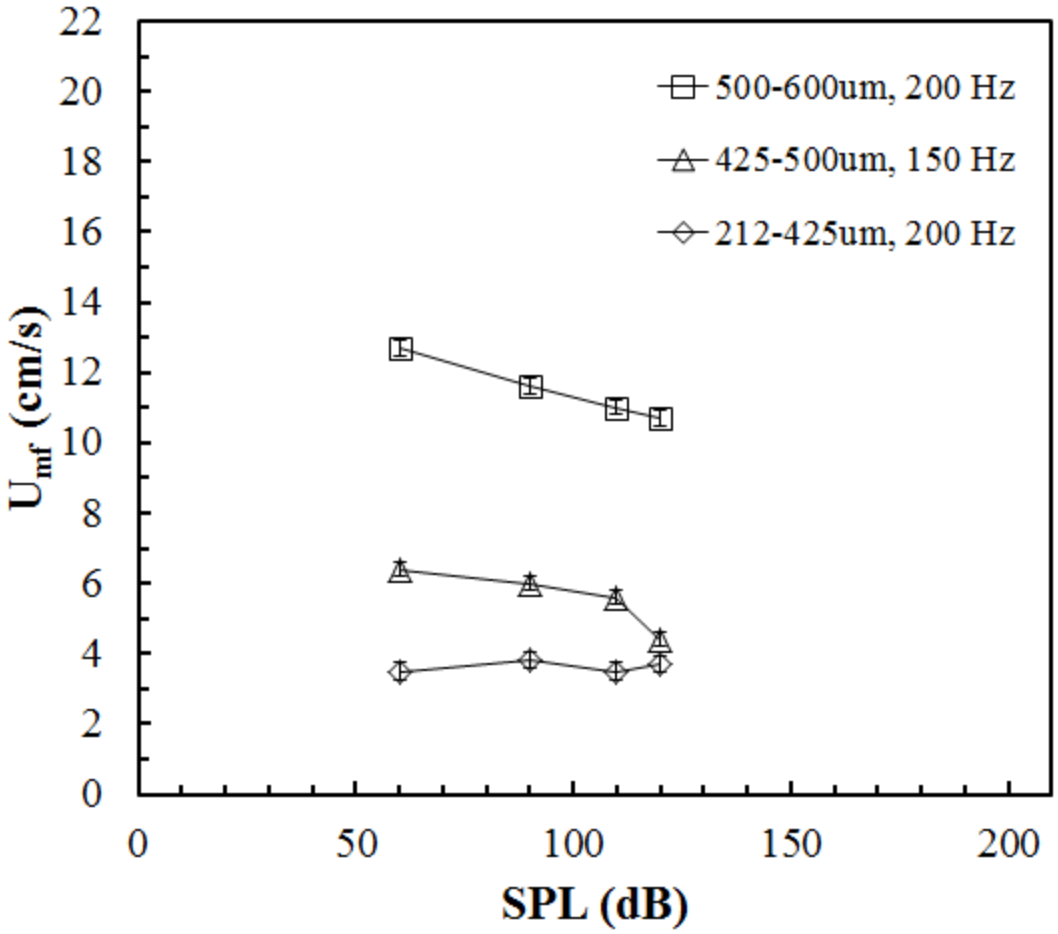

Figure 4.8: Minimum fluidization velocity as a function of sound pressure level (SPL) for walnut shell at H/D = 1.5.

4.3.3 Effect of Bed Height on the Minimum Fluidization Velocity.

As was stated in the introduction, several studies in the literature have concluded that minimum fluidization velocity for a particular material is independent of bed height. However, when an acoustic field was applied to the fluidized bed in this study, bed height was shown to influence U_{mf}.

Figure 4.9 shows the minimum fluidization velocity as a function of bed height for a bed of 500-600 µm glass beads at different frequencies. As Figure 4.9 shows, the minimum fluidization velocity exhibits a change as the H/D ratio changes when acoustics are applied but only a small

change, if at all, with no added acoustics. This phenomenon is observed for each of the frequency conditions tested. For 50 Hz and 200 Hz, the change in U_{mf} is more drastic between H/D ratios, meanwhile between 100-150 Hz, there is a change but it is not as severe as the one observed for the other frequencies. This shows again that the optimal frequency in which the bed achieves a better and more homogeneous fluidization is located between these frequency ranges. This phenomenon was also observed for ground walnut shell in Figure 4.10, however for ground walnut shell the severe changes on the minimum fluidization velocity are presented in the 50 Hz and 100 Hz frequencies, while in the 150 Hz and 200 Hz the changes are not as large. Also, it is important to notice that Figure 4.9 and Figure 4.10 exhibit opposite trends, while glass beads present a decline in the minimum fluidization velocity as the H/D ratio increases, ground walnut shell shows an increase in the minimum fluidization velocity as the H/D ratio increases. This behavior can be attributed to the fact that due to the physical characteristics of the materials, when the acoustic field is applied, materials react in a different way to the presence of the acoustic vibration. Glass beads being a more rigid material may be reflecting the acoustic vibration to the other particles, allowing the sound wave to travel all the way down to the lower region of the bed, making them easier to fluidize. On the other hand, ground walnut shell may be absorbing a portion of the acoustic vibrational energy, and as the H/D ratio increases, the sound energy reaching the bottom of the bed decreases. Therefore, with less acoustic energy reaching the bottom of the bed, the lower region becomes more packed, which requires an increase in the necessary superficial gas velocity to start fluidization.

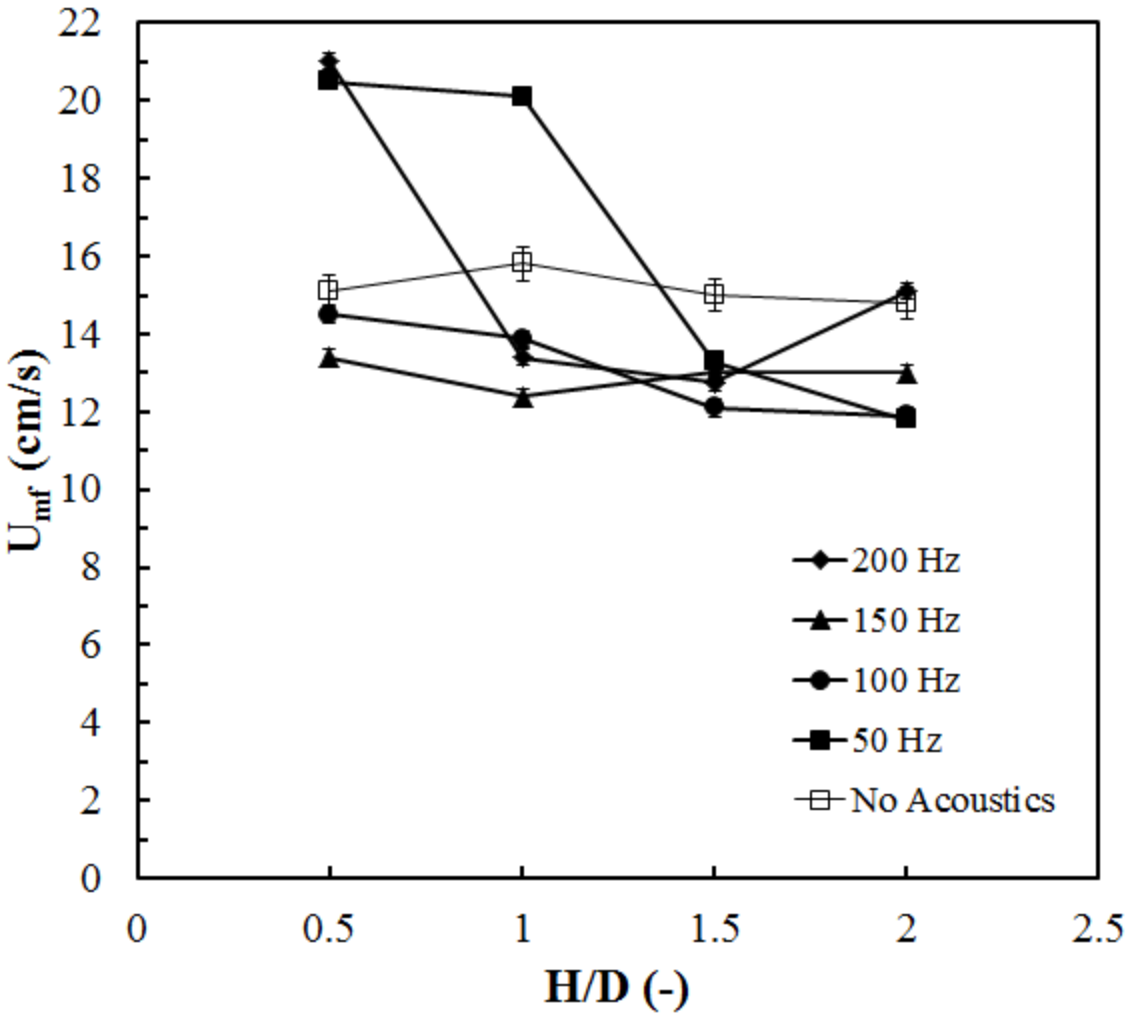

Figure 4.9: Minimum fluidization velocity as a function of bed height for 500-600 µm glass beads and SPL = 110 dB.

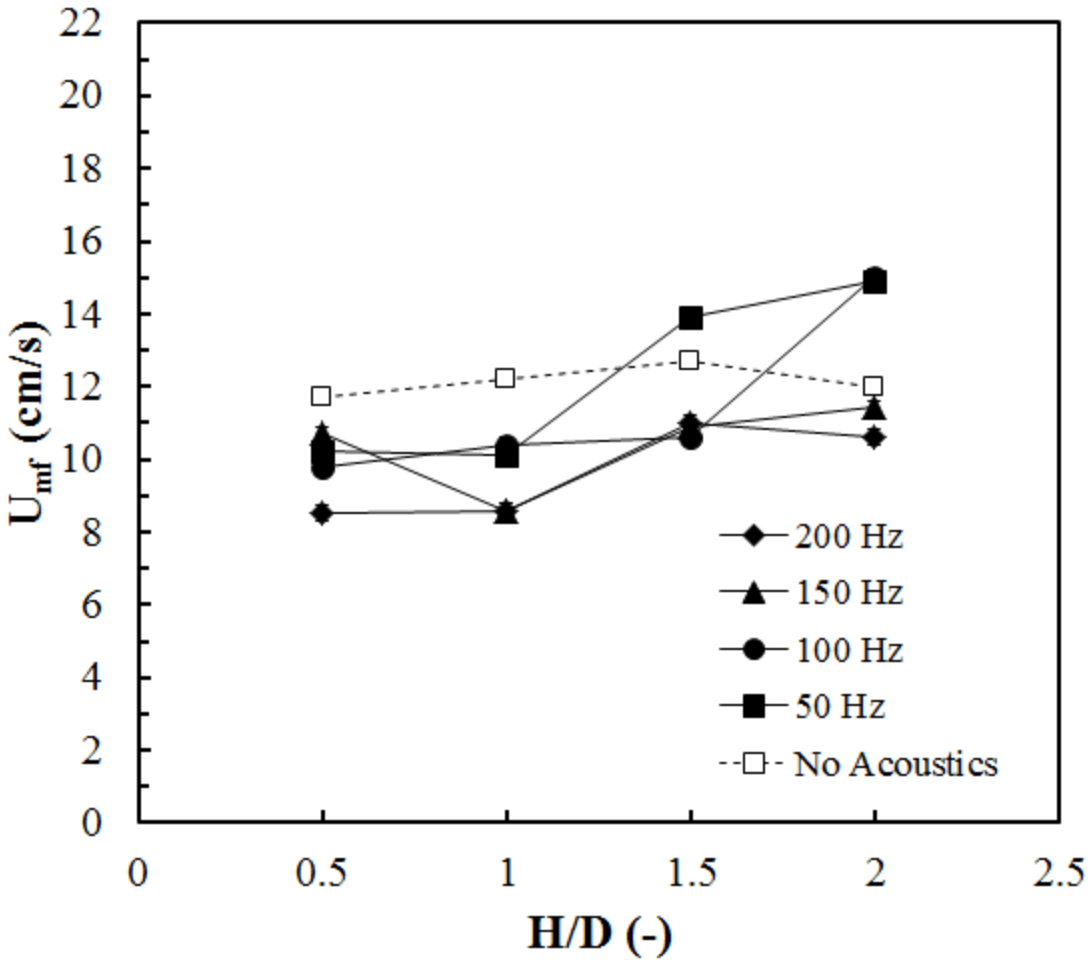

Figure 4.10: Minimum fluidization velocity as a function of bed height for 500-600 µm walnut shell and SPL = 110 dB.

Figure 4.11 shows that fluidization for glass beads is achieved with less superficial gas velocity at frequencies between 100 and 150 Hz for H/D = 0.5 and 1. When H/D = 1.5 or 2, U_{mf} is lowest between 50 and 100 Hz, which implies that as the surface of the bed approaches the acoustic source, lower frequencies are able to assist in material fluidization. On the other hand, Figure 4.12 shows that fluidization for walnut shell is achieved with less superficial gas velocity at frequencies between 100-200 Hz for all the H/D ratios.

Leu et al. (Leu et al., 1997) and Russo et al. (Russo et al., 1995) concluded that as the weight of the bed changed in a sound-assisted fluidized bed, the minimum fluidization velocity changed

over the entire frequency range in their study. They stated that this behavior is because the increase in the sound attenuation as the amount of solid increases reduced the average SPL under which beds of different weights are operated. They also showed that the change in the bed weight did not influence the trend exhibited by the minimum fluidization velocity as a function of frequency, and their results showed similar trends as the ones shown in Figures 4.11 and 4.12.

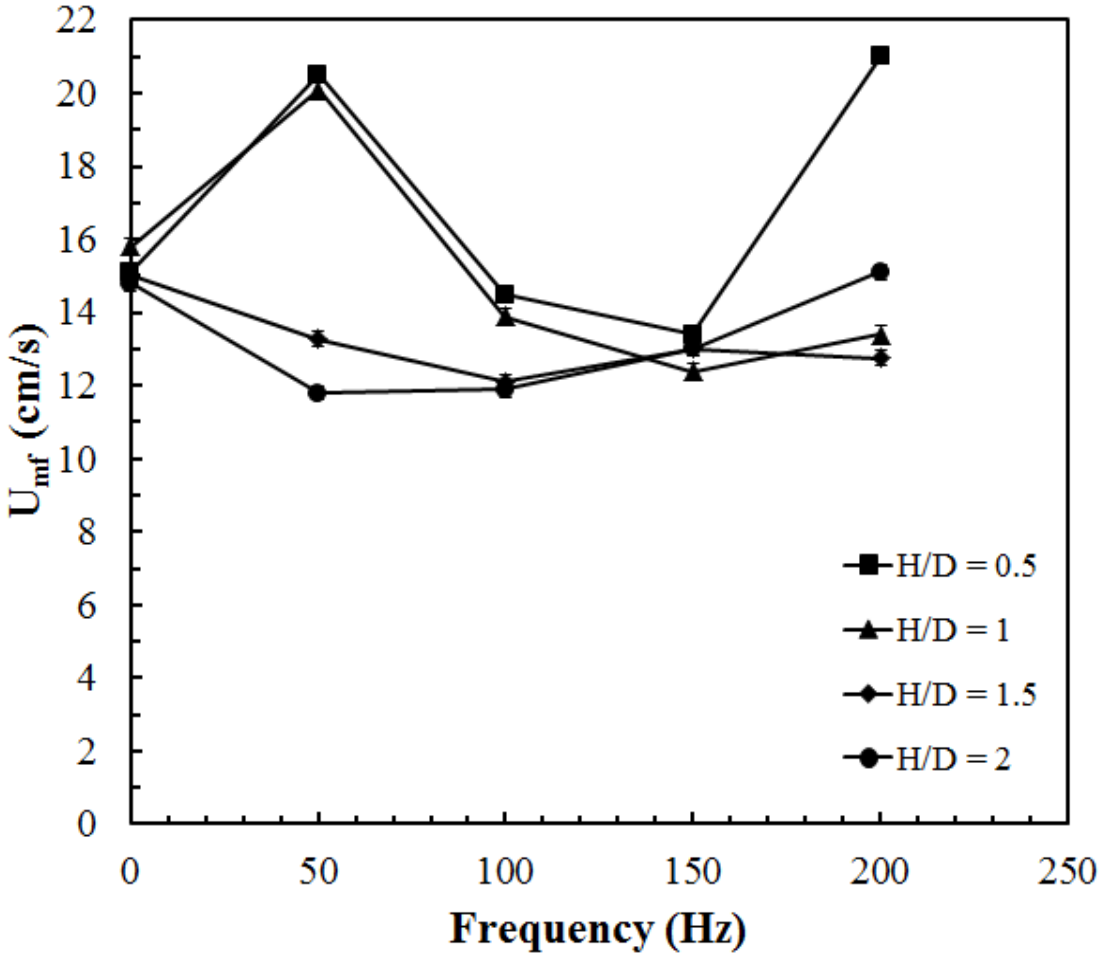

Figure 4.11: Minimum fluidization velocity as a function of frequency for 500-600 µm glass beads at different bed heights and SPL = 110 dB.

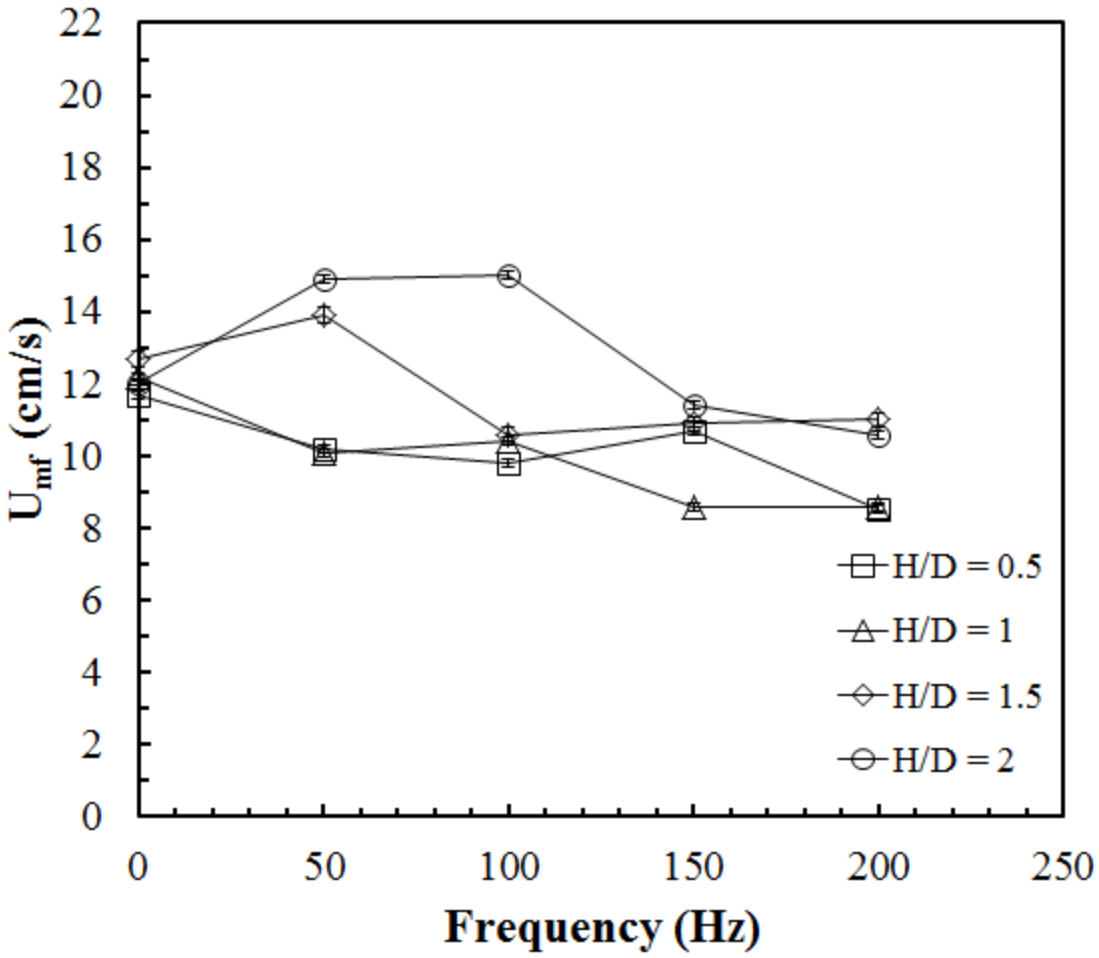

Figure 4.12: Minimum fluidization velocity as a function of frequency for 500-600 µm walnut shell at different bed heights and SPL = 110 dB.

Although U_{mf} displayed a height effect at different frequencies, the height effect was not observed when frequency was constant and the SPL increased in the glass bead beds. Figure 4.13 shows similar U_{mf} values for glass bead beds with different H/D ratios when the SPL is constant, but a decrease in U_{mf} as the SPL increases. In contrast, Figure 4.14 shows that for walnut shell beds, keeping the SPL constant and changing the H/D ratio produces a considerable change in U_{mf}, which implies that the material responds differently to the presence of a stronger acoustic vibration, causing the materials to behave differently. Moreover, Figure 4.14 shows that as SPL

increases, the minimum fluidization velocity decreases for ground walnut shell, but after a certain value of SPL, U_{mf} increases. This behavior was also observed by Leu et al. (Leu et al., 1997), where the minimum fluidization velocity decreased as the SPL increased until it reached a minimum or the power reached a critical value, which was a function of the bed height, the bed weight, and the distance the sound wave traveled. However, Leu et al. (Leu et al., 1997) observed that once a critical SPL was reached, the minimum fluidization became independent of SPL changes and just depended on frequency changes. Guo et al. (Guo et al., 2006) and Si and Guo (Si and Guo, 2008) revealed similar trends. Figure 4.13 does not reveal a critical SPL value for glass bead beds for the range of SPL tested in this study, while Figure 4.14 shows an increase in U_{mf} after a critical SPL value is reached. These different trends are observed because the critical power depends on bed characteristics, including bed material.

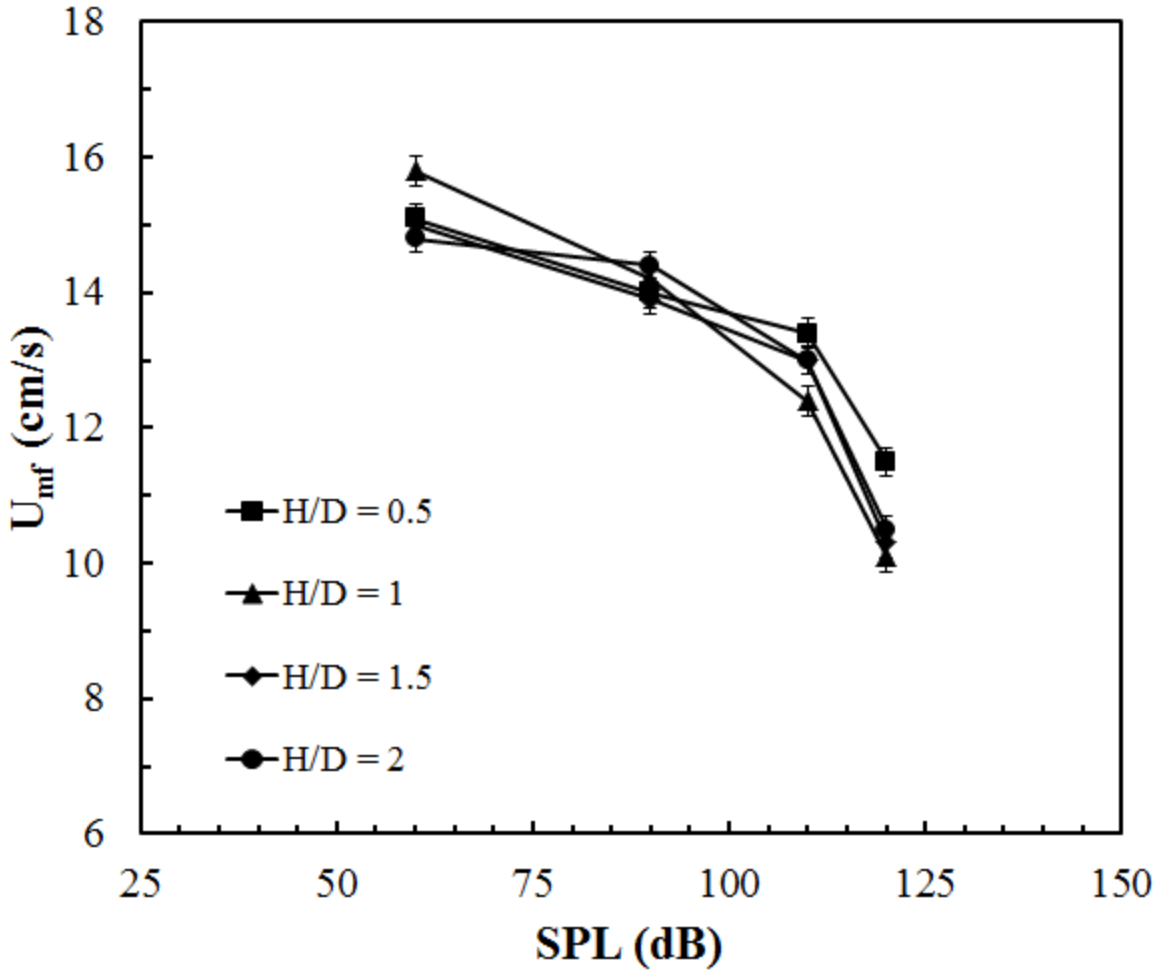

Figure 4.13: Minimum fluidization velocity as a function of SPL for 500-600 µm glass beads at different bed heights, at 150 Hz.

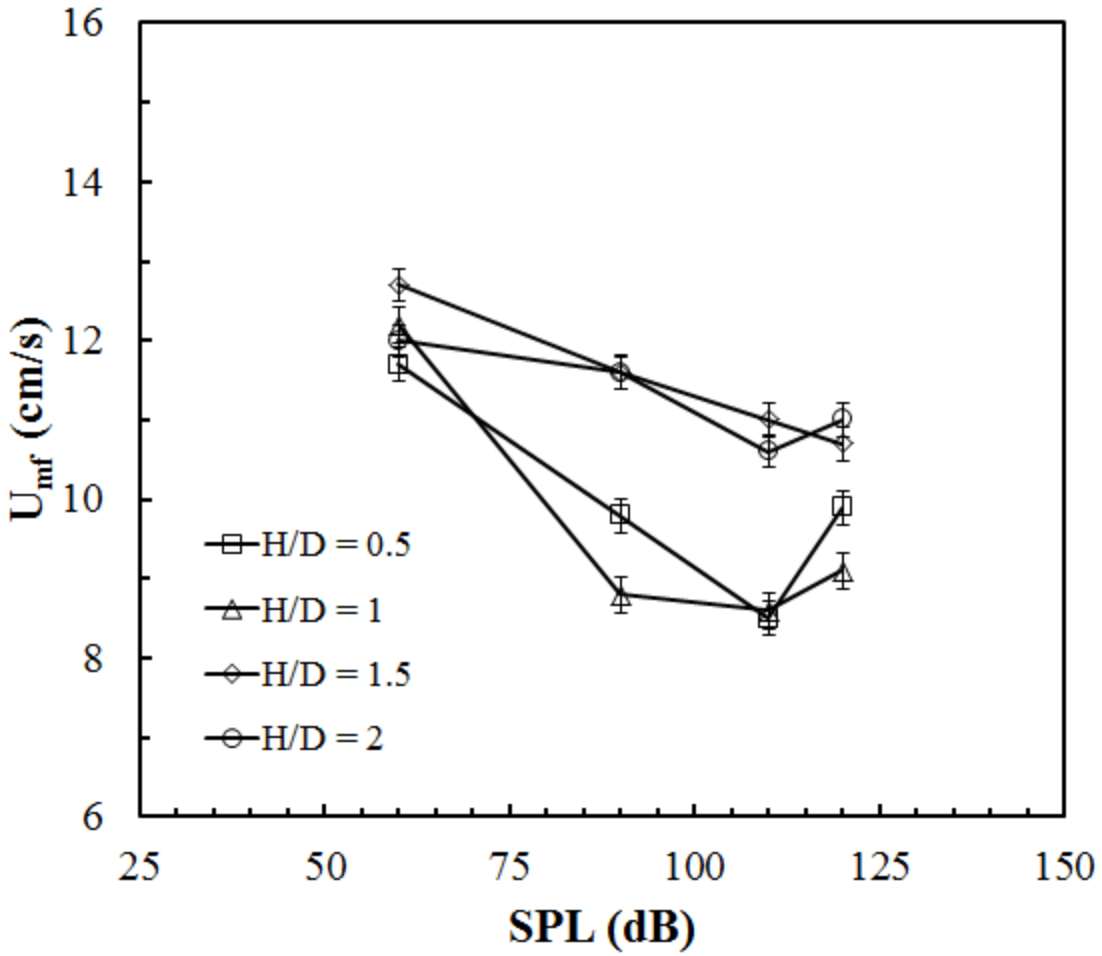

Figure 4.14: Minimum fluidization velocity as a function of SPL for 500-600 µm walnut shell at different bed heights, at 150 Hz.

4.4 Conclusions

The presence of an acoustic field in a fluidized bed filled with glass beads or walnut shell at different bed heights improved the ease of material fluidization (i.e., it lowered U_{mf}) in every particle size range studied.

Minimum fluidization velocity decreased with an increase in acoustic frequency until the material reached a point of homogeneous fluidization, beyond that point, U_{mf} started to increase. As sound pressure level increased the minimum fluidization decreased for both materials tested,

for the entire particle size range, and for the different bed height conditions. The increase in SPL provided additional energy that assisted fluidization.

Fluidized beds enhanced with acoustic sources exhibit dependence between bed height and minimum fluidization velocity. As H/D increased at a fixed frequency, there are changes in the minimum fluidization velocity; these changes did not happen when there was no acoustic field present in the bed. Moreover, at higher initial bed heights, the bed surface moved closer to the acoustic source and the frequency of the sound needed to achieve a homogeneous fluidization decreased.

Acknowledgements

This work was supported through Iowa State University.

CHAPTER 5: ACOUSTIC FLUIDIZED BED HYDRODYNAMICS CHARACTERIZATION USING X-RAY COMPUTED TOMOGRAPHY[1]

David Escudero[2] and Theodore J. Heindel

Department of Mechanical Engineering, Iowa State University
Ames, Iowa, 50011, USA
drescude@iastate.edu, theindel@iastate.edu

Abstract

Acoustic vibration in a fluidized bed can be used to enhance the fluidization quality of particulate matter; this particular noninvasive method provides no internal changes to the bed material structure. However, due to the complexity of this multiphase flow system, characterizing the hydrodynamics of a fluidized bed has become critical in understanding this system behavior. The local void fraction behavior in a cold flow 3D fluidized bed with and without acoustic intervention is investigated in this research. Several noninvasive techniques like gamma-ray computed tomography (GRT), X-ray computed tomography (XCT), or electrical capacitance tomography (ECT), can be used to study the void fraction distribution in multiphase flow systems. In this study, XCT imaging is used to determine the time-average local void fraction or gas holdup. Experiments are implemented in a 10.2 cm ID fluidized bed filled with glass beads or ground walnut shell, having a material density of 2500 kg/m^3 and 1440 kg/m^3, respectively, and particle size ranges between 212-600 μm. In this study, three different bed

[1] Originally published as: Escudero, D. R. and Heindel, T. J. (2014). "Acoustic fluidized bed hydrodynamics characterization using X-ray computed tomography." *Chemical Engineering Journal*. **243**: 411-420.

[2]Corresponding author: David Escudero G. (davidrescudero@gmail.com)

height-to-diameter ratios are examined: H/D = 0.5, 1 and 1.5. The loudspeaker's frequency, used as the acoustic source, is fixed at 150 Hz with a sound pressure level of 120 dB for glass beads, and 200 Hz and 110 dB for ground walnut shell. Local time-average gas holdup results show that the fluidized bed under the presence of an acoustic field provides a more uniform fluidization, the bed exhibits less channeling, and the jetting phenomena produced by the distributor plate is less prominent when compared to no acoustic field. Thus, acoustic intervention affects the local hydrodynamic behavior of the fluidized bed.

Keywords: Acoustics, fluidized bed, hydrodynamics, X-ray computed tomography.

5.1 Introduction

Multiphase hydrodynamics have a large impact on the performance of a fluidized bed. Gas holdup or void fraction is a parameter used to characterize the hydrodynamic structure of a multiphase flow system, and is defined as the volumetric gas fraction within the bed material. Several studies in the literature have determined the solid concentration (the inverse of gas holdup) in a gas-solid system for different fluidization regimes and different operational conditions in an attempt to understand the flow structures found in fluidized beds (Du et al., 2003, Zhu et al., 2008).

Several methods, both intrusive and nonintrusive, have been studied to improve the fluidization quality of granular material. These methods may also produce changes in the hydrodynamic behavior of the fluidized material. External stimuli, in the form of vibrations, have been used together with fluidization to treat cohesion problems. Vibrations, in fact, are able to interact directly with cohesive structures such as aggregates and channels (Barletta et al.,

2013). These vibrations can be applied to the fluidized bed in the form of mechanical vibrations or acoustic vibrations.

Studies in the literature have used mechanical vibrations to improve the fluidization quality of material that shows poor fluidization behavior (Marring et al., 1994, Zhang et al., 2012). For example, Barletta et al. (Barletta et al., 2008) studied the effects of mechanical vibration on fine powders. They found that bed packing degree reached by the vibrated bed without gas flow was always higher than that reached without vibration. Conversely, the pressure drop for a fluidized bed with vibration was equal to or less than the pressure drop obtained without vibration. These differences between conditions were more prominent when the frequencies tested were low and they become less noticeable at high frequencies. More recent studies performed by Barletta and Poletto (Barletta and Poletto, 2012), Barletta et al. (Barletta et al., 2013) and Levy and Celeste (Levy and Celeste, 2006) revealed similar results.

Acoustic fluidized beds have been researched intensively to understand the effects produced by the acoustic field on the fluidization behavior and quality in beds filled with different Geldart type particles. Leu et al. (Leu et al., 1997), Guo et al. (Guo et al., 2006), Kaliyaperumal et al. (Kaliyaperumal et al., 2011), and Levy et al. (Levy et al., 1997) all have used acoustic fields in fluidized beds to observed the different behavior that sound vibrations produced on the fluidization structure of the system.

Escudero and Heindel (Escudero and Heindel, 2013) studied the effects produced on the minimum fluidization velocity by the inclusion of an acoustic field for different Geldart type B particles. They showed that the presence of the acoustic field improved the ease of material fluidization by lowering the minimum fluidization velocity of every particle size and type they tested. Also, they found that fluidized beds enhanced with an acoustic source exhibited a

dependence between bed height and minimum fluidization velocity; these changes where not observed when the acoustic field was not present, confirming the results of Leu et al. (Leu et al., 1997).

Herrera and Levy (Herrera and Levy, 2001) used visual observations as well as invasive techniques such as fiber optic probes to measure the bubbling characteristics of a Geldart type A fluidized bed. Using these techniques, they determined that high values of the sound pressure level affected the fluidization behavior of the bed and had a large impact on the bubble characteristics, such as size and frequency. Other studies have shown additional effects in the fluidization characteristics of granular material under the presence of an acoustic source (Si and Guo, 2008, Guo et al., 2011).

Different noninvasive techniques can be used to determine local void fraction distributions in multiphase systems. Mandal et al. (Mandal et al., 2012) used gamma densitometry to study the void fraction distribution in an unary and packed fluidized bed. They determined that packed beds produced a more homogeneous fluidization than unary fluidized beds. Veera (Parasu Veera, 2001) also used gamma densitometry to study gas holdup profiles in bubble columns and showed how useful this technique can be for understanding different flow behaviors in laboratory or industrial scale bubble columns. Finally, Du et al. (Du et al., 2005) used electrical capacitance tomography to investigate local void fraction distributions in various fluidized beds; they showed that radial symmetry was observed when the bed was operated in the turbulent fluidization regime.

X-rays have been used to study multiphase fluidized systems for several decades (Yates et al., 2002). They are a commonly employed noninvasive technique because they are safer than other nuclear based techniques (they can be turned on and off at will), have high resolution, and

can be controlled by varying the voltage or current to improve penetration or contrast (Heindel, 2011).

Heindel et al. (Heindel et al., 2008) developed an X-ray visualization facility to study the different characteristics of opaque multiphase flows, from bubble columns to fluidized beds, with good both spatial and temporal resolution depending on the type of imaging technique used. Their facility is capable of producing three different X-ray imaging techniques: X-ray radiography, X-ray stereography, and X-ray computed tomography.

X-ray computed tomography (XCT) generates a 3D image of the object of interest. X-rays pass through the object and the intensity values are recorded from several projections by an imaging device. After the images are collected, computer algorithms reconstruct the images to produce a 3D representation of the object. However, due to the high amount of projections that must be acquired in order to obtain a whole reconstruction of the object, this technique does not have a good temporal resolution. On the other hand, the multiple projections give a high spatial resolution to this technique, a characteristic that can be used to determine the local time-average gas holdup in a very efficient way (Escudero, 2010).

Moreover, XCT data analysis allows for the calculation of time-average local gas or solid holdup. Escudero and Heindel (Escudero, 2010, Escudero and Heindel, 2011) studied the effects of bed height, superficial gas velocity, and bed material on the local time-average gas holdup of a 10.2 cm fluidized bed. They identified fluidization hydrodynamic affects using different bed materials (glass beads, ground corncob, and ground walnut shell), superficial gas velocities (U_g), and height-to-diameter ratios (H/D). They found that as superficial gas velocity increased, the overall gas holdup increased for every bed height studied. Flow behavior was also affected by the increase in superficial gas velocity. Increasing bed height, particularly at the higher gas flow

rates, enhanced bubble coalescence creating slugs that flow thorough the center of the bed, producing regions of low gas holdup near the walls of the fluidized bed. Also, the effects of bed height observed in the time-average local gas holdup varied depending of the bed material tested. Finally, they determined that as material density decreased, gas holdup increased.

Most of the studies concerning acoustic fluidized beds available in the literature used both invasive and noninvasive measurement techniques to describe the hydrodynamic characteristics of the bed. Fiber optic systems, visual observations, pressure fluctuation analysis, or camcorder systems are some of the techniques used in the studies summarized in the previous paragraphs. However, non-invasive techniques such as X-ray computed tomography have not been used in sound assisted fluidized beds to determine qualitative and quantitative local void fraction distribution characteristics. The goal of this study is to alleviate this shortcoming and characterize the local void fraction distribution of an acoustic 3D fluidized bed using X-ray computed tomography.

5.2 Experimental Setup

A cylindrical cold flow fluidized bed reactor is used in this study. A detailed description of the fluidized bed reactor, as well as the equipment used for supplying the fluidizing gas for the specific conditions of each experiment can be found in (Escudero, 2010, Escudero and Heindel, 2011), since the same equipment was used for these studies. Figure 5.1 shows a schematic of the fluidized bed reactor.

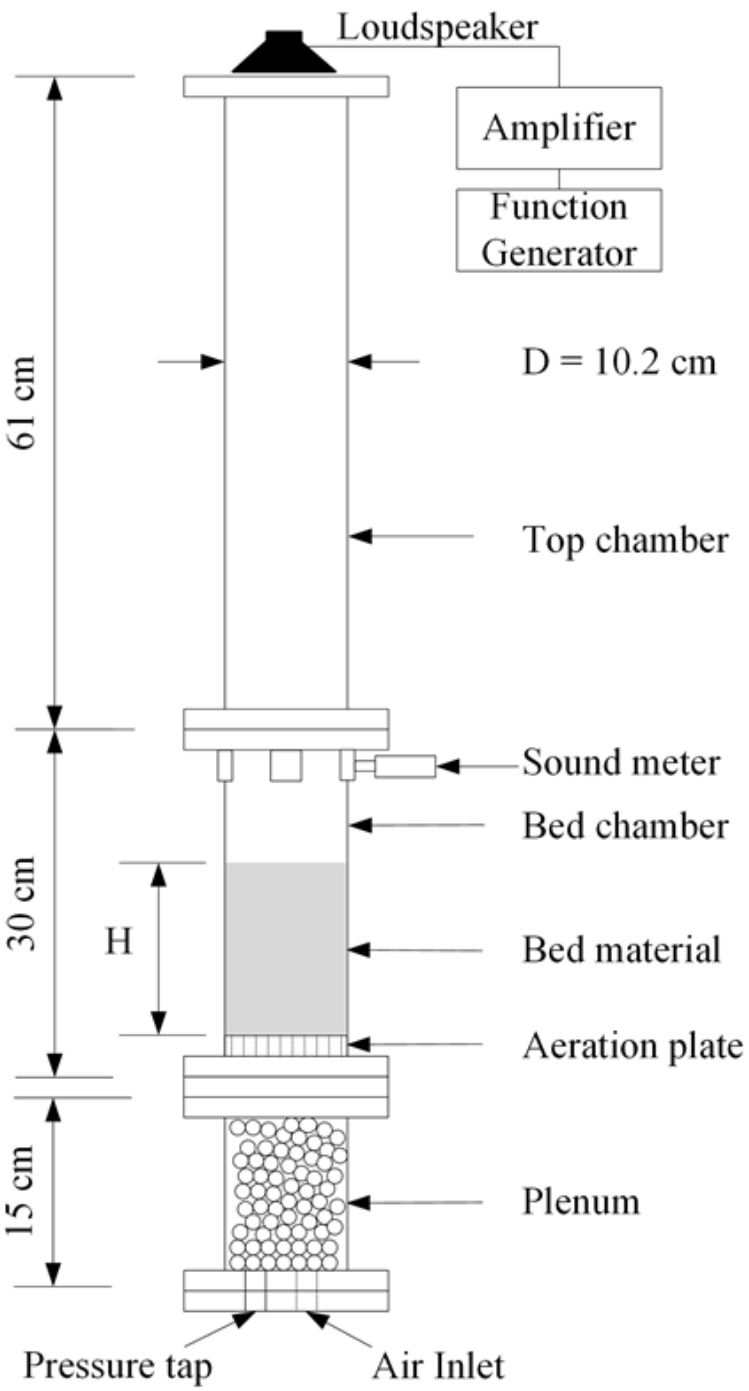

Figure 5.1: Cold flow fluidized bed reactor (not to scale). The static bed height is identified by H.

In order to modify the fluidized bed into an acoustic fluidized bed, acoustic vibrations have to be added to the system. The details of the different sound equipment used in this research can

be found in (Escudero and Heindel, 2013). To measure the power of the sound (Sound Pressure Level) that is emitted by the speaker, a mini digital sound level meter with a maximum pressure level of 130 dB and an approximate error of less than 1% is located at the top of the bed chamber. Refer to Figure 5.1 to see the setup for the entire experiment.

The fluidizing materials are glass beads (ρ_{glass} = 2500 kg/m^3) and ground walnut shell ($\rho_{walnut\ shell}$ = 1440 kg/m^3) over three different size ranges (212-425 μm, 425-500 μm, and 500-600 μm). The materials are divided into the different size classes by initially filling a 600-800 μm sieve with the desired material. The 500-600 μm, 425-500 μm, and 212-425 μm sieves are then added sequentially to the sieve stack, with a bottom under the smallest sieve. With the help of a mechanical shaker, the sieve stack is vibrated for about 20 minutes; this process is repeated several times to ensure that the desired particle size range is retained in the respective sieve.

The bed bulk density was determined using the material mass and the static bed volume. Bed material is slowly added until the desired static bed height is reached, which corresponds to H/D = 0.5, 1, and 1.5. Before the bed height is measured, the bed is fluidized and then allowed to collapse to avoid any packing effects due to the filling process. The material mass is then measured and the given bed bulk density is calculated. Table 5.1 summarizes the general bed characteristics. Note that, as shown, the bed measured bulk density was the same for each H/D ratio and particle size range for the respective particle types.

Table 5.1: Summary of bed material properties.

	Glass Beads		**Walnut Shell**	
H/D	**Bed Mass (g)**	**Bulk density (kg/m^3)**	**Bed Mass (g)**	**Bulk density (kg/m^3)**
0.5	620	1505	250	610
1	1240	1505	500	610
1.5	1860	1505	750	610
Diameter (μm)	212-425, 425-500, 500-600		212-425, 425-500, 500-600	
Particle Density (kg/m^3)	2500		1440	

Humidified air is used to reduce the electrostatic effects that may appear during the fluidization process. The relative humidity level of the air measured inside the fluidized bed range between 55 to 70% depending of the time of year. This simple solution has been implemented in the laboratory and in several studies found in the literature (Baron et al., 1987, Escudero, 2010, Zhang et al., 2010, Escudero and Heindel, 2013).

X-ray computed tomography (CT) scans are captured with and without acoustic intervention at different H/D ratios (H/D = 0.5, 1, 1.5) and different superficial gas velocities U_g = 1.5 and 3 U_{mf}, where U_{mf} is the minimum fluidization velocity previously determined (Escudero and Heindel, 2013). Note that as determined by Escudero and Heindel (Escudero and Heindel, 2013) and shown in Table 5.2, U_{mf} is a function of the flow conditions (i.e., acoustics, particle type, particle size) and the specific U_{mf} is used as the reference value for the conditions tested in this study unless otherwise noted.

Table 5.2: Summary of U_{mf} conditions.

Glass Beads				**Ground Walnut Shell**			
Particle Diameter (µm)	**H/D**	**Case**	**U_{mf} (cm/s)**	**Particle Diameter (µm)**	**H/D**	**Case**	**U_{mf} (cm/s)**
212-425	0.5	Acoustic	8.1	**212-425**	0.5	Acoustic	3.7
	1	Acoustic	8		1	Acoustic	3.9
	1.5	Acoustic	8.3		1.5	Acoustic	3.7
	0.5, 1, 1.5	No Acoustic	8.8		0.5, 1, 1.5	No Acoustic	4
425-500	0.5	Acoustic	9.1	**425-500**	0.5	Acoustic	4.8
	1	Acoustic	8.8		1	Acoustic	3.7
	1.5	Acoustic	8.5		1.5	Acoustic	4.4
	0.5, 1, 1.5	No Acoustic	11		0.5, 1, 1.5	No Acoustic	6.6
500-600	0.5	Acoustic	11.5	**500-600**	0.5	Acoustic	8.5
	1	Acoustic	10.1		1	Acoustic	8.6
	1.5	Acoustic	10.3		1.5	Acoustic	11
	0.5, 1, 1.5	No Acoustic	15		0.5, 1, 1.5	No Acoustic	12.2

The X-ray equipment used in this research is described in detail by Heindel et al. (Heindel et al., 2008), and only the procedure used for this study is described here. First, the X-ray source that is located opposite the CT detector is warmed up at the same time the thermoelectric cooler on the camera is simultaneously cooled to 0°C to reduce noise and allow for long CT scans. Custom X-ray imaging software captures the CT images, controls the camera settings, and controls the rotation ring motion. After completing the warm-up process, the X-ray voltage and current, as well as the camera exposure time and binning options are adjusted. For this study, the power settings are constant at a voltage of 150 keV and a current of 3 mA for glass beads, and 130 keV and 3 mA for ground walnut shell; the exposure time is set to 1 second per projection (360 projections total) and the binning is set to 4×4. Next, the fluidized bed is placed in the imaging region and the scintillation crystals in the detector are excited with X-rays for about 20 minutes.

After the CT data are generated, the files are reconstructed using standard algorithms (Heindel, 2011). Volume files are reconstructed and analyzed using custom software that allows selecting the region of interest (ROI) in the image and generating 2-D images of different planes. For this study, three viewing axes are selected (Figure 5.2), images in the x-y plane at different axial heights, x-z plane in the center of the bed, and y-x plane passing through the center of the bed. A false color scale is then applied to each image to provide a better appreciation for the flow structure.

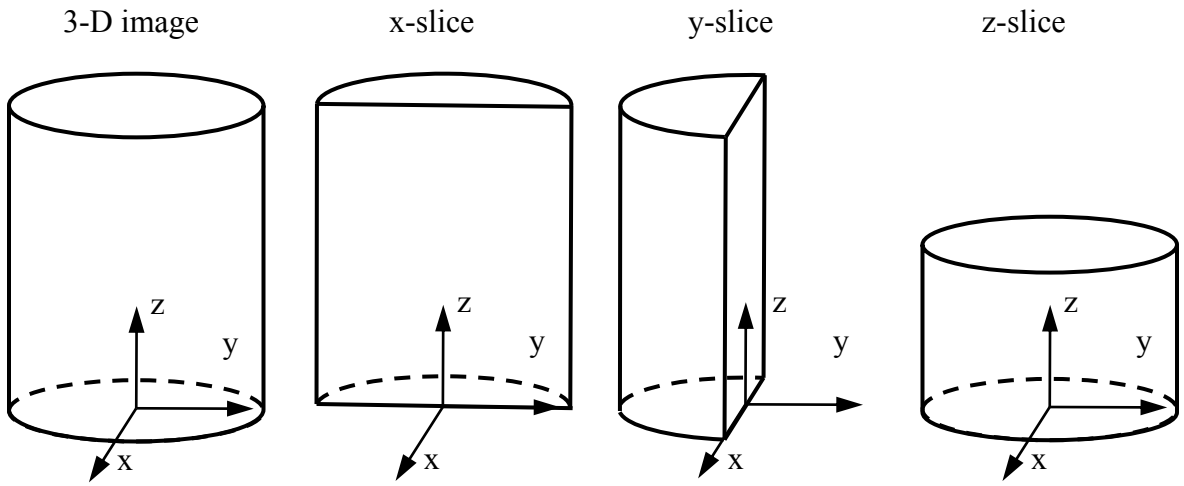

Figure 5.2: CT imaging slices planes.

Time-average local gas holdup information is calculated using the data obtained from the CT reconstruction volume files. Void fraction or gas holdup is the amount of gas present in the solid material, and is useful to characterize the hydrodynamic behavior of this gas-solid multiphase flow system. Quantifying the local time-average gas holdup, ε_g, requires the CT intensity of the empty reactor (I_g), a CT intensity of the reactor filled with a fixed bed of the bulk material (I_b), and a CT intensity of the reactor under the specified fluidization conditions (I_f). To ensure the same response for each condition from the detector system, each CT is taken with the same X-ray source power settings for the respective conditions. The local time-average gas holdup is then determined from the two reference CT images and the flow CT image (Escudero and Heindel, 2011):

$$\varepsilon_g = \frac{I_f - I_b + \left(I_g - I_f\right)\left(\varepsilon_{g,b}\right)}{I_g - I_b} \tag{5.1}$$

where the bulk void fraction, $\varepsilon_{g,b}$, is defined as:

$$\varepsilon_{g,b} = 1 - \frac{\rho_b}{\rho_p} \tag{5.2}$$

where ρ_b and ρ_p are the measured bulk and particle density, respectively. Further details of the data processing techniques are found in (Escudero, 2010).

5.3 Results and Discussion

5.3.1 Qualitative observations of the effects of acoustics on the time-average local gas holdup

Two-dimensional time-average local gas holdup maps sliced horizontally at specified bed heights can be obtained to show qualitative characteristics of the acoustic effects. These images do not show particle agglomerates, instead they show the local void fraction distribution inside the bed with different colors representing different void fraction values. A more uniform void fraction distribution implies a more uniform solid distribution within the fluidized bed. Images of z-slice gas holdup for 500-600 μm glass beads beds at a superficial gas velocity of $U_g = 3U_{mf}$ for different H/D ratios with and without the influence of an acoustic field are shown in Figure 5.3. The z-slice images are taken at seven different axial heights, h, measured from the aeration plate.

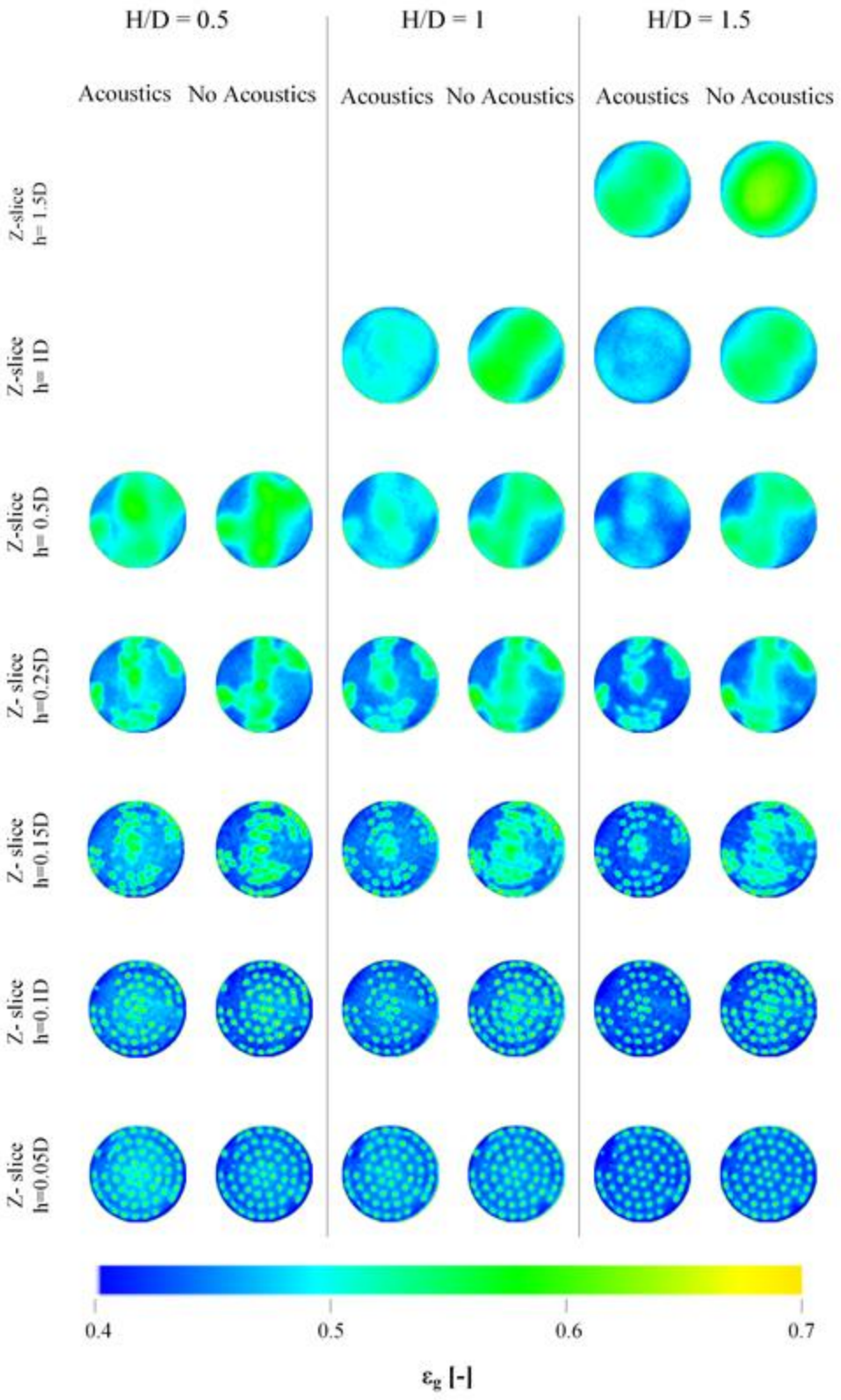

Figure 5.3: Gas holdup for the 500-600 μm glass bead beds at different H/D ratios and $U_g = 3U_{mf}$.

As shown in Figure 5.3, z-slice images at low axial height locations (h= 0.05D, 0.1D, and 0.15D) at every H/D ratio show multiple air jets (discrete regions of higher void fraction) that are caused by the aeration holes of the distributor plate. More active jets can be observed in the images without the presence of an acoustic field, and they merge at lower bed positions; this phenomenon is attributed to the fact that the volume of air that is passing through the no acoustic bed material is slightly higher than the flow rate that is passing through the bed with the acoustic field present because the minimum fluidization velocities are slightly different (Table 5.2).

Moreover, the z-slice images located at h = 0.25D show that for the acoustic condition, some of the jets still have not merged with adjacent jets, which indicates zones of high gas holdup concentrations next to zones of low gas holdup concentration. In contrast, for the no acoustic condition, jet merging has already happened at h = 0.25D and the merged jets penetrate farther into the bed.

Similar void fraction distributions are observed in all the slices in Figure 5.3 for H/D = 0.5, independent of the presence of an acoustic field. However, as the H/D ratio increases, particularly when H/D > 0.5 where the bed height is far enough away from the aeration region, the void fraction distribution in the bed for both conditions differ. Gas holdup images from the acoustic bed show more uniform gas holdup concentration throughout the bed. This void fraction distribution may suggest that the acoustic vibration imposed on the system allows for more bed uniformity. Also, this effect in the void fraction distribution as H/D ratio increases can be attributed to the way the sound wave propagates through the material. When the sound wave reaches the material, the sound pressure level is highest at the top of the bed, but the sound pressure decreases as it travels down into the bed. These differences in sound pressure level at different axial location in the z-direction create different void fraction distributions inside the

bed. In contrast, the no acoustic images show higher gas holdup concentrations through the center of the bed and lower gas holdup concentration near the wall of the bed, suggesting that air is migrating toward the bed center, and it reaches the top of the bed, solid material is being thrown towards the wall, which falls back into the bed.

Figure 5.4 shows images of z-slice gas holdup for 500-600 μm ground walnut shell beds at a superficial gas velocity of $U_g = 3U_{mf}$ for different H/D ratios with and without the influence of an acoustic field. As Figure 5.4 shows, the difference in the gas holdup structure between the acoustic and no acoustic condition for every height to diameter ratio is minimal. Regions of high gas holdup for both conditions occur in the middle of the bed as the bed surface is approached, with low gas holdup located near the bed walls, suggesting material is thrown out of the bed through the center of the bed and then reenters the bed through the outside region. The z-slice qualitative images for ground walnut shell beds show that acoustics do not significantly modify the void fraction distribution of the bed for this particular material and particle size range.

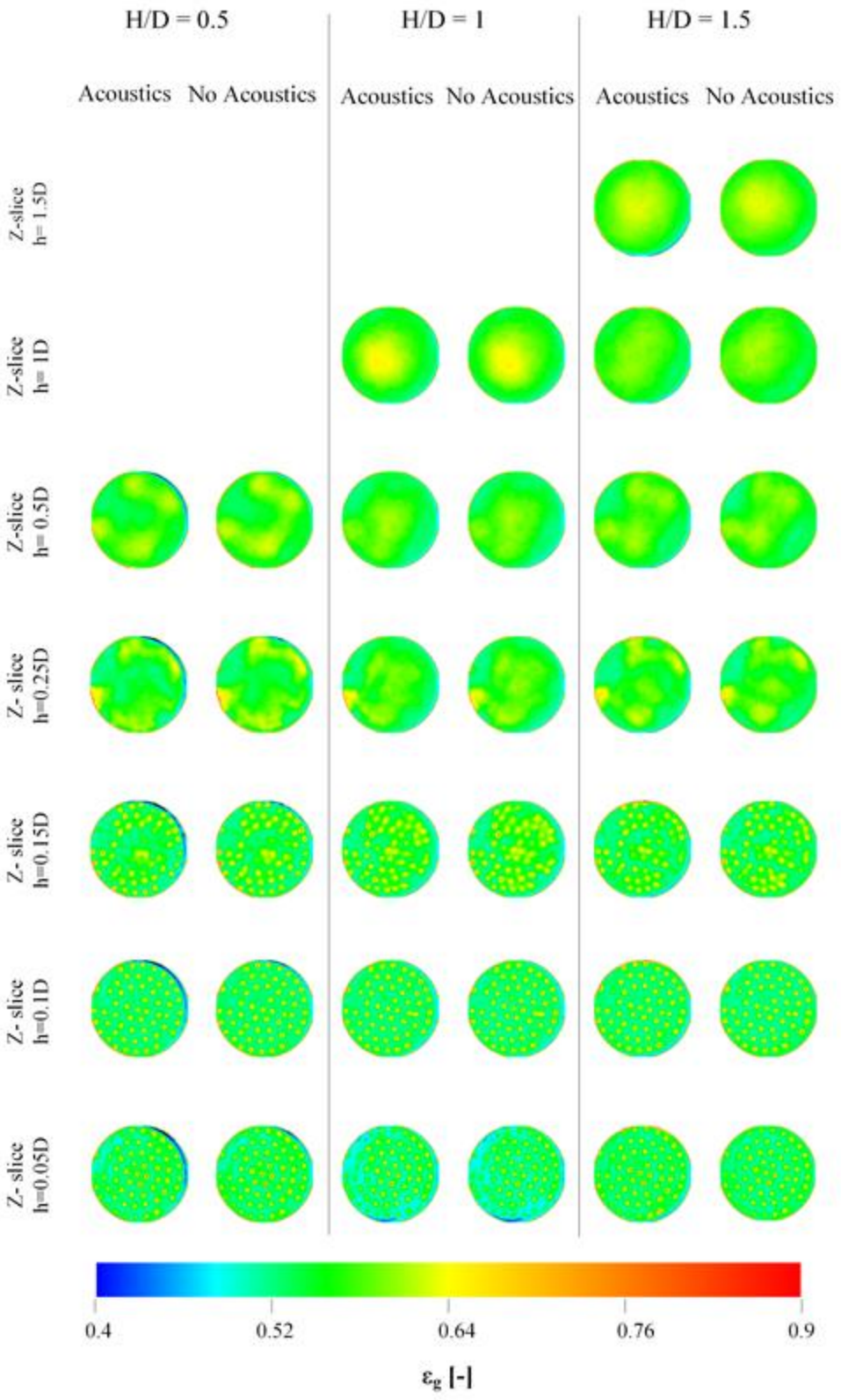

Figure 5.4: Gas holdup for the 500-600 μm ground walnut shell beds at different H/D ratios and $U_g = 3U_{mf}$.

Various glass bead particle sizes were tested to observe if acoustic effects are influenced by particle diameter. Figure 5.5 shows different 2D gas holdup maps for the three particle sizes tested at H/D = 1 and a superficial gas velocity $U_g = 3U_{mf}$. Each y-slice encompasses the entire bed diameter through the center of the bed.

Similar void fraction distributions can be observed for the smallest glass bead particle size ranges (212-425 and 425-500 μm) for both conditions, suggesting that the acoustic field does not produce a significant effect in these ranges.

For the largest particle size range tested (500-600 μm), acoustics do have an effect on the void fraction structure in the bed. Looking at the y-slices in Figure 5.5, low gas holdup regions are located towards the wall of the acoustic fluidized bed, while the region in the center of the bed presents a higher but uniform gas holdup region. In contrast, the no acoustic fluidized bed has even higher gas holdup in the bed but it is concentrated in the bed central region.

The differences in void fraction distribution are attributed to the fact that the addition of the vibrations produced by the sound field in the fluidized bed prevents bubbles from coalescing and forming larger bubbles that rise through the center of the bed while dispersing the solid particles towards the wall region. It is hypothesized that the sound energy is able to maintain bubbles in the smaller size range and produce a more uniform gas distribution deeper in the bed as Figure 5.5 shows for 500-600 μm glass beads.

For the case of ground walnut shell, Figure 5.6 shows different 2D gas holdup maps for the same fluidization conditions and bed height as Figure 5.5. Figure 5.6 shows that the acoustic condition produces a lower gas holdup concentration due to the fact that the amount of air passing through the material is lower than the no acoustic case, based on the effects that acoustics have on the minimum fluidization velocity (Table 5.2). However, the general

hydrodynamic structures observed in Figure 5.6 are similar for every particle size range tested, which may suggest that the properties of the acoustic waves (frequency and sound pressure level) selected do not affect the behavior of the material. Different properties of the sound field may affect the void fraction distribution for this particular material.

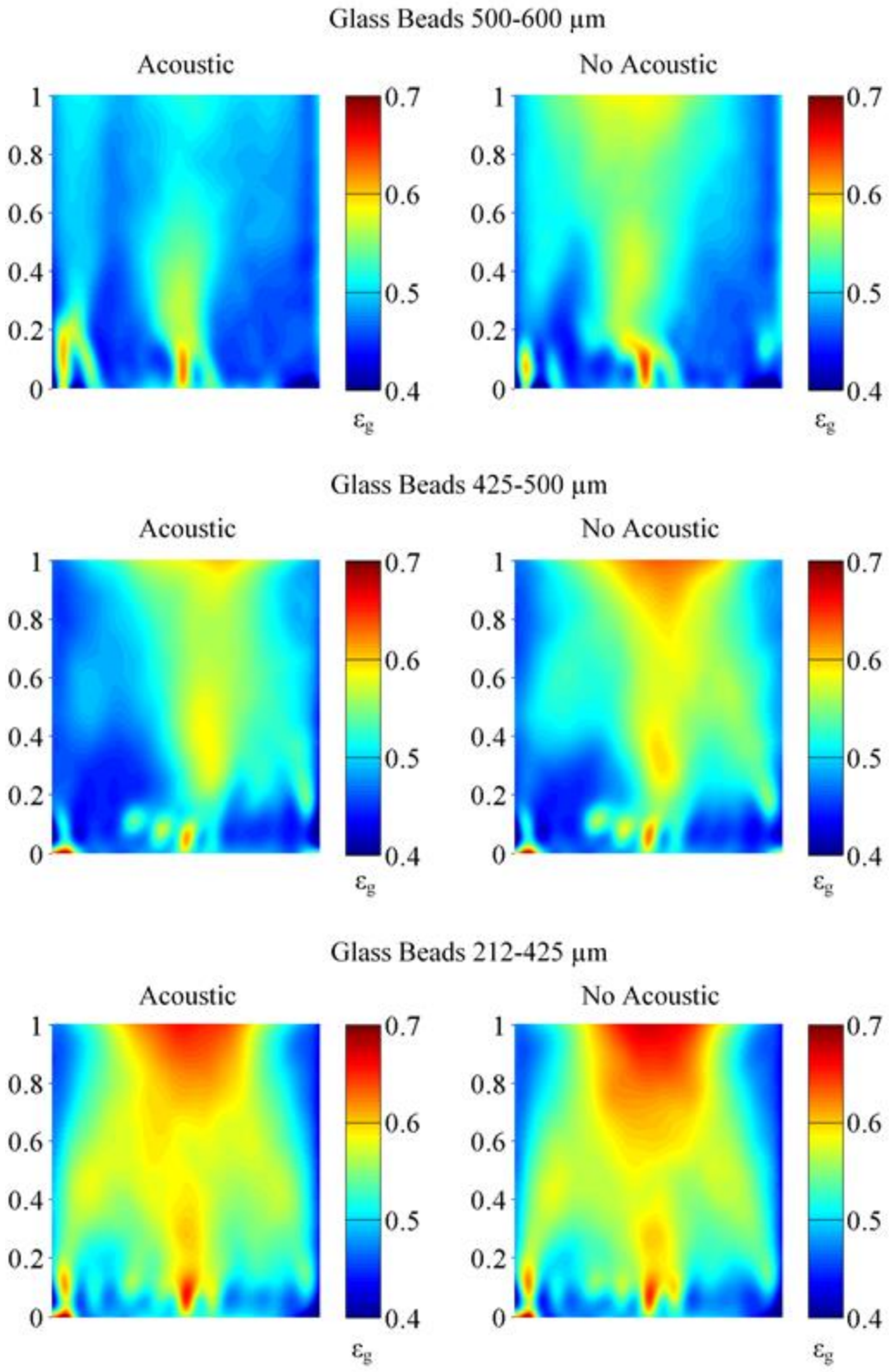

Figure 5.5: Gas holdup y-slice maps at $U_g = 3U_{mf}$ and H/D = 1 for glass beads of different particle size ranges.

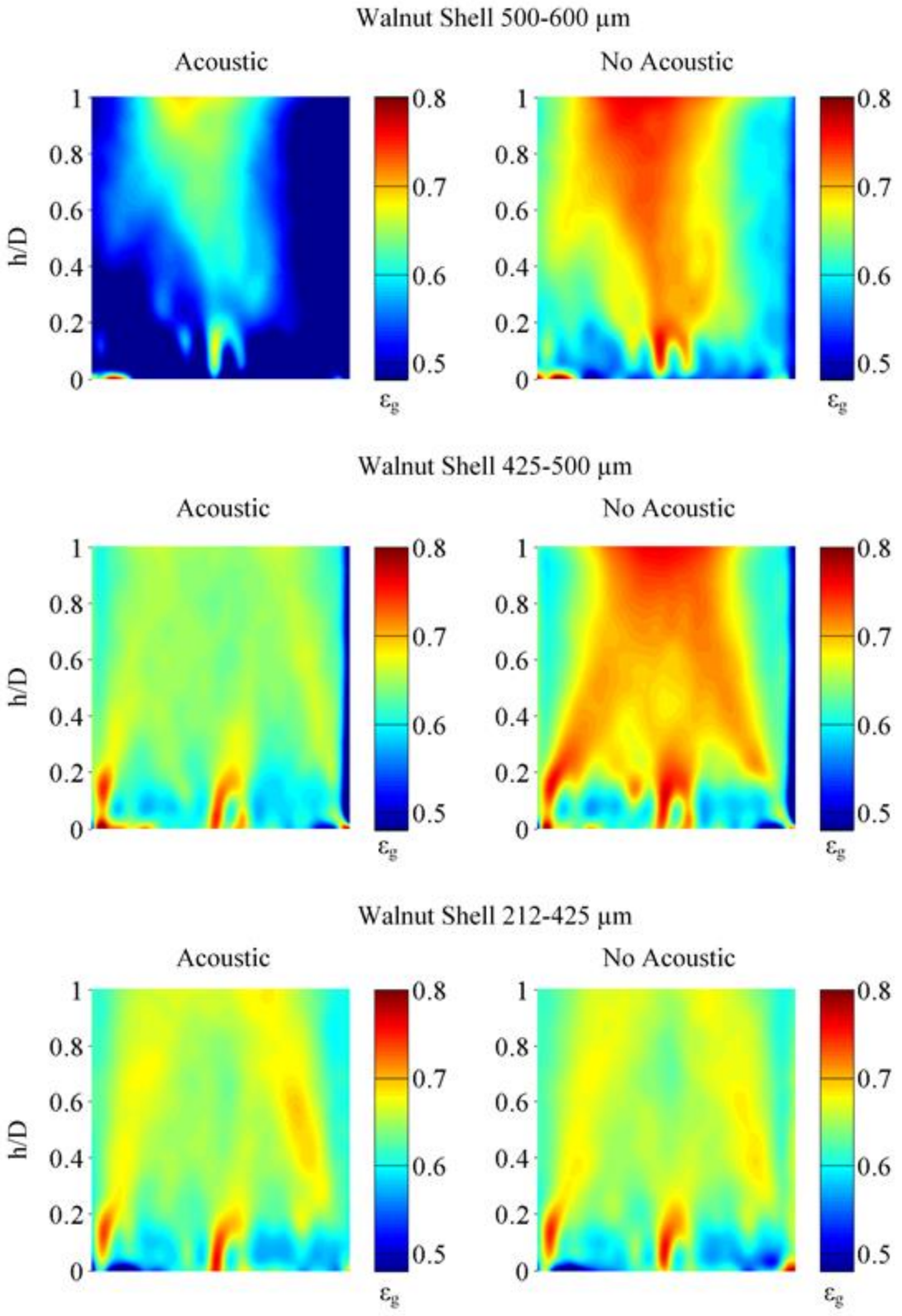

Figure 5.6: Gas holdup y-slice maps at $U_g = 3U_{mf}$ and H/D = 1 for ground walnut shell of different particle size ranges.

5.3.2 Quantitative results of the effects of acoustics on the time-average local gas holdup

The horizontal averaged local time-average gas holdup is plotted as a function of height to determine quantitatively the variation of the gas holdup through the entire bed, with and without acoustic intervention. Figure 5.7 shows these trends for 500-600 μm glass beads at H/D = 1 for a superficial gas velocity of $U_g = 3U_{mf}$. As shown in Figure 5.7, at a lower bed height ($h/D \leq 0.25$, where h is the local bed height measured from the aeration plate), both conditions presented variations that are attributed to the jetting phenomena near the distributor plate. As h/D increases (moving higher in the bed), gas holdup remains fairly constant for both cases; however, the acoustic condition shows a more uniform (i.e., constant) gas holdup distribution throughout the entire bed, which was also observed in the qualitative images (Figures 5.3 and 5.5). Near the top of the bed ($h/D \approx 1$), the no acoustic condition has a higher bed expansion due to a slightly higher gas flow rate (Escudero and Heindel, 2013), which causes more material to be expelled from the bed and then fall back into the bed. Similar trends as the ones shown in Figure 5.7 are observed when the superficial gas velocity changes.

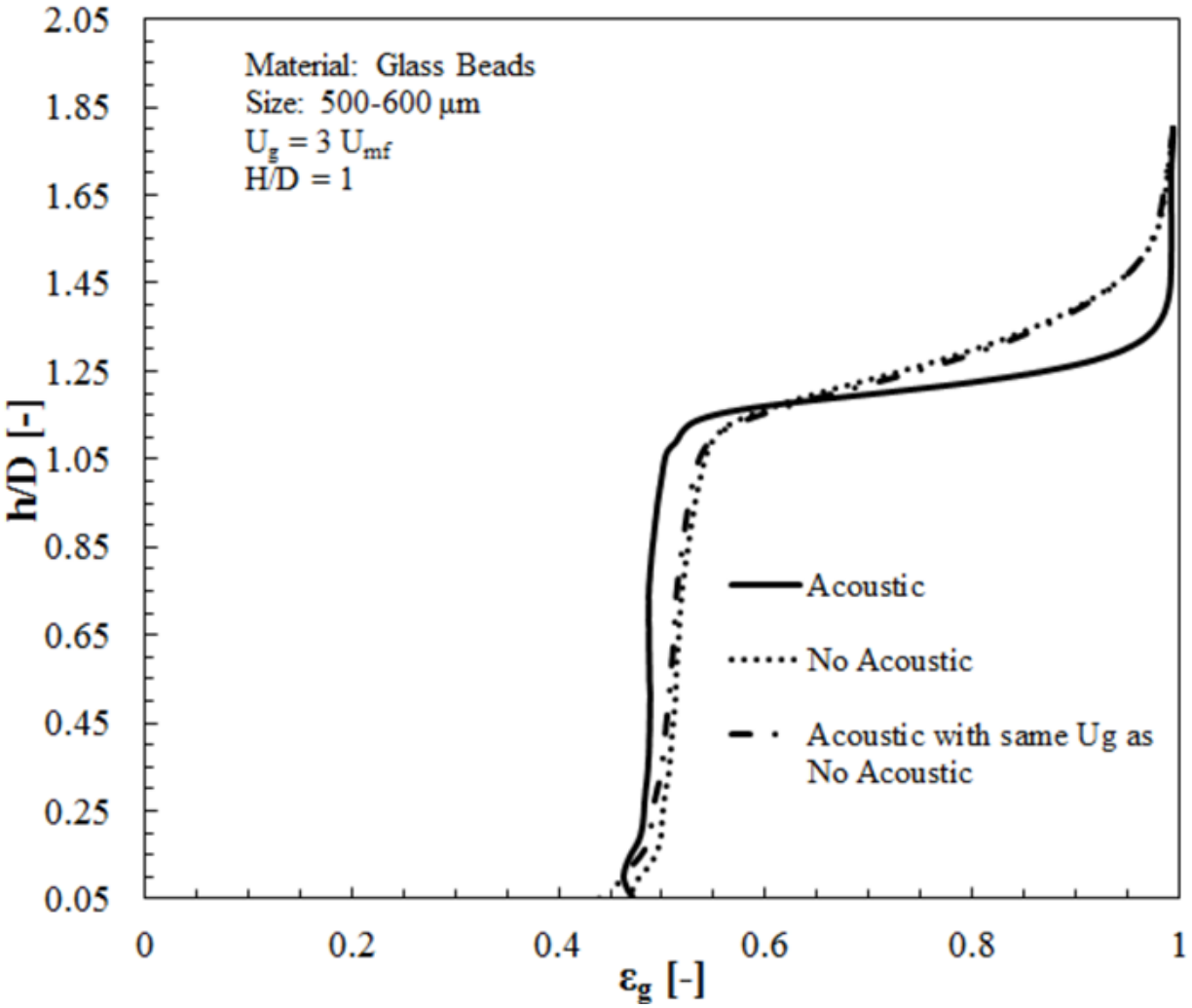

Figure 5.7: Horizontal average gas holdup for 500-600 µm glass bead bed with H/D =1, and with and without acoustic intervention and $U_g = 3U_{mf}$.

Moreover, when the acoustic field is applied to a bed that is fluidized with the same superficial gas velocity (U_g) as the no acoustic bed, the differences in the gas holdup values and in the uniformity of the gas holdup throughout the entire bed are minimal, suggesting that the acoustic field has no effect when the same superficial velocity is applied to the bed. However, it is important to clarify that Figure 5.7 represents the planar average at different height locations, and does not represent local variations of the gas holdup values, and thus does not show local variations of the hydrodynamic behavior in the fluidized bed.

Figure 5.8 shows the gas holdup as function of height for glass beads at two different superficial gas velocities. At the lower superficial gas velocity, the effects caused by the acoustic field are minimal – gas holdup is fairly uniform for both conditions. The main difference is that the acoustic condition has a lower bed expansion when U_g is fixed relative to U_{mf}, which differs slightly between the acoustics and no acoustics case. Similar trends are observed for ground walnut shell.

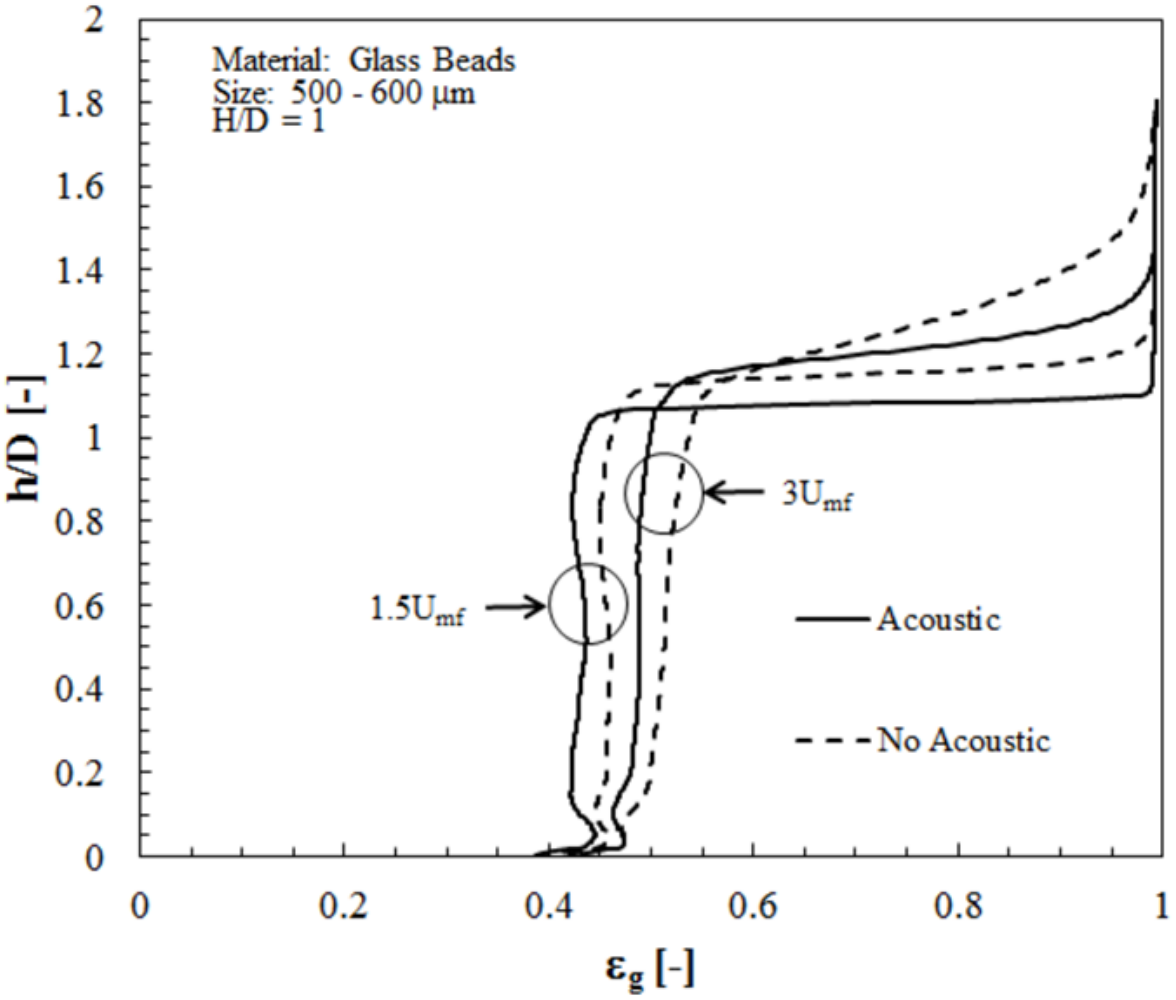

Figure 5.8: Effect of superficial gas velocity on horizontal average gas holdup for different U_g at H/D = 1.

Finally, local time-average gas holdup is plotted as a function of location along two mutually perpendicular lines that pass through the center of the bed for all the particle sizes tested at H/D = 1 and $U_g = 3U_{mf}$. Figure 5.9a shows the local gas holdup data along the x-slice at an axial height h = 0.25D (2.5cm), while Figure 5.9b shows the data along the y-slice. The local rise and fall in local gas holdup is attributed to the presence of jets from the aeration plate.

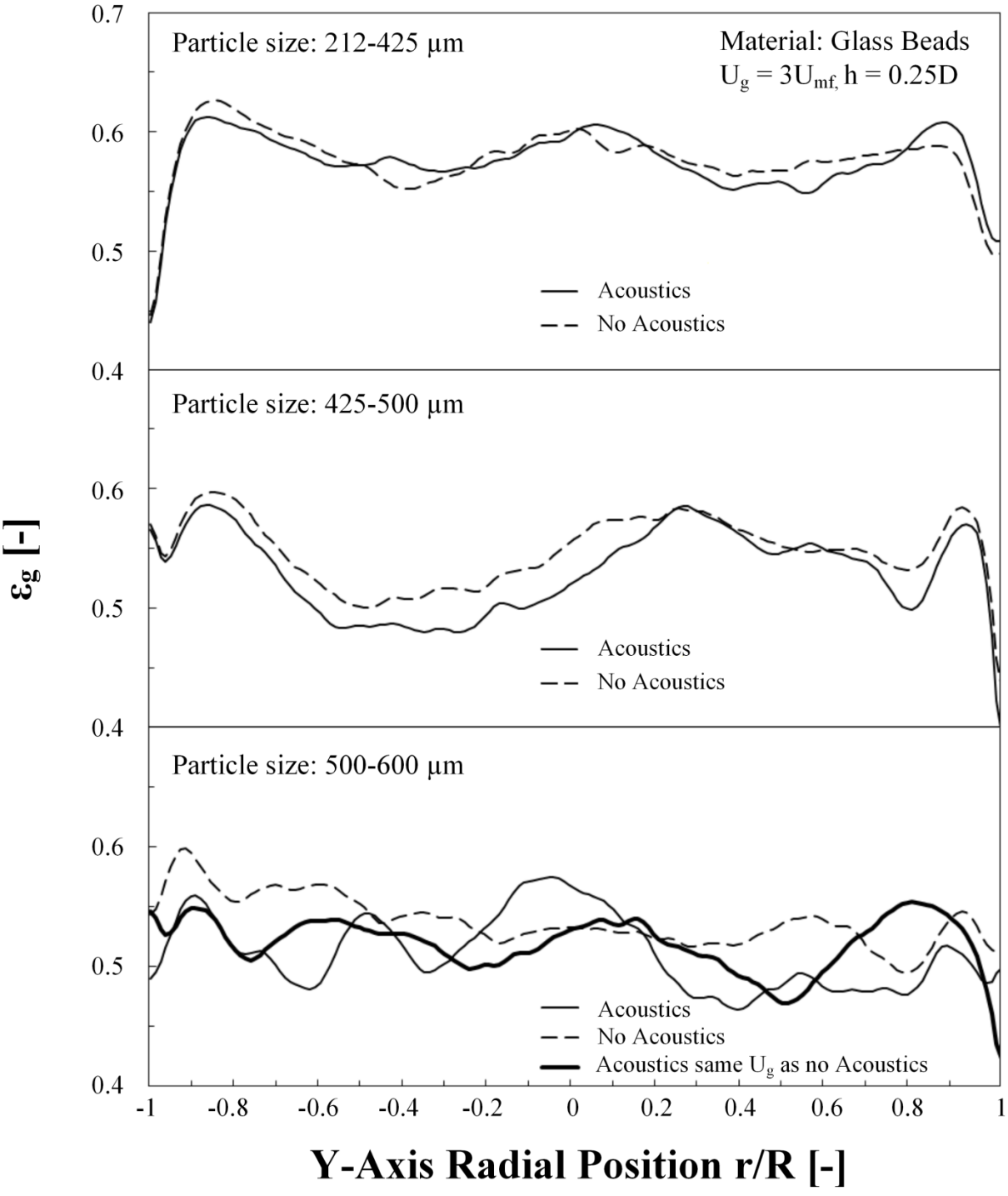

Figure 5.9a: Local gas holdup along the x-slice, as a function of location at h = 0.25D for different size ranges of glass beads.

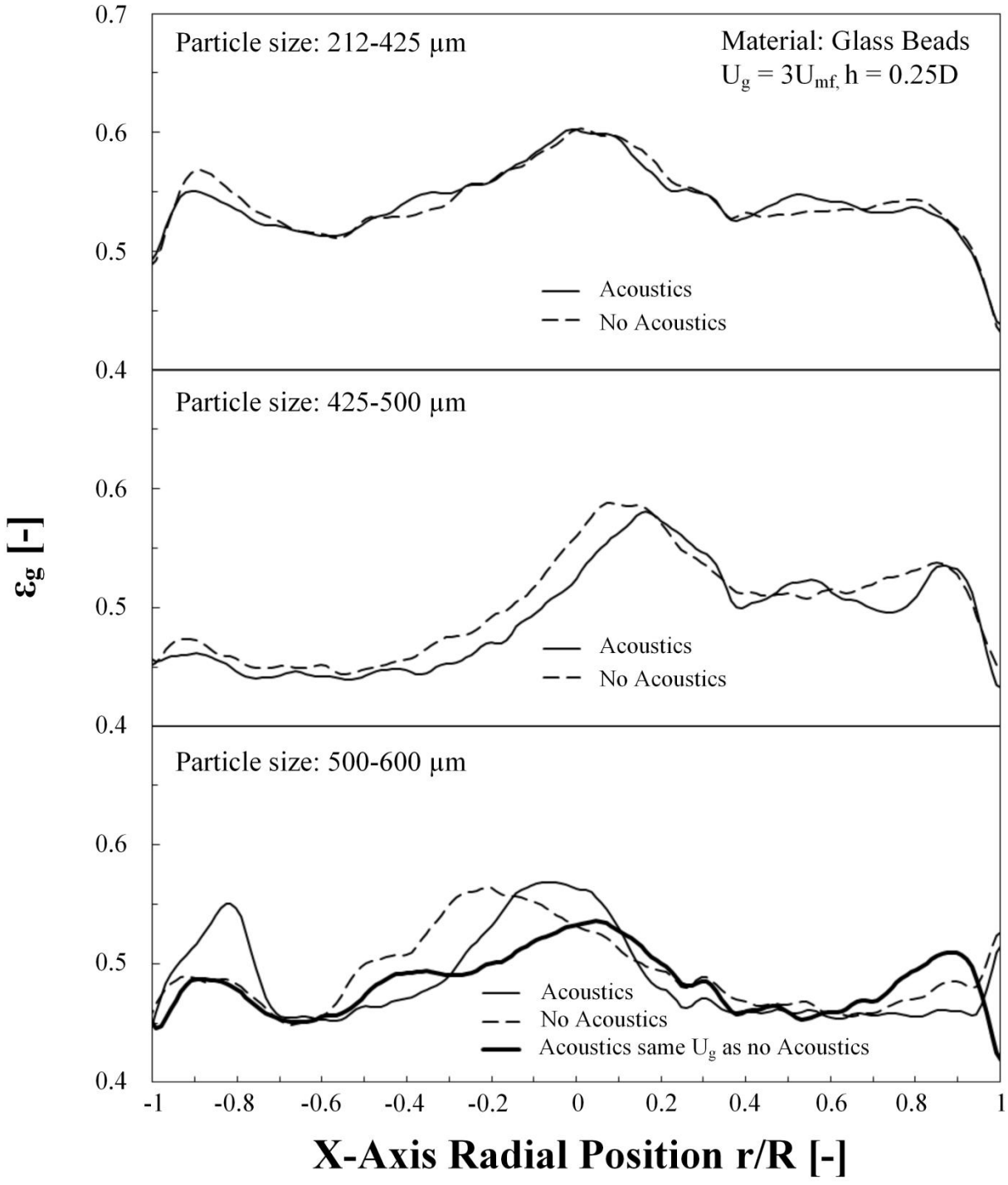

Figure 5.9b: Local gas holdup along the y-slice, as a function of location at h = 0.25D for different size ranges of glass beads.

It is observed in Figure 5.9 that the differences in the trends between acoustic and no acoustic curves for particle sizes of 212-425 μm and 425-500 μm are minimal, suggesting that acoustics do not influence the hydrodynamic behavior of the fluidized bed for these particle sizes. However, the 500-600 μm glass bead curves show that the acoustic data observe more rises and falls in the gas holdup values (Figure 5.9a) due to local jets that have not yet merged with adjacent jets. In contrast, the no acoustic curve in the same radial position as the acoustic curve does not show these local variations in the gas holdup value, which may indicate that the local jets have lost their identity at that particular height in the bed. Similar trends are observed when the acoustic field is applied to the 500-600 μm glass bead bed which was fluidized at the same U_g as the one without the acoustics intervention.

Figure 5.10a shows the local gas holdup data along the x-slice at an axial height h = 1D (10.2 cm), while Figure 5.10b shows the same conditions along the y-slice. Again the differences in gas holdup trends observed in glass beads with particle size ranges below 500-600 μm between the acoustic and the no acoustic case are minimal, hence the void fraction distribution is not influence by the acoustic vibrations. For the 500-600 μm glass beads, some differences can be observed in Figure 5.10a and 5.10b, where for the acoustic case, there is a more uniform gas holdup distribution through the center of the bed while the no acoustic case presents an increase in the gas holdup all the way through the center of the bed and then shows a decrease in the gas holdup near the walls. These variations again are attributed to the fact that the sound energy produced by the acoustic field maintains smaller bubble sizes which create a better and more uniform distribution between the gas and solid particles throughout the bed, especially in the center region of the fluidized bed. Similar results were observed by (Cao et al., 2010) using experimental and numerical methods in a gas-solid fluidized bed of FCC particles.

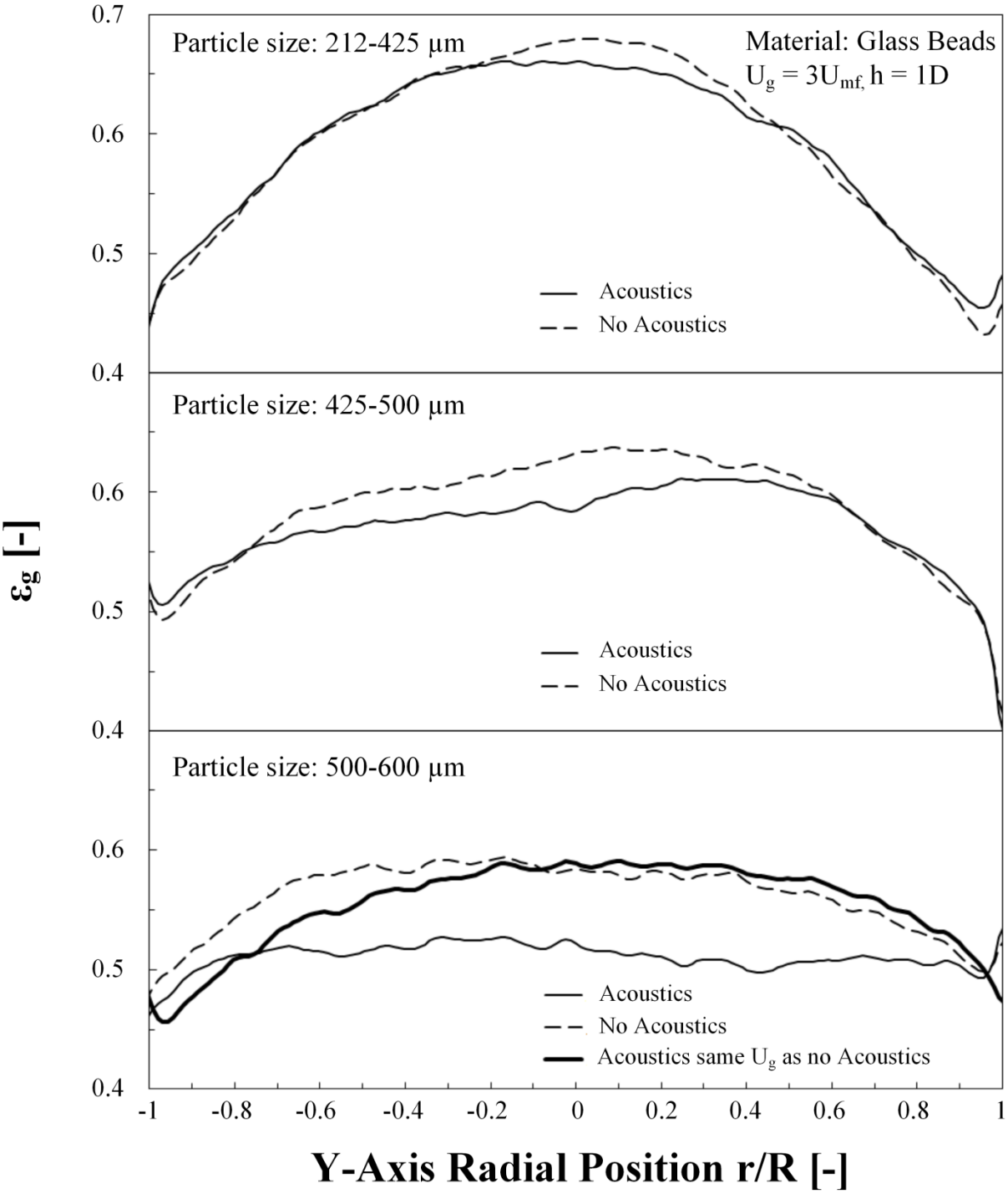

Figure 5.10a: Local gas holdup along the x-slice, as a function of location at h = 1D for different size ranges of glass beads.

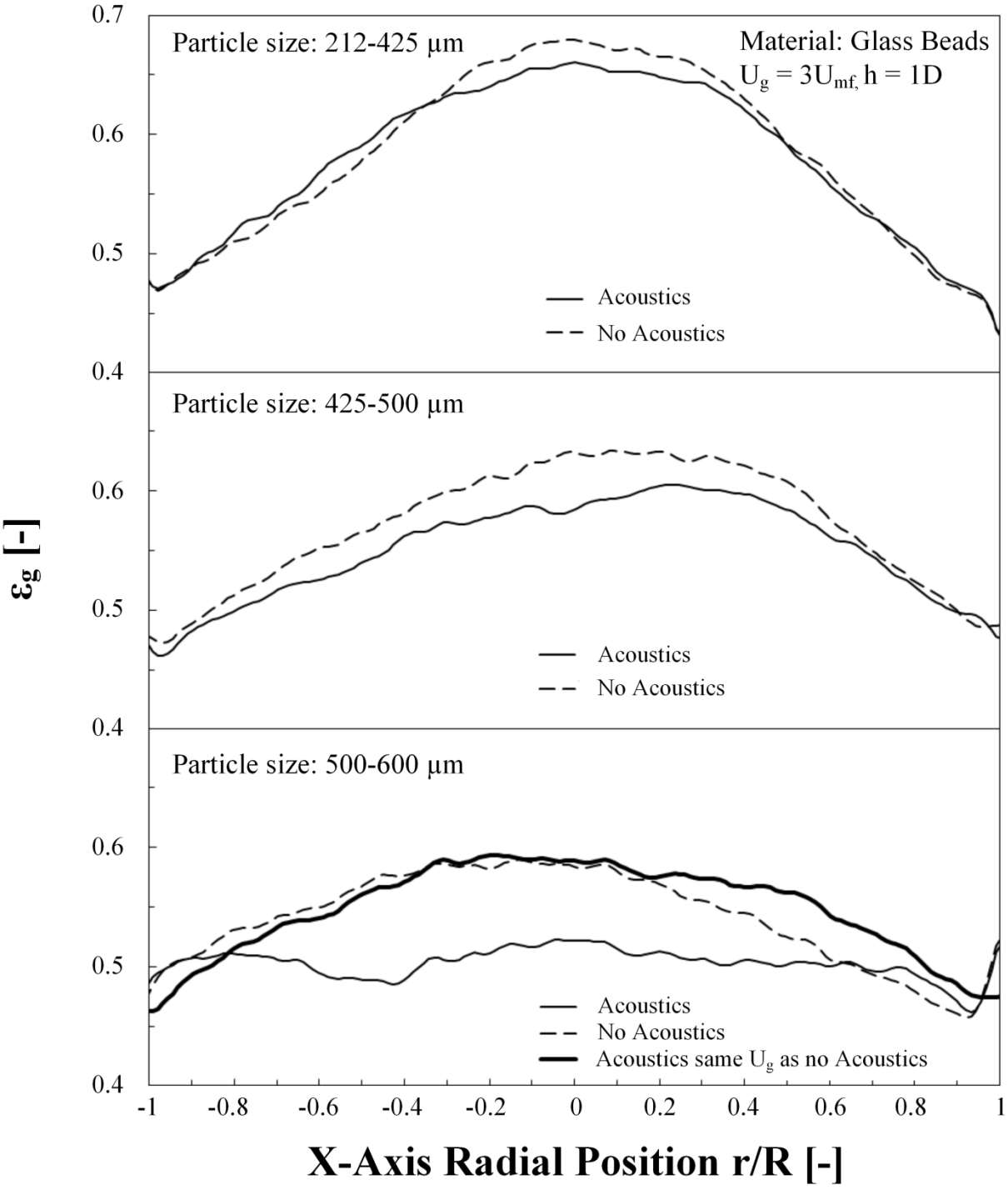

Figure 5.10b: Local gas holdup along the y-slice, as a function of location at h = 1D for different size ranges of glass beads.

Figure 5.11 shows the variations of the local time-average gas holdup for ground walnut shell at h = 0.25D and $U_g = 3U_{mf}$. The trends in the gas holdup for the acoustic and the no acoustic case for every particle size range presents minimum differences between them, corroborating what the qualitative images have shown; the only observable difference is that the no acoustic case produced a higher gas holdup concentration compared to the no acoustic case.

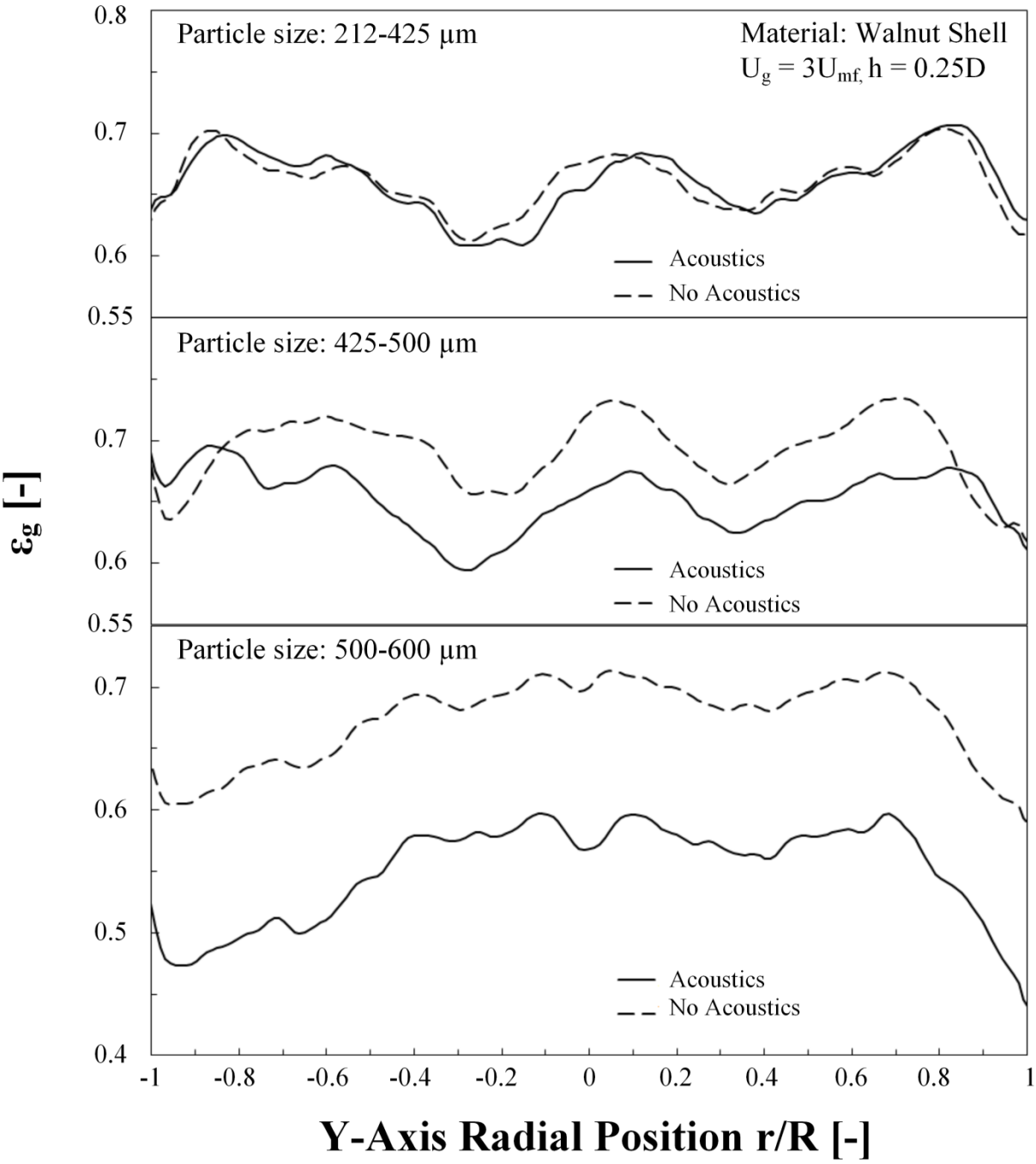

Figure 5.11a: Local gas holdup along the x-slice, as a function of location at h = 0.25D for different size ranges of ground walnut shell.

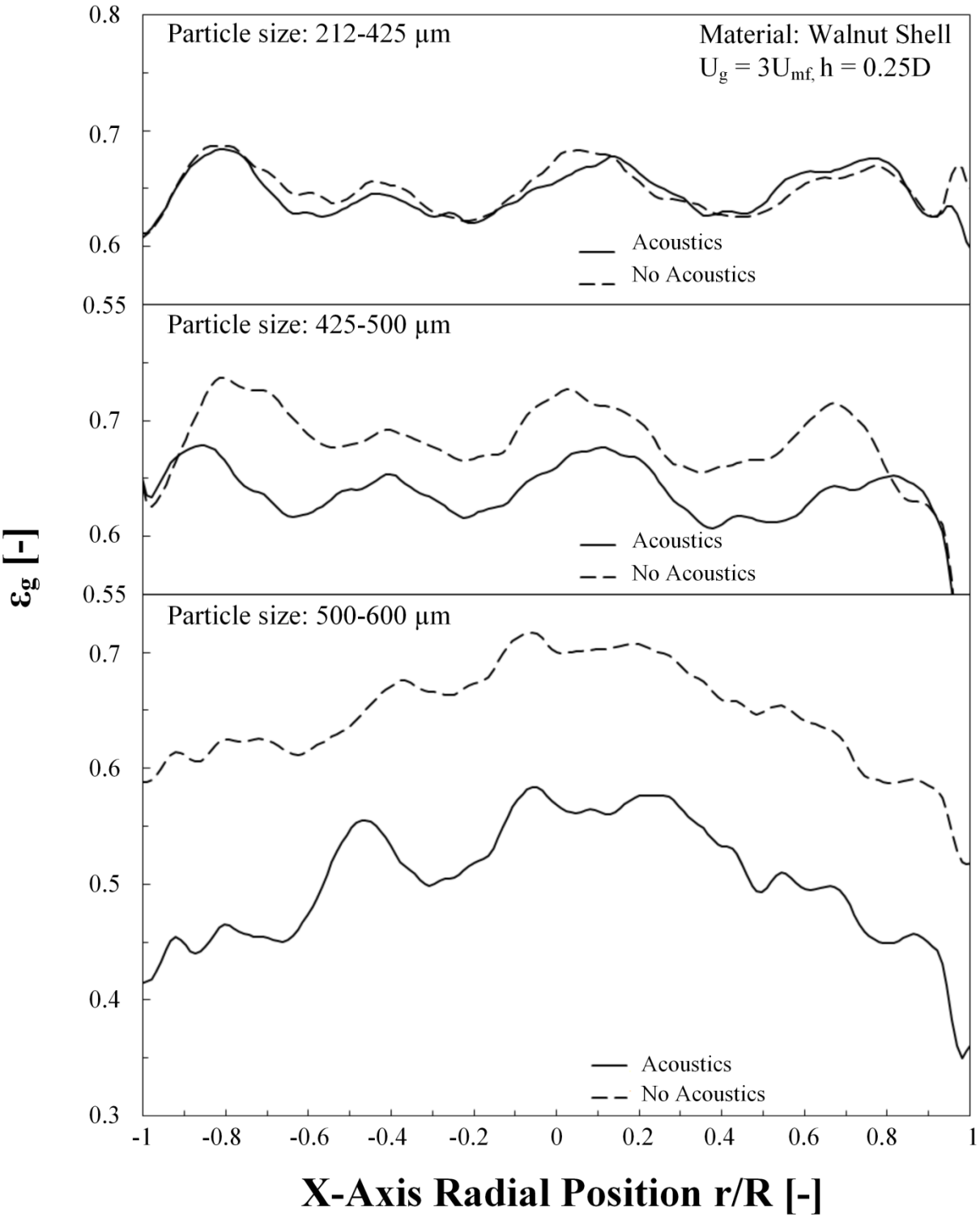

Figure 5.11b: Local gas holdup along the y-slice, as a function of location at h = 0.25D for different size ranges of ground walnut shell.

Figure 5.12 shows that as the axial height increases farther into the bed, the trends in the gas holdup concentration between each size range is the same, with the exception for the particle size range of 425-500 μm, where the acoustic case show a more uniform distribution of the gas holdup along the entire bed, while the no acoustic case presents an increase in the gas holdup concentration in the middle section of the bed. This phenomenon is attributed to the fact that as Escudero and Heindel (Escudero and Heindel, 2013) have shown, the effects of frequency and sound pressure level were influenced by the ground walnut shell particle size; the acoustic conditions of this study for ground walnut shell (200 Hz, 110 dB) had a more prominent effect on the gas holdup concentration for the material at the 425-500 μm range. This effect can also be observed in the qualitative images shown in Figure 5.6.

Also, at this particular frequency and sound pressure level, there could be less sound wave attenuation as it passes through the ground walnut shell for the 425-500 μm size range. A decreased sound wave attenuation implies that the sound energy that is reaching the particles is higher, which can explain the different behavior observed in ground walnut shell. Variations in the sound wave attenuation also explains why the trends observed between the no acoustic and the acoustic case for ground walnut shell at 425-400 μm are very similar (Figure 5.11), but as we increase the axial height (Figure 5.12), the differences between the gas holdup concentration presents differences between conditions; the sound energy reaching the upper region of the bed is higher than that reaching the lower region of the bed. Hence, there is insufficient sound energy in the lower bed region to influence any changes in the bed void fraction distribution.

It is also interesting that both in Figures 5.11 and 5.12, the gap present in the gas holdup concentration between the no acoustic and acoustic conditions for all particles size ranges (except the 425-500 μm and h = 1D case) increases as the particle size increases, and it is

constant through the entire bed height. This phenomenon may be attributed to the properties of the material (density, morphology); however additional analysis is needed to better understand this behavior.

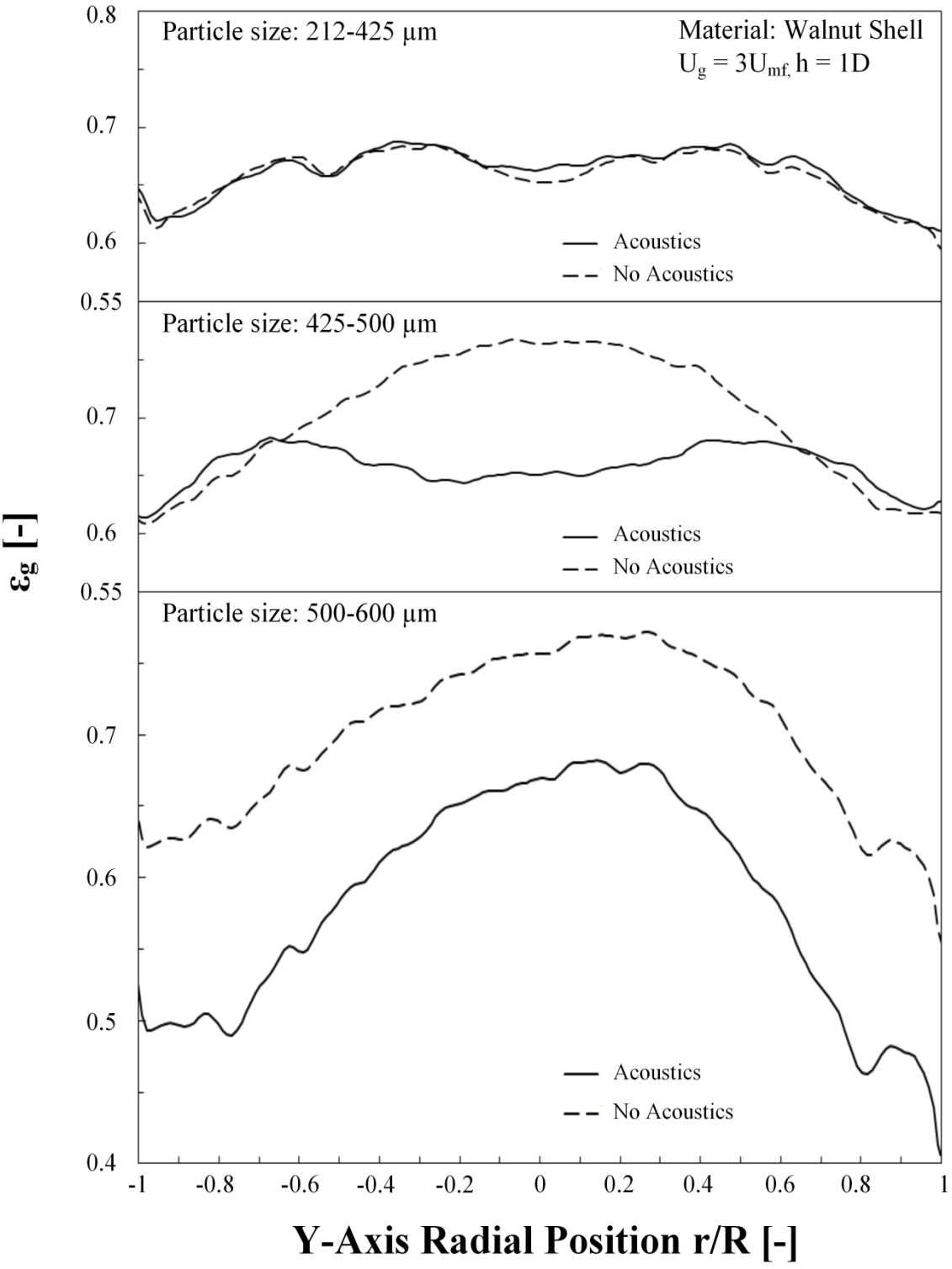

Figure 5.12a: Local gas holdup along the x-slice, as a function of location at h = 1D for different size ranges of ground walnut shell.

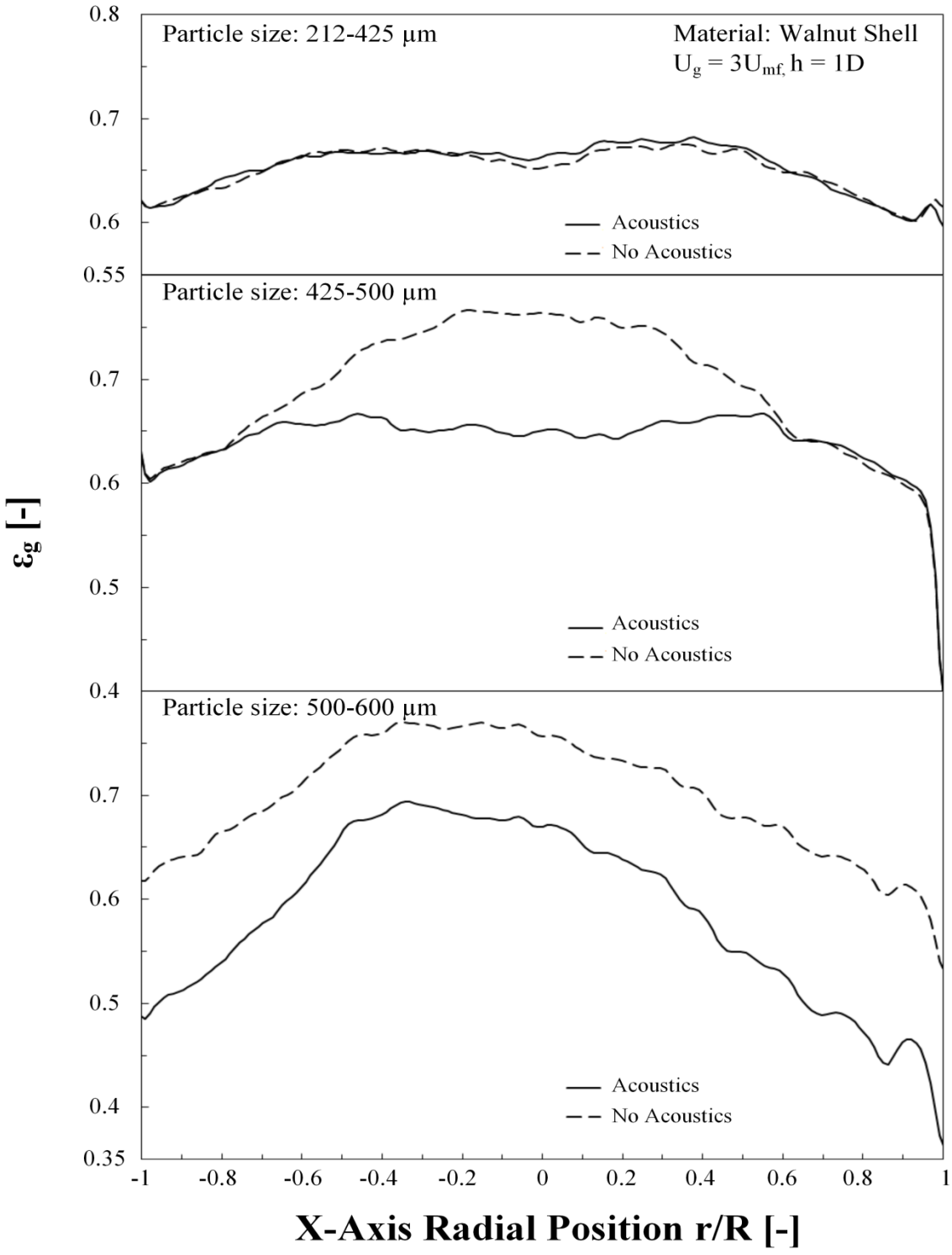

Figure 5.12b: Local gas holdup along the y-slice, as a function of location at h = 1D for different size ranges of ground walnut shell.

5.4 Conclusions

Local time-average gas holdup values obtained for fluidized beds filled with glass beads showed that the presence of an acoustic field produced a more uniform void fraction distribution compared to a fluidized bed without any acoustic intervention.

The acoustic field also influenced the jetting phenomena present near the aeration plate, where it was observed that the jets in the acoustic fluidized bed merged higher in the bed compared to the no acoustic condition. It was also observed that acoustic fluidized beds had fewer amounts of active jets than the no acoustic fluidized bed conditions, which allowed a more homogeneous gas holdup region deep into the bed.

Glass bead beds with small particles size ranges of 212-500 μm did not show any influence of acoustic intervention. Particles in the 500-600 μm range were influenced by acoustics and produced a more homogenous void fraction distribution for a fixed U_g relative to U_{mf}.

The presence of the acoustic field in a ground walnut shell fluidized bed had a strong dependence with the particle size ranges tested. For the particular frequency and sound pressure level tested, two out of the three particle size ranges did not exhibit any significant change in the void fraction distribution of the fluidized bed compared to the no acoustic case. While the 425-500 μm particle size ranges did exhibit differences between the acoustic and no acoustic case in void fraction distribution.

Acknowledgements

The X-ray facility used in this work was developed with support from the National Science Foundation under Grant No. CTS-0216367 and Iowa State University. The work in this study was supported through Iowa State University.

CHAPTER 6: CHARACTERIZING JETTING IN AN ACOUSTIC FLUIDIZED BED USING X-RAY COMPUTED TOMOGRAPHY[1]

David R. Escudero[2] and Theodore J. Heindel

Department of Mechanical Engineering

Iowa State University

Ames, Iowa 50011

Abstract

Understanding the jetting phenomena near the gas distributor plate in a fluidized bed is important to gas-solids mixing, heat and mass transfer, and erosion on any bed internals, which can all affect the performance of the bed. Moreover, acoustic vibration in a fluidized bed can be used to enhance the fluidization quality of the particulate matter and influence the jetting behavior. Characterizing the jetting structure using X-ray computed tomography in a 3D fluidized bed, with and without acoustic intervention, is the focus of this study. A 10.2 cm ID fluidized bed filled with glass beads and ground walnut shell, with material density of 2500 kg/m^3 and 1440 kg/m^3, respectively, and particle sizes ranging between 212-600 μm, is used in these experiments. X-ray computed tomography (CT) imaging is used to determine local time-average gas holdup. From this information, qualitative and quantitative characteristics of the hydrodynamic structure of the multiphase flow system are determined. Local time-average gas holdup images of the fluidized bed under acoustic intervention at a high superficial gas velocity

[1] In preparation for submission to *Chemical Engineering Journal.*
[2] Corresponding author

show that jets produced near the aeration plate merge with other jets at a higher axial position of the bed compared to the no acoustic condition. Acoustic fluidized beds also have a fewer number of active jets than the no acoustic fluidized bed, which allowed for a more homogeneous gas holdup region deep in the bed. Hence, the acoustic presence has a significant effect on the jetting phenomena near the fluidized bed distributor plate.

Keywords: Acoustic fluidized bed, hydrodynamics, jetting, X-ray computed tomography.

6.1 Introduction

Jetting has been studied extensively in the gas-solid fluidized bed literature; see for example Yang and Keairns (Yang and Keairns, 1987), Ettehadieh et al. (Ettehadieh et al., 1988), Guo et al. (Guo et al., 2001, Guo et al., 2001), Chen et al. (Chen et al., 2008), or Müller et al. (Müller et al., 2009). However, most of the studies focused on jetting produced by using a central vertical nozzle or focused on jetting produced by a horizontal nozzle penetrating a lightly fluidized bed. There is limited information available from studies of jetting produced by the distributor plate of a fluidized bed, even though the hydrodynamics that are produced around this area are of extreme importance to the performance of the bed.

Yang (Yang, 1998) made a comparison of the vertical jetting phenomena between a 30 cm and a 3 m diameter fluidized bed. He studied the momentum dissipation, the jet penetration depth, and the jet velocity profile by visual observation. He also proposed several correlations for the parameters studied above.

Wang et al. (Wang et al., 2010) used electrical capacitance volume tomography (ECVT) to calculate the volumetric solids holdup (related to the gas holdup) of a bubbling gas-solid fluidized bed with a corresponding horizontal penetrating the bed from the side. They concluded that the solids holdup in the region of the gas-solid mixture jet was higher than in the region near

a pure gas jet. Also, the penetration length of the horizontal gas-solid mixture jet was larger than a horizontal gas jet alone.

Jet structure in a 3D fluidized bed was studied by Pore et al. (Pore et al., 2010) using magnetic resonance imaging. They used different distributor plate configurations to study the jet-jet interactions, and the jet-wall interactions. They obtained maps of solid concentrations to investigate the jet stability under the different distributor configurations. They concluded that depending on the design of the distributor plate, the closer the jets are to each other, the more they bend toward each other. Likewise, jets that are near the wall have a tendency to bend towards the wall.

Guo et al. (Guo et al., 2010) studied the flow characteristics in a fluidized bed with jetting produced by a horizontal nozzle under acoustic assistance. They investigated the jet penetration depth and the particle concentration using an optical probe. They concluded that the jet penetration depth increased when an acoustic field of a certain sound pressure level and frequency was applied to the fluidized bed; they also concluded that sound waves have a different effect on particle concentration depending on the region of the bed.

Sound assisted fluidized beds have been studied in the literature because it has been shown that the inclusion of sound vibrations can help overcome fluidization problems in certain material types. Different behavior under sound vibrations have been observed by several investigators (Leu et al., 1997), (Guo et al., 2006), (Kaliyaperumal et al., 2011), (Levy et al., 1997).

Visual observations as well as invasive techniques have been used to determine the different characteristics of fluidized beds under the presences of acoustic waves (Herrera and Levy, 2001,

Si and Guo, 2008). Noninvasive techniques have also been used to investigate the effects of acoustic waves on the void fraction distribution in fluidized beds.

X-ray imaging has been used to study fluidized systems for several years (Heindel, 2011). They are a commonly employed noninvasive technique because they are safer than other nuclear based techniques (they can be turned on and off at will), have high spatial resolution, and can be controlled by varying the voltage or current to improve penetration or contrast; other nonintrusive techniques (gamma-ray computed tomography, electrical capacitance tomography, magnetic resonance imaging, etc.), that can also be used to study the characteristics of fluidized beds.

Heindel et al. (Heindel et al., 2008) developed an X-ray visualization facility to study different characteristics of opaque multiphase flows, from bubble columns to fluidized beds. Their facility is capable of utilizing three different X-ray imaging techniques: X-ray radiography, X-ray stereography, and X-ray computed tomography (CT).

X-ray CT imaging generates a 3D density map (image) of the object of interest. X-rays pass through the object and the intensity values are recorded with an imaging device from several projections. After the various projections are collected, computer algorithms reconstruct them to produce a 3D image of the object. However, due to the large number of projections that must be acquired in order to obtain a complete reconstruction of the object, this technique generally has poor temporal resolution. On the other hand, the multiple projections give a high spatial resolution to this technique, a characteristic that can be used to determine the local time-average gas holdup in a very efficient way (Escudero, 2010).

Escudero and Heindel (Escudero, 2010, Escudero and Heindel, 2011) used X-ray CT imaging to determine local time-average gas holdup in a 10.2 cm diameter fluidized bed to study the

effects of bed height, superficial gas velocity, and bed material on local conditions. They determined that the fluidization hydrodynamics are affected by using different bed materials (glass beads, ground corncob, and ground walnut shell), superficial gas velocities (U_g), and height-to-diameter ratios (H/D).

Most of the studies on jetting have focused in the hydrodynamic distribution created by a single central or horizontal nozzle. The goal of this study is to focus on the jetting phenomena created by the distributor plate of an acoustic fluidized bed using images obtained via X-ray computed tomography.

6.2 Experimental Setup

Certain aspects of the experimental setup are described in this section. A cylindrical, D = 10.2 cm diameter, cold flow sound assisted fluidized bed reactor is used in this study. To induce the acoustic vibration in the fluidized bed, a loudspeaker is located at the top of the fluidized bed. This speaker emits sine waves that are generated using a function generator at different frequencies with a specific amplitude controlled by an amplifier, more details of the entire setup can be found in Escudero and Heindel (Escudero and Heindel, 2014).

The distributor plate used for this study is fabricated from a 1.27 cm thick acrylic plate with 62, 1 mm diameter holes spaced approximately 1.27 cm apart in a circular grid for a total open area of 0.60 % (Figure 6.1).

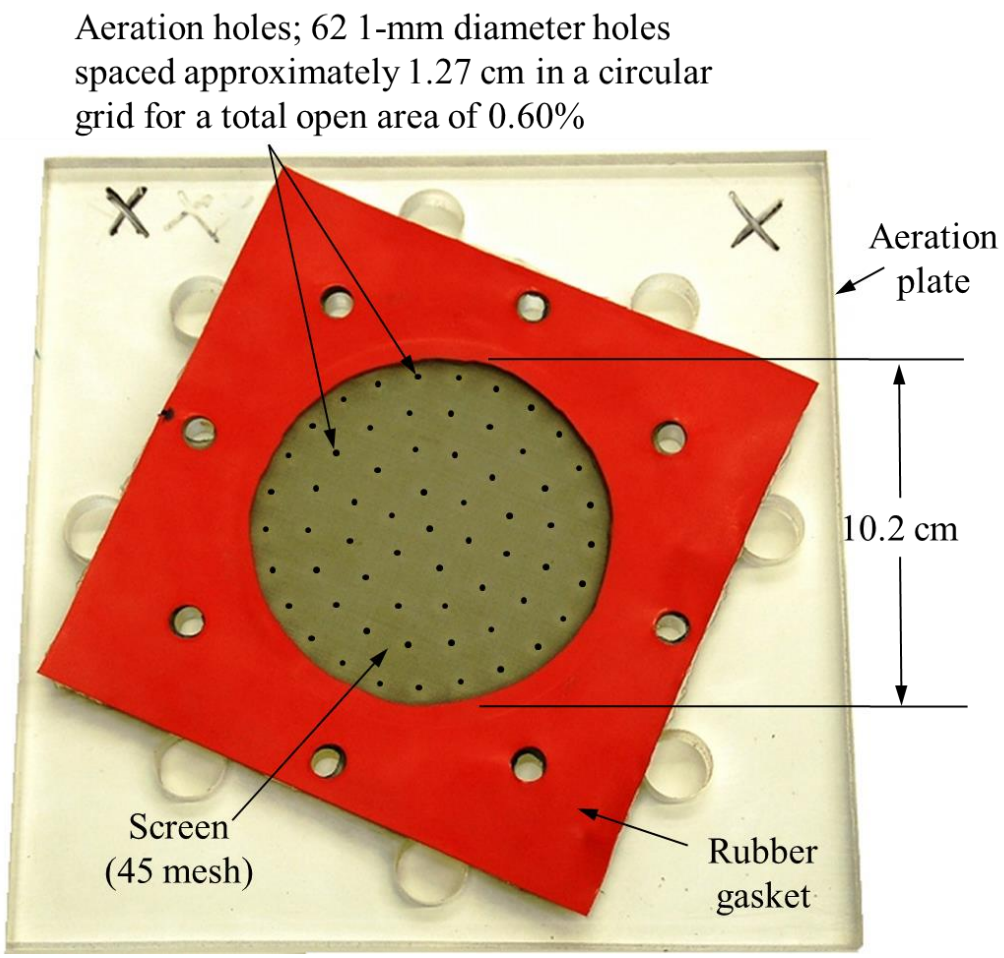

Figure 6.1: Actual aeration plate used in this study.

The acoustic conditions used in this study in terms of frequency and sound pressure level were fixed at 150 Hz and 120 dB for glass beads, and 200 Hz and 110 dB for ground walnut shell, which are the conditions determined by Escudero and Heindel (Escudero and Heindel, 2013) to produce the lowest minimum fluidization velocities for the given conditions.

The materials used in these experiments are glass beads (ρ_{glass} = 2500 kg/m^3) and ground walnut shell (ρ_{walnut} = 1440 kg/m^3), with particles sizes that range from 212 – 600 μm. The material is sifted several times using a mechanical shaker and sieves with different mesh sizes to ensure the material falls in the desired particle size range. The bed bulk density was determined

using the material mass and the static bed volume. Bed material is slowly added until the desired static bed height (H) is reached, which corresponds to H/D = 0.5, 1, and 1.5. Before the bed height is measured, the bed is fluidized and then allowed to collapse to avoid any packing effects due to the filling process. The material mass is then measured and the given bed bulk density is calculated. Table 6.1 summarizes the general bed characteristics.

Table 6.1: Summary of material properties.

	Glass Beads			Ground Walnut Shell		
H/D	**0.5**	**1**	**1.5**	**0.5**	**1**	**1.5**
Bed Mass (g)	620	1240	1860	250	500	750
Bulk density (kg/m^3)	1505	1505	1505	610	610	610
Diameter (µm)	212-425, 425-500, 500-600			212-425, 425-500, 500-600		
Particle Density (kg/m^3)	2500			1440		
U_{mf} no acoustic bed (cm/s)	8.8	11	15	4	6.6	12.2
U_{mf} acoustic bed (cm/s)						
212-425 µm	8.1	8.0	8.3	3.7	3.9	3.7
425-500 µm	9.1	8.8	8.5	4.8	3.7	4.4
500-600 µm	11.5	10.1	10.3	8.5	8.6	11

X-ray computed tomography (CT) scans are captured with and without acoustic intervention at different H/D ratios (0.5, 1, 1.5) and different superficial gas velocities $U_g = 1.5\ U_{mf}$ and $3\ U_{mf}$, where U_{mf} is the minimum fluidization velocity previously determined (Escudero and Heindel, 2013). The minimum fluidization velocity differs between the acoustic and the no acoustic fluidized bed.

The X-ray equipment used in this research is described in detail by Heindel et al. (Heindel et al., 2008); the procedure used for this study is described in detail in (Escudero and Heindel, 2014).

To calculate the local time-average gas holdup information, data obtained from the CT reconstruction volume files are used. Gas holdup is the volumetric gas fraction present in the

gas-solid fluidized bed, and is useful to characterize the hydrodynamic behavior of this multiphase flow system. Escudero and Heindel (Escudero and Heindel, 2011, Escudero and Heindel, 2013, Escudero and Heindel, 2014) describe the mathematical equations used to quantify the local time-average gas holdup, ε_g; the data obtained from that previous study are used to analyze the jetting phenomena that occurs near the distributor plate with and without acoustic intervention.

Using image analysis software, each of the volumetric pixels (voxels) in the gas holdup volume file is analyzed to determine the edge of each jet present inside the fluidized bed. To identify the jets, the voxel of interest is first determined to be located inside the fluidized bed. Then, the center of the fluidized bed is located in the xy-plane. Once the center is located, the radius of the fluidized bed is determined (for the parameters of this study, the radius of the fluidized bed is equal to 86 voxels). Once the radius is determined, the next step is to ensure that the distance from the center of the bed to the voxel of interest is less than or equal to the radius of the bed.

To identify a jet, the gas holdup in a voxel of interest is compared to the neighboring local average gas holdup value. The local average gas holdup is determined by averaging the neighboring voxel gas holdup found in the same xy-plane and within a specified radius of the voxel of interest, making sure that only voxels that are within the fluidized bed are used in the average. The local average contains only voxels located in a single xy-plane because the vertically changing interface between the jet and the rest of the bed would otherwise skew the average. The average is localized so that sharp differences, such as that between a jet and the rest of the bed, are more clearly defined.

A circular area for the local average value is used because the jets are assumed to be roughly circular, and the bed is circular. The optimal radius for the local average area is approximately the distance from the center of a jet to the next closest jet. This is done to minimize the effect of the surrounding jets. If surrounding jets are included in the averaging region, a higher value of local average gas holdup can be obtained, skewing the average producing unfavorable results. Figure 6.2 demonstrates this principle; for this study the optimal radius is 18 voxels. The area inside the black circle is the region included in the average of the gas holdup values.

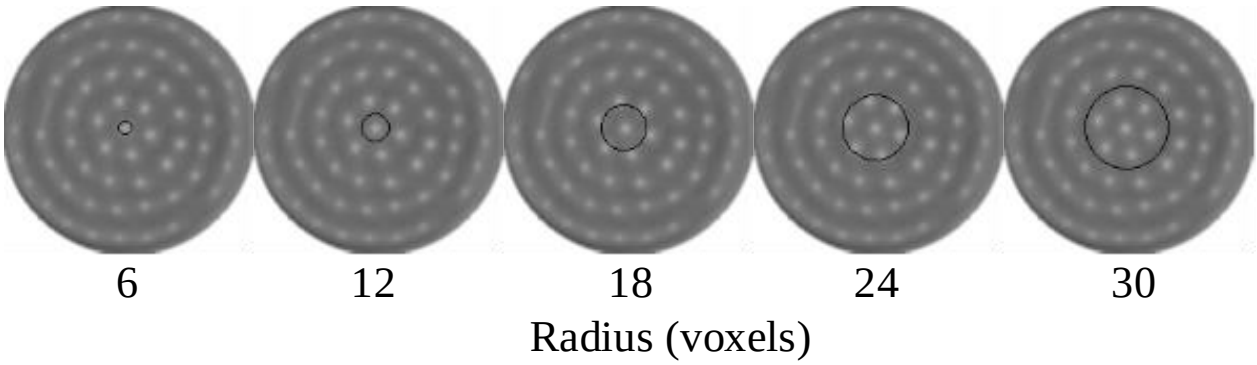

Figure 6.2: Different radius averaging regions for jet identification. The lighter regions indicate a higher gas holdup, indicating a jet location.

Finally, if the gas holdup value in the voxel of interest is a specified threshold greater than the local average (10% for this study), it is marked as likely being located within a jet. Otherwise, it is left unmarked. The jet regions are then identified as all white and the non-jet region is identified as all black. Figure 6.3 shows y-slice planes at different thresholds for glass bead and ground walnut shell volume files, respectively. The threshold of 10% is chosen based on the number of voxels marked as a jet. Beyond 10%, the number of voxels marked as jets decrease, artificially eliminating useful data.

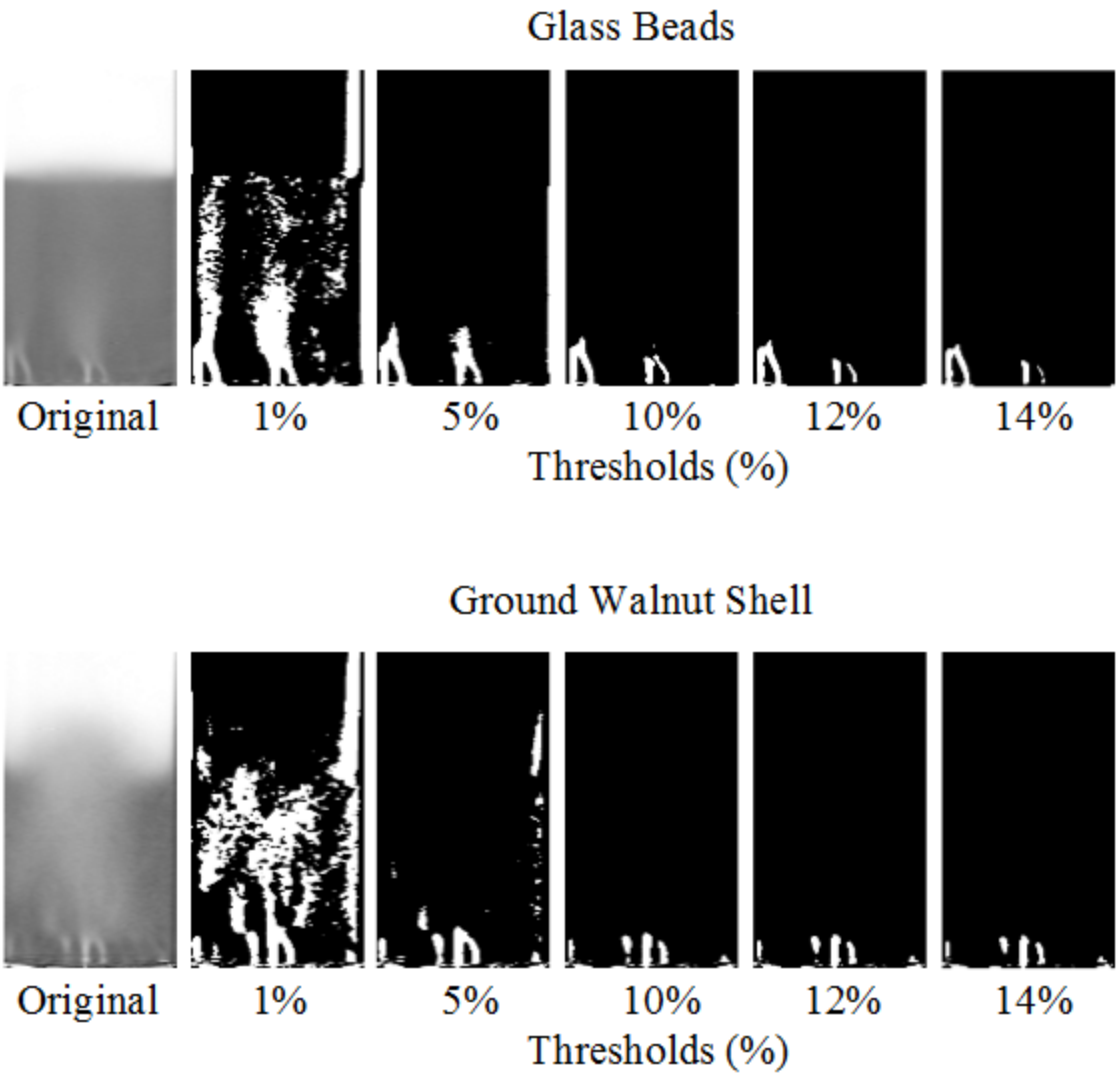

Figure 6.3: Different threshold percentages for glass beads and ground walnut shell.

To define individual jets, the image of the fluidized bed is assumed to be located in 3D space such that the aeration plate is located at z-slice = 0 and all voxels have positive, integer values for all x, y, and z locations within the bed. The image is analyzed by looking at all the local voxel gas holdup values, compared to the local voxel average, in one xy-plane and then continuing to the next xy-plane.

Each jet is defined in a grouping of voxels that are determined to have a local gas holdup higher than the local average by the given threshold. For each voxel defined to be in a jet, it is first checked to see if the voxel of interest, labeled as (x, y, z), is found adjacent to a jet grouping. If so, the voxel is added to the jet grouping. If not, a new jet group is defined starting with the voxel of interest.

Eventually, jets merge and lose their individual identities but are still strong enough to be considered jets. Therefore, the merged jets are divided so that a more accurate description of the jets can be given. In order to do this, the jets are assumed to have an approximate circular cross-section, and the center of each jet is calculated in each xy-plane. If an area of voxels that are marked as within a jet by the initial analysis is determined to be over the centers of more than one jet, the marked area is divided such that the voxels closest to each jet center are added to that jet's group.

The initial analysis that defines which voxels are within jets will necessarily have some voxels marked as within jets that are not actually part of a jet. This "noise" is eliminated with filtering in the identification of individual jets. One filter through which the data are passed determines if the group of voxels identified as a jet begins at the aerator plate. If it does not, then the group of pixels is not a jet. If the number of identified jets is still higher than the number of aeration holes in the aeration plate, another filter successively removes the groups with the smallest number of voxels identified until the appropriate number of jets is established. It is assumed that the small number of voxels in the group indicates that the group is not a jet and is simply "noise" from the original analysis.

Several parameters have been used to characterize jet geometric features. For this study, the jet length (L_j) and expansion angle (α_j) (Figure 6.4) are determined using the image analysis

software, then these parameters are compared with proposed correlations available in the literature (Table 6.2) to validate the method used in this study. All of the correlations presented in Table 6.2 are for multiple vertical jets without any acoustic intervention.

Table 6.2: Jet length and half angle published correlations

References	Correlation
Jet Length	
Blake et al. (Blake et al., 1990)	$\frac{L_j}{d_o} = 22.1 \times \left(\frac{U_j^2}{g d_o}\right)^{0.268} \left(\frac{\rho_f}{\rho_p}\right)^{0.189} \left(\frac{\rho_p U_j d_p^2}{\mu d_o}\right)^{-0.163} \left(\frac{D}{d_o}\right)^{0.077} \left(\frac{P_o}{d_o}\right)^{-0.102}$
Muller et al. (2009)	$\frac{L_j}{d_o} = 8.7 \times \left(\frac{\rho_f d_o}{\rho_p d_p}\right)^{0.64} \left(\frac{U_j^2}{g d_o}\right)^{0.31}$
Rees et al. (2006)	$\frac{L_j}{d_o} = 2.77 \times \left(\frac{d_o^2}{A_o}\right)^{0.29} \left(\frac{U_j^2}{g d_o}\right)^{0.24} \left(\frac{U_{mf}^2}{g d_o}\right)^{-0.034}$
Wen et al. (Wen et al., 1982)	$\frac{L_j}{d_o} = 1.15 \times 10^4 \times \left(\frac{\left(U_j - U_{mfj}\right)^2}{g d_p}\right)^{0.42} \left(\frac{\rho_f}{\rho_p}\right)^{1} \left(\frac{\rho_f d_p \left(U_j - U_{mfj}\right)^2}{\mu}\right)^{-0.42} \left(\frac{d_p}{d_o}\right)^{0.66}$
Jet Half Angle	
Rees et al. (2006)	$\alpha_j = 2.86 \times \left(\frac{d_o^2}{A_o}\right)^{-0.41} \left(\frac{U_j^2}{g d_o}\right)^{-0.059} \left(\frac{U_{mf}^2}{g d_o}\right)^{0.33}$

For each group identified as a jet, the jet length must be identified. In order to do this, the xy-plane in which a jet no longer has any voxels identified as within a jet directly above it is defined as the top of the jet. The number of voxels between the aeration plate and the top of the jet are counted, and the number of voxels is then converted into a physical distance using a conversion factor based on the resolution of the CT images originally obtained using x-rays. This conversion factor accounts for 0.59 mm per voxel.

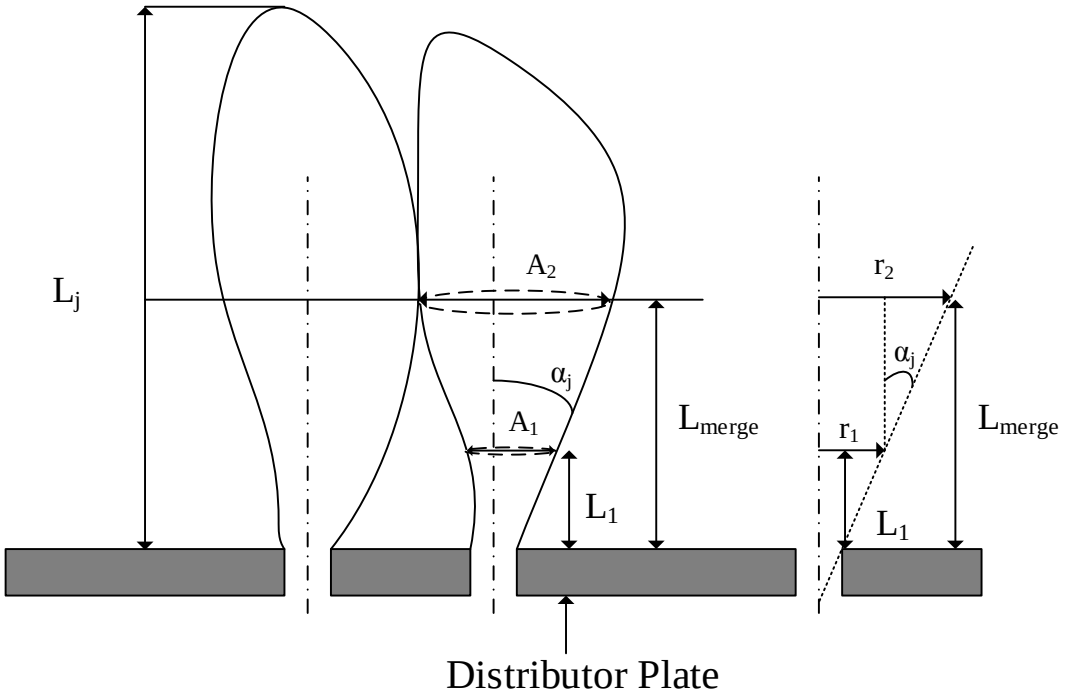

Figure 6.4: Geometrical parameters of the jets.

In order to define a jet expansion angle (α_j), the jets are assumed to be approximately conical in shape. Also, the expansion angle is calculated using only voxels located beneath the point at which the jet touches another jet and thereby merges. The height (L_1) and area of the smallest cross section of a jet (A_1) beneath a merged region is recorded as well as the merge height (L_{merge}) and area of the largest cross section of a jet (A_2) beneath the merged region. From the areas, the effective radii of the respective cross sectional areas are calculated. Using the distance between the cross sectional areas and their lengths above the distributor plate, the expansion angle can be calculated via similar triangles (Figure 6.4):

$$\alpha_j = \tan^{-1}\left[\frac{(r_2 - r_1)}{(L_{merge} - L_1)}\right] \tag{6.1}$$

6.3 Results and Discussion

6.3.1 Qualitative characterization

Figure 6.5 and Figure 6.6 shows different 2D images through the center of a fluidized bed of 500-600 µm glass beads and ground walnut shell with and without acoustic intervention for two different superficial gas velocities, respectively. The images in Figure 6.5 and 6.6 represent the original gas holdup volume file in grayscale next to the black and white images that were created using the jet identifier software. Note that only jets identified in this plane are visible, but in general, the entire 3D jet region is identified.

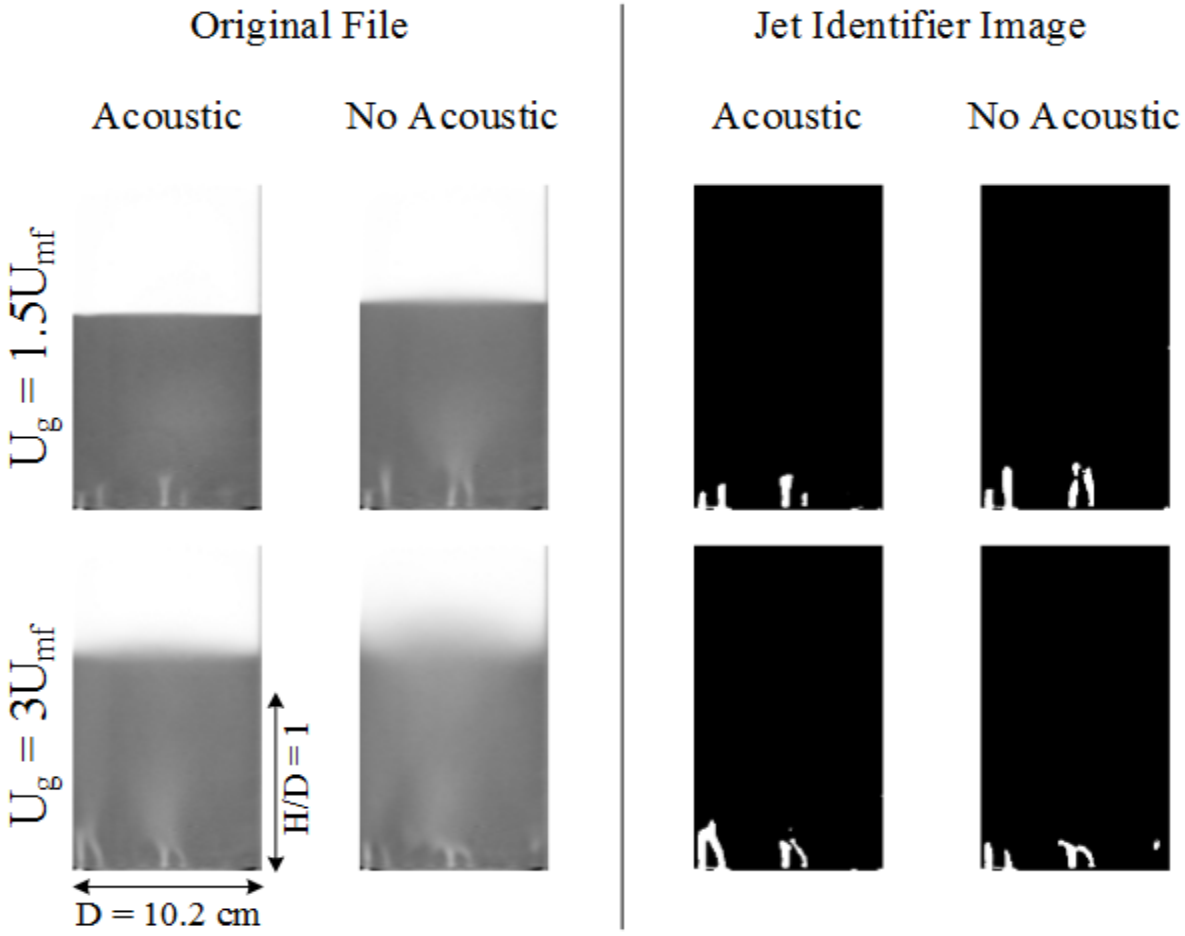

Figure 6.5: Single slice images of jetting for 500-600 µm glass beads with and without acoustic intervention for $U_g = 1.5U_{mf}$ and $U_g = 3U_{mf}$.

As Figure 6.5 shows for $U_g = 1.5U_{mf}$, the no acoustic fluidized bed condition exhibit larger jets that penetrate farther into the bed than the ones observed in the acoustic fluidized bed. In contrast, Figure 6.6 shows larger jets for the no acoustic condition at lower superficial gas velocity for ground walnut shell. Moreover, by examining multiple 2D slice images for $U_g = 1.5U_{mf}$, both materials show more jet-jet interactions in the no acoustic case, where jet merging is more prevalent. This phenomenon can also be observed in the original image.

As the superficial gas velocity increases to $U_g = 3U_{mf}$, jets become larger for the acoustic condition for both materials. This phenomenon is attributed to the fact that as superficial gas velocity increases, the effect of the acoustic vibrations is more prominent where the vibrations produced by the sound waves create paths where air can easily break through, allowing the jets to be larger in size than the jets produced without any acoustic excitation.

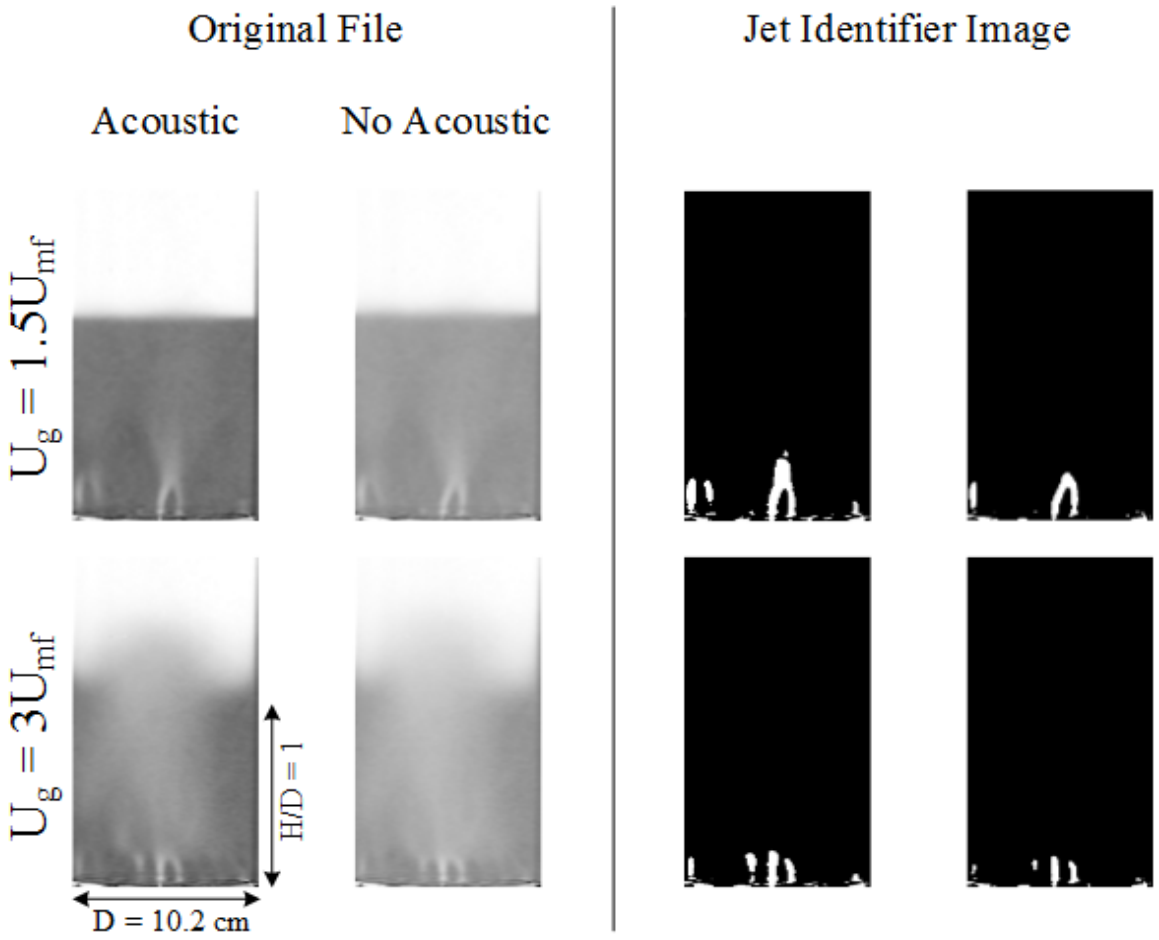

Figure 6.6: Single slice images of jetting for 500-600 µm ground walnut shell with and without acoustic intervention for $U_g = 1.5U_{mf}$ and $U_g = 3U_{mf}$.

Different particle sizes were tested to compare the different effects, if any, that the acoustic vibration has on jetting when the particle diameter is changed while the superficial gas velocity remains constant at $U_g = 3U_{mf}$. As shown in Figure 6.7 for glass beads, the differences in jetting between the acoustic and the no acoustic case are more apparent for the 500-600 µm particles. Similar results are found in ground walnut shell particle beds. However, to fully understand and visualize the effects of acoustic vibration on the jetting phenomena, different 3D images of the jets produced by the aeration plate for both conditions were created and presented in Figure 6.7.

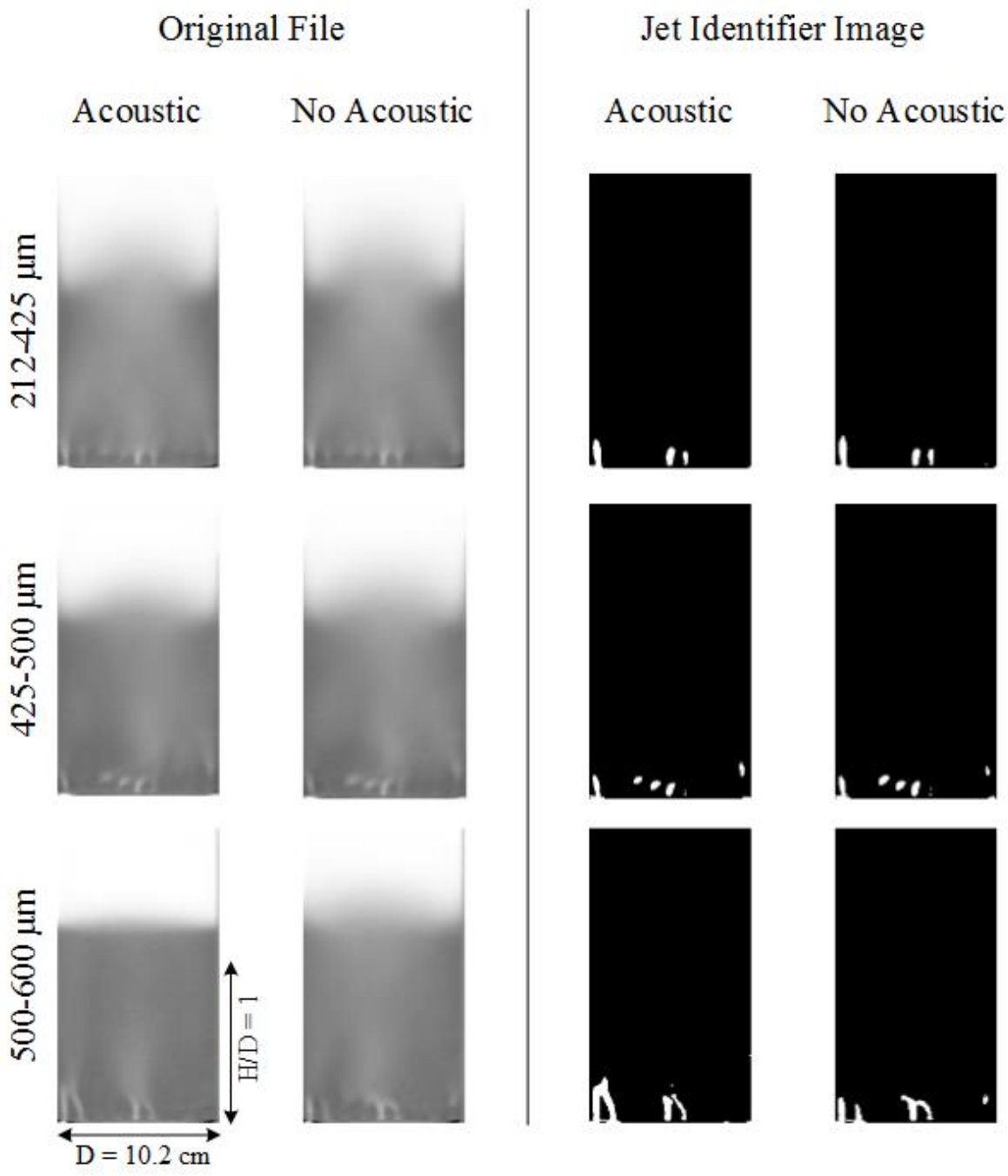

Figure 6.7: Single slice images of jetting at $U_g = 3U_{mf}$ for glass beads with different particle size ranges.

Figures 6.8a and 6.8b show 3D representations of the jets produced by the aeration plate for a bed of 425-500 µm glass beads with and without acoustic intervention, respectively. As shown

for both conditions, the structure and length of the jets are similar, and the direction at which they extend in both images is also similar. It is interesting to see that four jets merge in the same location for both conditions. Figures 6.8a and 6.8b clearly show that for this particular particle size range and material, the addition of sound vibrations produces a negligible qualitative change in the jetting phenomena in a fluidized bed. Similar results were observed in the smallest particle size range for both materials.

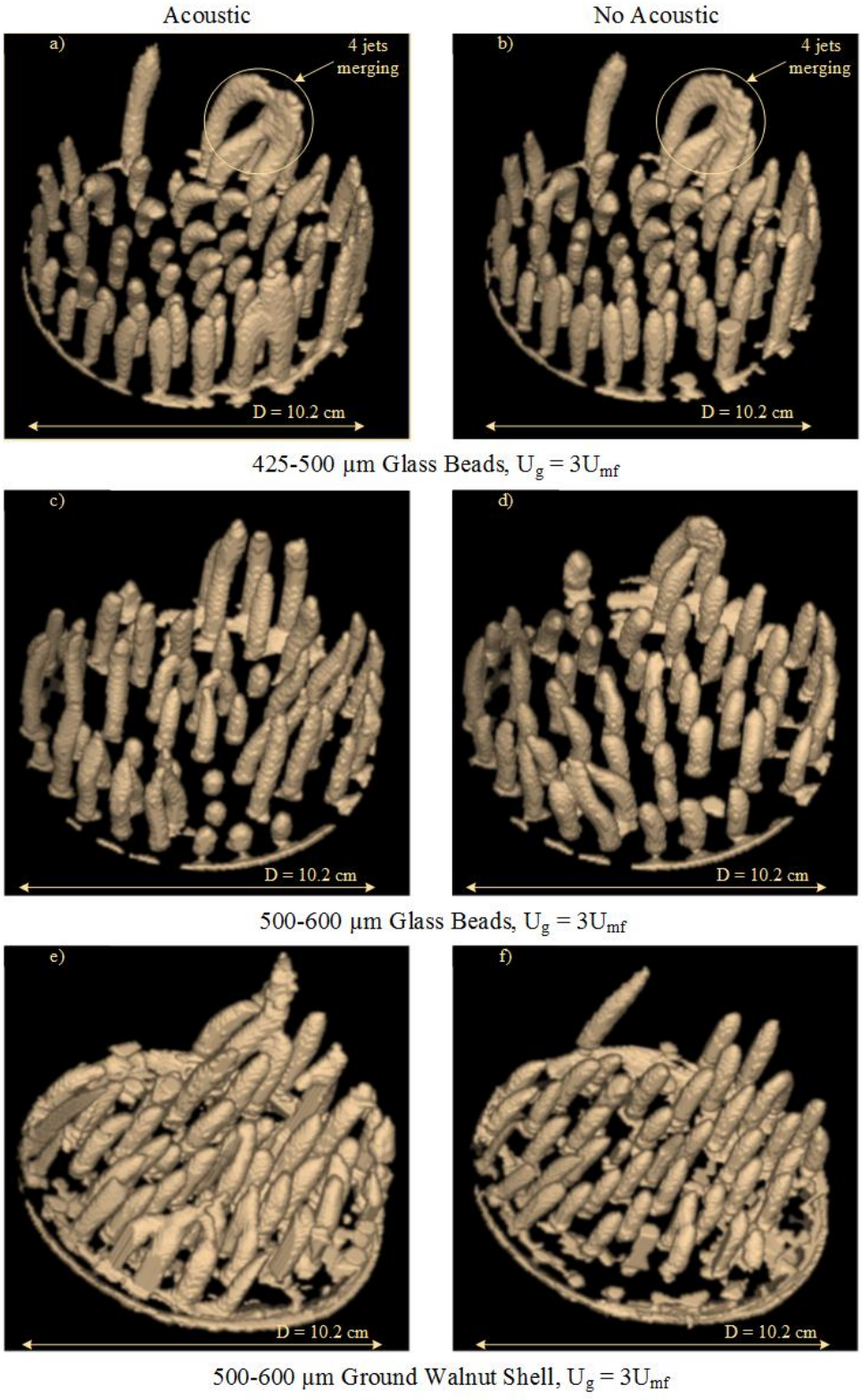

Figure 6.8: 3D image of the jets for a fluidized bed of glass beads (425-500 µm, 500-600 µm) and ground walnut shell (500-600 µm) with and without acoustic intervention.

Conversely, Figures 6.8c and 6.8d show the 3D representation of the jets for 500-600 µm glass beads. As Figure 6.8c shows when the fluidized bed has acoustic intervention, the length of the jets appear to be longer than the same jets shown in Figure 6.8d without acoustic intervention particularly the jets that are located near the walls of the fluidized bed; emphasizing the observations from the 2D images in Figures 6.5 and 6.7.

Moreover, these images show than for the acoustic case, there are less active jets present in the fluidized bed, some of the holes from the distributor do not show any jet formation compared to the same holes in the no acoustic case; this difference is attributed to the different superficial gas velocity that is applied to the fluidized bed, which is a consequence of different minimum fluidization velocities in the presence of the acoustic wave inside the fluidized bed (Escudero and Heindel, 2013).

In addition, 3D representation of the jets in a ground walnut shell fluidized bed (Figure 6.8e and 6.8f) show that for the acoustic case the jets are larger than the jets for the no acoustic case. Moreover, the acoustic case for ground walnut shell shows more jet to jet interaction than the no acoustic case. In both cases, the jets apparently have a tendency to bend towards the center of the bed than towards the walls of the fluidized bed as previous studies showed when the superficial gas velocity is higher than the minimum fluidization velocity (Pore et al., 2010).

6.3.2 Quantitative characterization

Using the images obtained for the previous analysis, important features of the jets can be determined. Figure 6.9 shows the average jet length as a function of the jet velocity for the different correlations summarized in Table 6.2, as well as the results obtained for the experimental data, for 500-600 µm glass beads with and without acoustic intervention. The error

bars in the figure represent the error associated with the calculations of the jet length using the image analysis software.

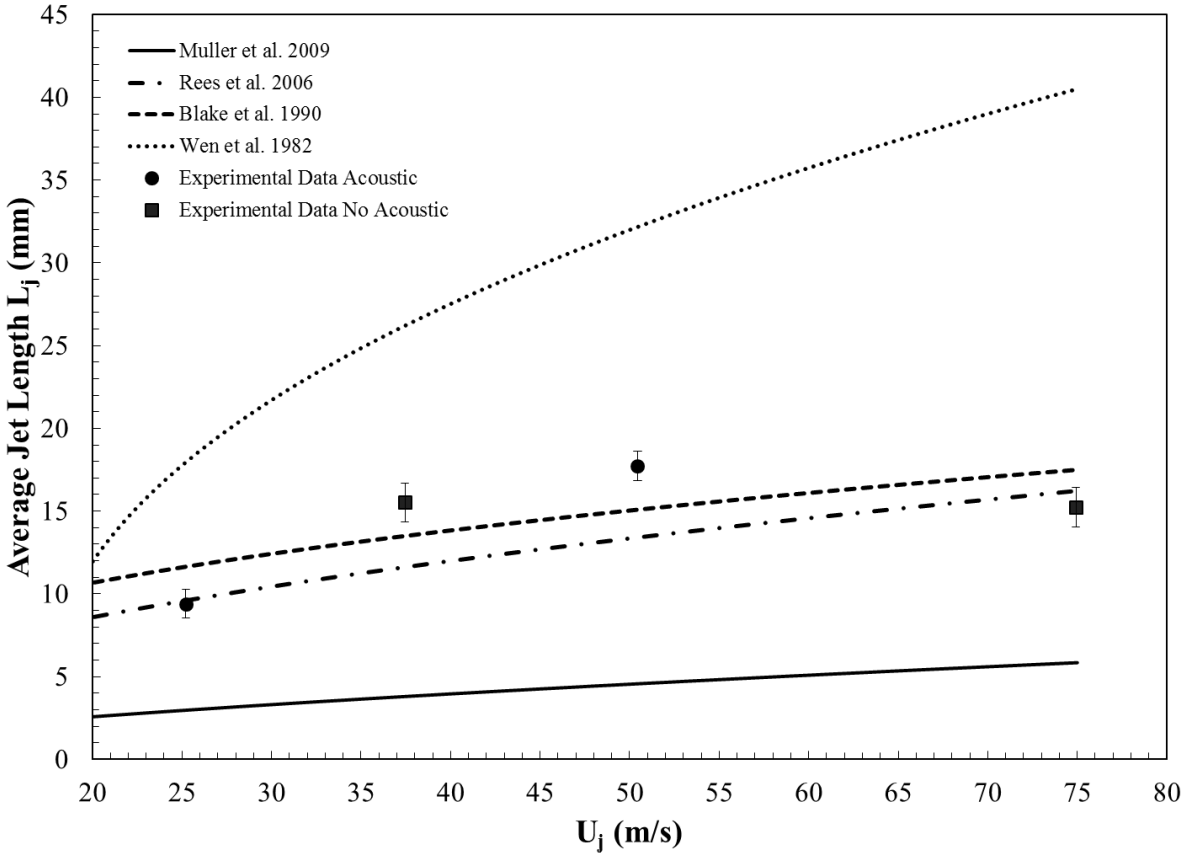

Figure 6.9: Average jet length as a function of jet velocity for a fluidized bed of 500-600 μm glass beads with and without acoustic intervention.

As seen in Figure 6.9 as the jet velocity increases the average jet length from the correlations increase, due to the fact that for these correlations the average jet length is directly proportional to the jet velocity. However, the no acoustic experimental data does not follow the trend observed by the correlations even though the magnitudes obtained for the average jet length at the two different tested velocities correlate well with the values obtained by two of the correlations. Conversely, as the jet velocity increases, the experimental average jet length for the acoustic bed shows an increase, following the trend obtained with the correlations. The fact that under the acoustic case the average jet length does increase with an increasing velocity can be

explained by the fact that with the additional vibration imparted to the particles cause the jets to penetrate farther into the bed, allowing the jets to grow longer before they merge with adjacent jets. These results can be observed also in the qualitative images (Figure 6.8c and 6.8d).

For the ground walnut shell case, the average jet length for the acoustic and the no acoustic intervention decreases slightly as jet velocity increases. This particular behavior was also observed in the qualitative image (Figure 6.6). It is hypothesized that because the ground walnut shell is less dense than the glass beads, the jets merge and lose their identity as the jet velocity increases. Note, however, that actual jet length in ground walnut shell beds is larger than that in glass bead beds, and the acoustic bed has slightly larger jet lengths that the no acoustic bed.

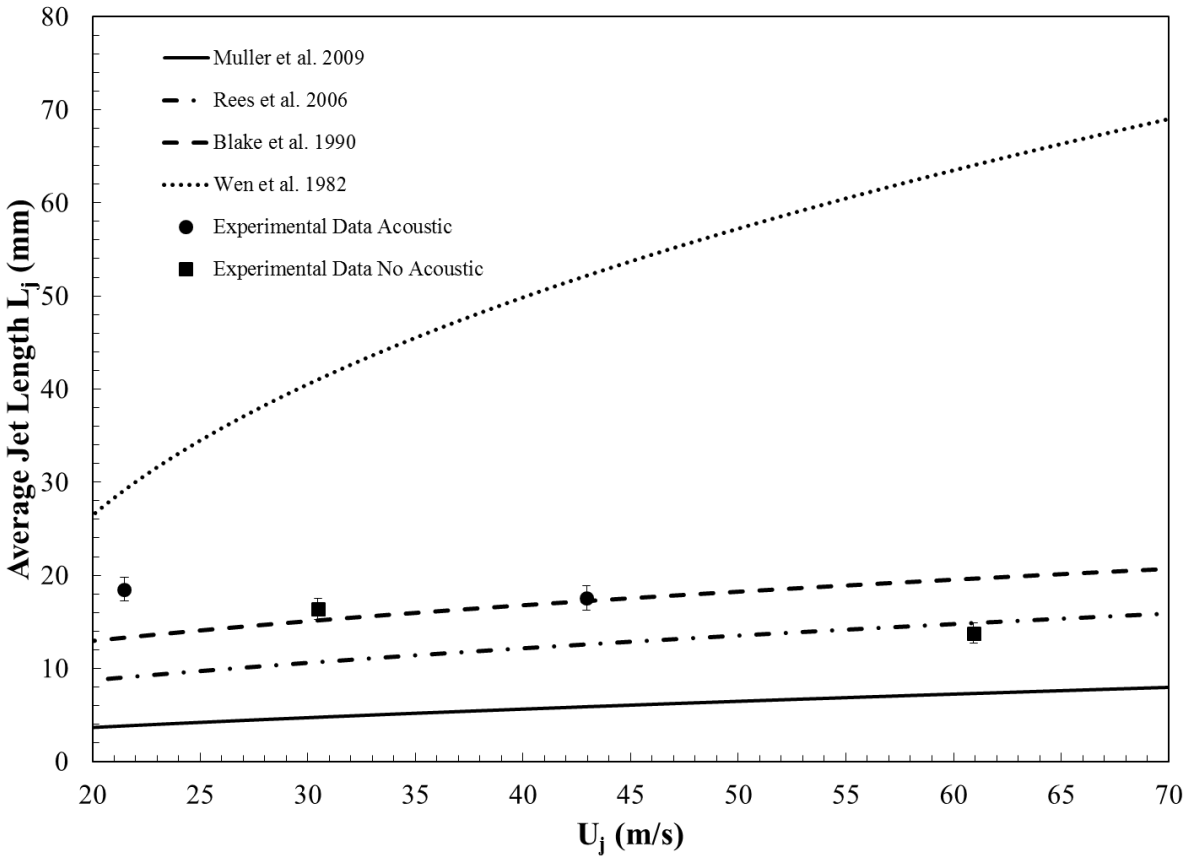

Figure 6.10: Average jet length as a function of jet velocity for a fluidized bed of 500-600 μm ground walnut shell with and without acoustic intervention.

The average jet length between the fluidized bed with and without acoustic intervention can be observed in Figures 6.11 and 6.12 for glass beads and ground walnut shell for two different particles sizes, respectively. Figure 6.11 shows that for jet velocities closer to the minimum fluidization velocity ($U_j/U_{mf} = 1.5$) and for a finer particle size there is an slight increase in the average jet length (~3.3%) when the fluidized bed is under the acoustic intervention. Moreover, at the same jet velocities for the larger particles the no acoustic case exhibit larger jet lengths than the acoustic case, which was also concluded from the qualitative images (Figure 6.5). The error bars in the figures represent the error associated with the calculations of the jet length using the image analysis software.

As the jet velocity increases in comparison with the minimum fluidization velocity ($U_j/U_{mf} = 3$), the average length of the jets for the acoustic case for the two different particle sizes are approximately 9-16% larger than the no acoustic case, suggesting again that the addition of the sound vibrations creates, on average, longer jets inside the fluidized bed. The presence of the sound energy in the fluidized bed allows larger bubbles to break into smaller ones, increasing the presence of solid particles; this increase in solid concentration increases the jet momentum dissipation allowing the jets to penetrate further into the bed. This phenomenon is more clearly observed at high jet velocities for both of the bed materials used in the study (Figure 6.11 and Figure 6.12).

It is also interesting to notice that at the same jet velocity, as particle size increases the average jet length decrease for the bed material without acoustic intervention (Figure 6.11 and Figure 6.12). This phenomenon is attributed to the fact that as particle size increases, the drag force produced by the jet increases suggesting there is more gas bypassing between the particles

and the gas phase, creating a decrease in the jet length. When acoustic vibration is applied, the previously described phenomenon is not observed for both glass beads and ground walnut shell.

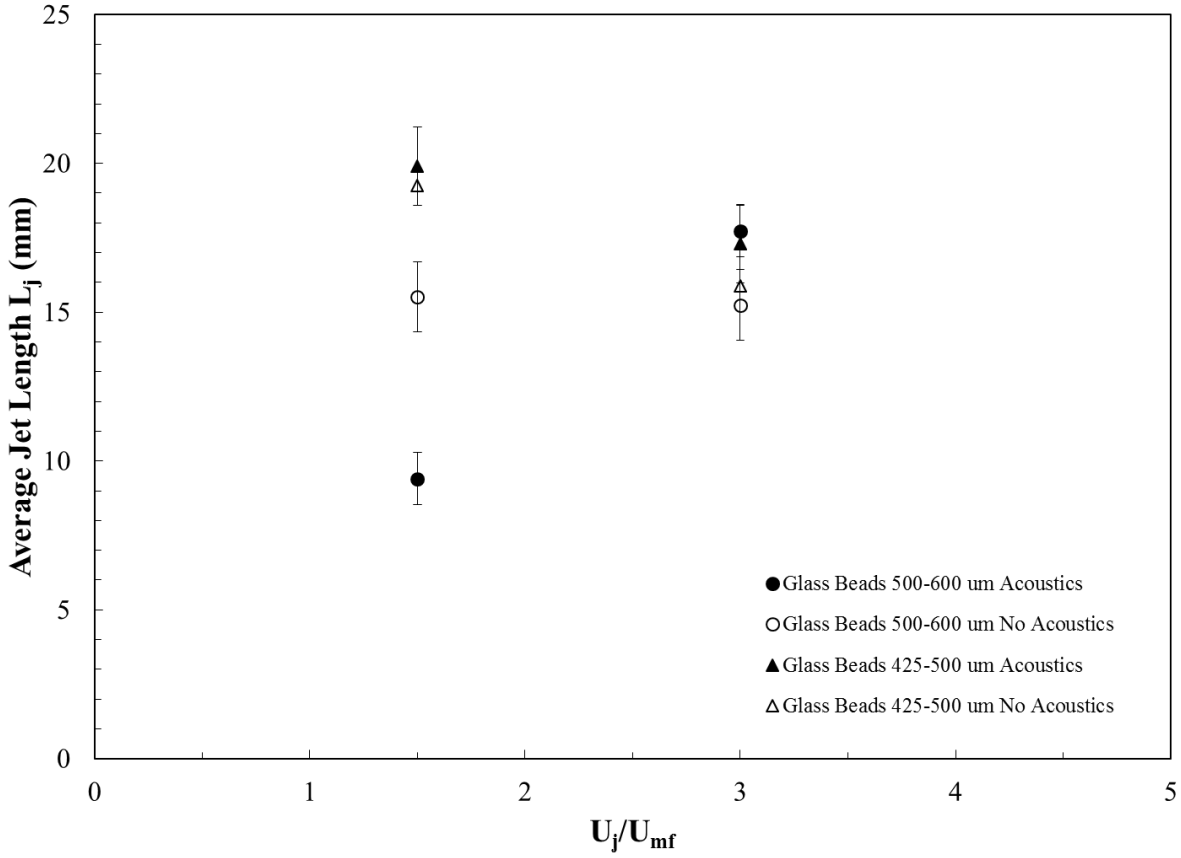

Figure 6.11: Average jet length as a function of U_j/U_{mf} for glass beads with different particle size with and without acoustic intervention.

The expansion angle of the jets is calculated using the procedure explained above. Figure 6.13 shows the comparison of the experimental results obtained for glass beads with and without acoustic intervention with the correlation proposed by Rees et al. (Rees et al., 2006). The correlation over predicts the measurements of this study; however, for both cases, as the jet velocity increases, the expansion angle decreases, following the trend observed by the correlation and by others in the literature.

Figure 6.14 shows that for the smaller particles of glass beads with and without acoustic intervention, there is an increase in the average expansion angle as the jet velocity increases,

suggesting that as the jet velocities increase, jets are spreading more quickly out of the holes of the distributor plate. Conversely, with larger particles, the jet expansion angle decreases as jet velocities increase, indicating that when larger particles surround the jets, there is no room for them to spread as fast as with smaller particles, thus, creating smaller expansion angles.

Furthermore, as Figures 6.13 and 6.14 show, when acoustic vibrations are applied to the fluidized bed, a higher expansion angle is generally observed when compared to a no acoustic case.

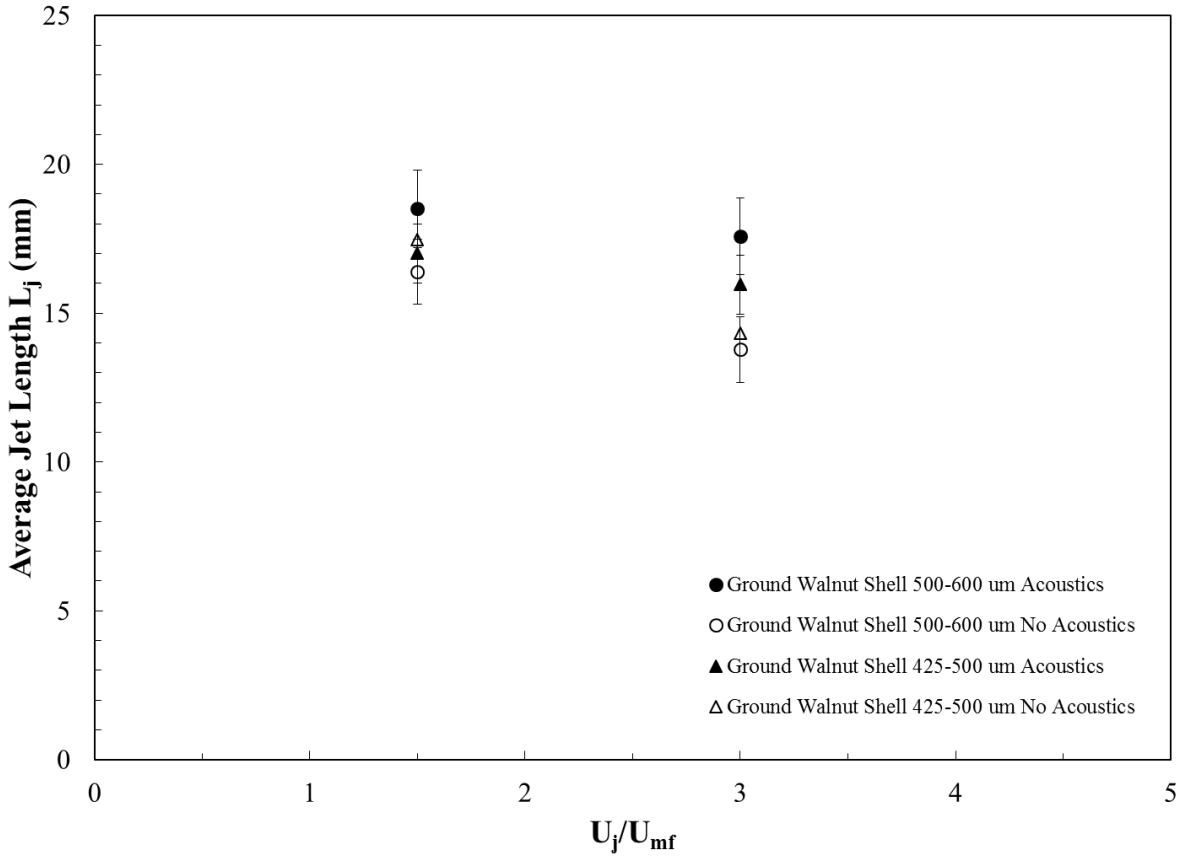

Figure 6.12: Average jet length as a function of U_j/U_{mf} for ground walnut shell with different particle size with and without acoustic intervention.

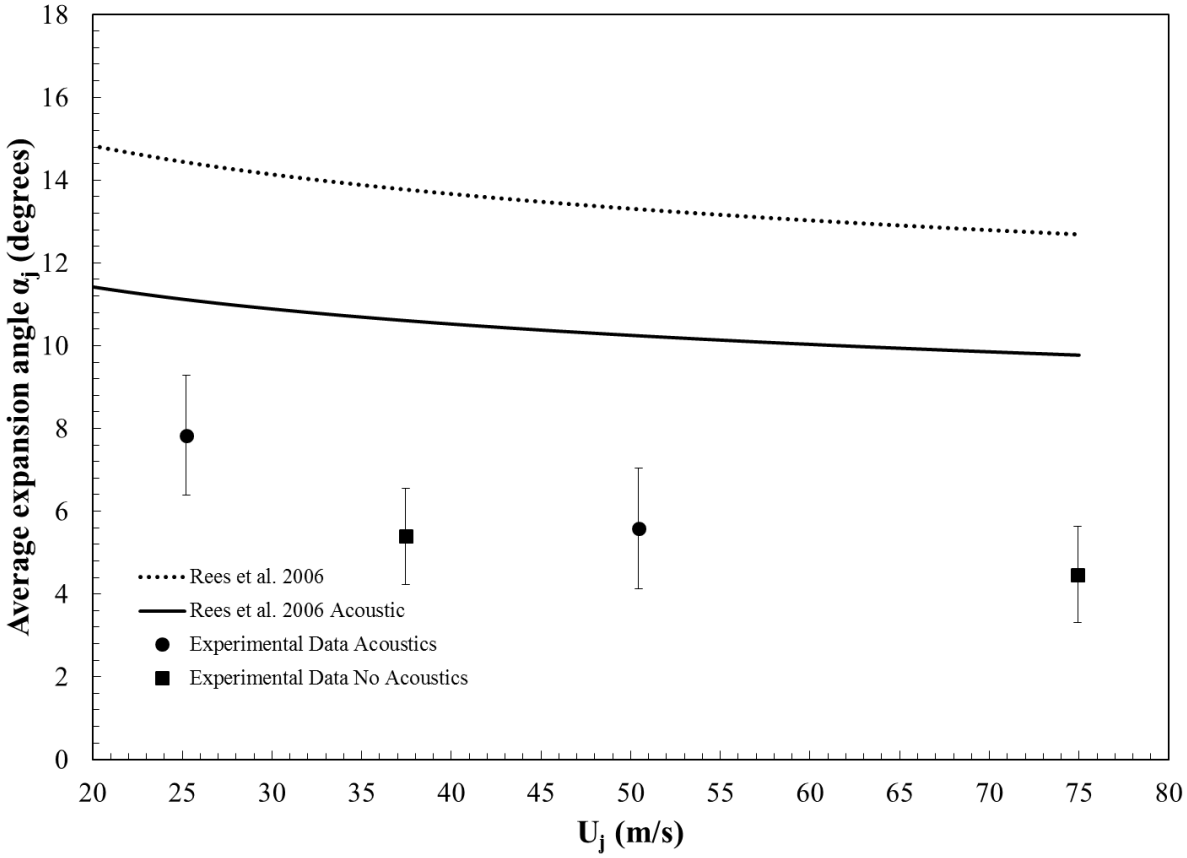

Figure 6.13: Average expansion angle as a function of jet velocity for a fluidized bed of 500-600 μm glass beads with and without acoustic intervention.

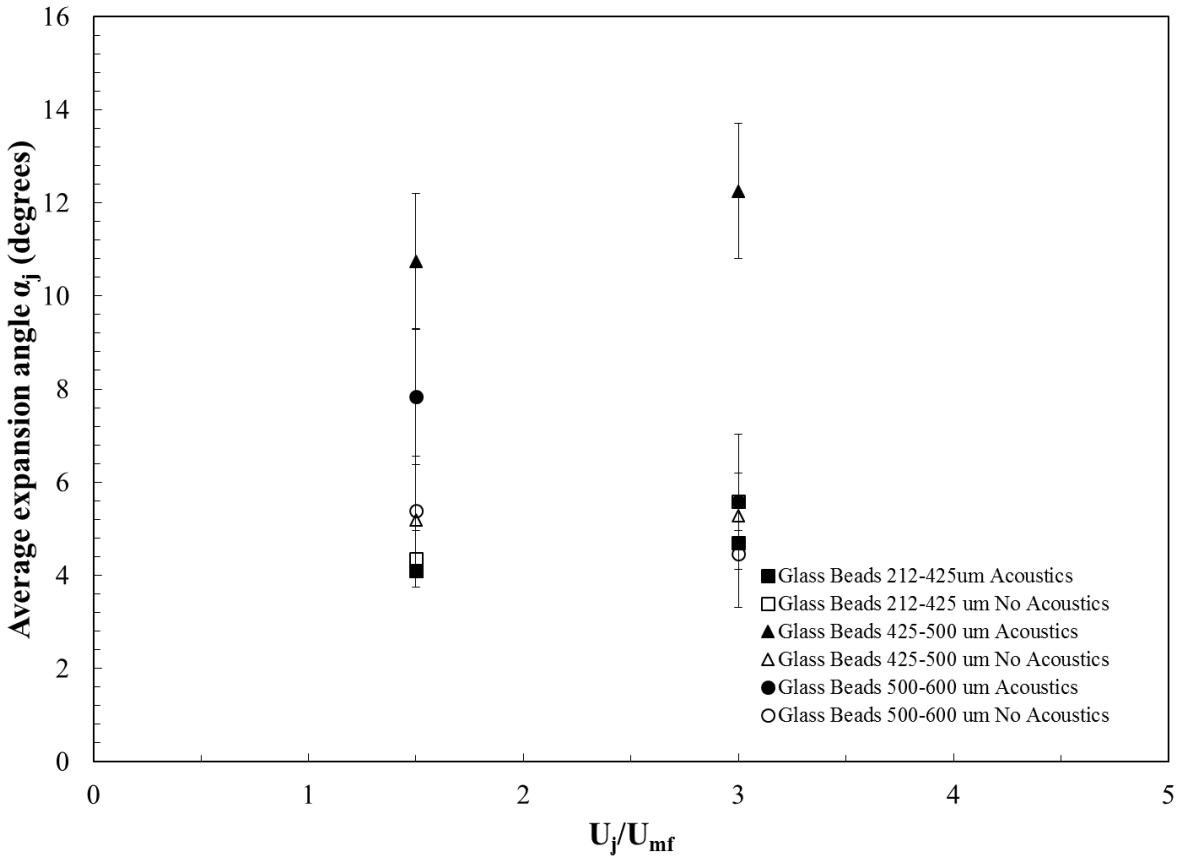

Figure 6.14: Average expansion angle as a function of U_j/U_{mf} for glass beads with different particle size with and without acoustic intervention.

6.4 Conclusions

X-ray computed tomography was used to qualitatively and quantitatively identify features of the jetting phenomena produced by a distributor plate in a fluidized bed with and without acoustic sound vibrations.

Jets produced at higher superficial gas velocities near the distributor plate under the effect of acoustic vibration extend deeper into the bed material, merging with other jets at higher axial positions compared to the jets produced with no acoustic vibration.

Acoustic sound vibrations allowed larger bubbles to break into smaller ones, increasing the presence of solid particles; thus reducing the jet momentum dissipation loss which allowed the

jets to have a higher average jet length compared with the fluidized bed without acoustics vibrations. The addition of acoustic vibrations also produced an increase in the jet expansion angle.

Due to the difference in superficial gas velocity, which is a consequence of the presence of the acoustic waves, the acoustic fluidized bed presented less active jets in the bed with a particle size greater than 500 μm, therefore less jetting phenomena near the distributor than the no acoustic fluidized bed conditions is observed, allowing it to have a better distribution of the void fraction throughout the entire fluidized bed.

Nomenclature

A_o	Area of distributor plate available per orifice; $\frac{\pi D^2}{4N}$	$[m^2]$
A_1	Smallest cross sectional area of the jet	$[m^2]$
A_2	Largest cross sectional area of the jet	$[m^2]$
D	Internal diameter of the fluidized bed	[m]
d_o	Orifice diameter	[m]
d_p	Mean diameter of a bed particle	[m]
g	Gravitational acceleration	$[m/s^2]$
H	Bed height	[cm]
L_j	Average jet length	[mm]
L_1	Height of the smallest cross sectional area of the jet	[m]
L_{merge}	Height at which two jets merged	[m]
N	Number of holes in the distributor plate	
P_o	Pitch distance between holes in distributor plate	[m]

U_g	Superficial gas velocity	[m/s]
U_j	Jet velocity within an orifice; $U_j = \frac{U_g D^2}{N d_o^2}$	[m/s]
U_{mf}	Minimum fluidization velocity	[m/s]
U_{mfj}	Jet velocity when $U=U_{mf}$	[m/s]

Greek Letters

α_j	Expansion angle	[degrees]
μ_f	Air viscosity	[Pa.s]
ρ_f	Air density	[kg/m^3]
ρ_p	Particle density	[kg/m^3]

Acknowledgements

The X-ray facility used in this work was developed with support from the National Science Foundation under Grant No. CTS-0216367 and Iowa State University. This work in this study was supported through Iowa State University. DRE would like to thank Ms. Claire Funke for initiating the jet identification analysis.

CHAPTER 7: ACOUSTIC STANDING WAVES IN FLUIDIZED BEDS[1]

David R. Escudero[2] and Theodore J. Heindel

Department of Mechanical Engineering

Iowa State University

Ames, Iowa 50011

Abstract

In order to analyze and understand the effects of acoustic waves on the hydrodynamic structures within a fluidized bed, it is important to describe the sound wave behavior inside the bed. A one dimensional model based on the acoustic standing waves theory is applied to an empty 10.2 cm fluidized bed, and to the same fluidized bed filled with glass beads and ground walnut shell at a fixed bed height. The beds are fluidized at different superficial gas velocities, and different sound pressure levels along the length of the fluidized bed are recorded and compared to model values. Results show that for an empty fluidized bed, the sound pressure level exhibits the behavior of a standing wave and shows good agreement with the proposed model. When material is present and the bed is fluidized, the sound pressure level is attenuated due to the presence of the solid material, resulting in a lower sound pressure level at the distributor plate and higher sound pressure level values at the free surface of the fluidized bed.

Keywords: Acoustic model, fluidized bed, sound pressure level, standing waves.

---

[1] In preparation for submission to *Chemical Engineering Journal.*

[2] Corresponding author

7.1 Introduction

Sound assisted fluidized beds have been studied in the literature because it has been shown that the inclusion of sound vibrations can help overcome fluidization problems in certain bed material types (Leu et al., 1997; Guo et al., 2006; Kaliyaperumal et al., 2011; Levy et al., 1997). Knowing how sound waves travel through fluidized bed material and interact with the gas and solid region of the bed is important to better understand the response of an acoustic fluidized bed.

Selected studies have proposed acoustic models to simulate the sound wave propagation in a fluidized bed.

Herrera et al. (Herrera et al., 2002) proposed a one dimensional model using the theory of standing waves to determine the important parameters that affect the sound pressure amplitude throughout the bed. They determined a good agreement between their experimental data and the data obtained from the model. They also concluded that the wave number (k), which is a parameter affected by the frequency and the speed of sound, along with the bed height, are the most important parameters that determined the sound pressure amplitude of the sound waves throughout the fluidized bed.

Cao et al. (Cao et al., 2010) modified the Syamlal-O'Brien drag model to include acoustic behavior; using CFD software they obtained a good agreement between the simulations and the experimental data. They determined that the radial volume fraction increases with an increase in the sound pressure level. They also concluded that the bubble size decreased and the amount of bubbles increased when the sound pressure level was increased.

The following study uses the 1D model of Herrera et.al (Herrera et al., 2002) to determine its applicability to describe the results in a fluidized bed filled to different heights of glass beads or

ground walnut shell. The goal is to better understand the behavior of the sound wave inside this particular gas-solid system.

7.2 Experimental Setup

Sound pressure level emitted by a loudspeaker at different operational frequencies (50, 100, 150, 200 Hz) while keeping the amplitude of the acoustic wave source constant, were obtained to understand the behavior of the sound wave inside a fluidized bed. The goal was to determine the change in the sound pressure level as a function of height through the fluidized bed.

An EMM 6 Dayton Audio Measurement Microphone was utilized to measure the sound pressure level produced by the loudspeaker to determine how the sound pressure level changes as a function of height. The microphone was first calibrated using a calibration file for the given microphone and the Room Equalizer Wizard audio analysis software. Once the microphone was calibrated, it was located at different axial positions inside the fluidized bed. In each axial position, a function generator which serves as the acoustic source, was set to an initial frequency of 50 Hz and the amplifier was set to specified amplitude. The sound pressure level at the microphone was recorded using the audio analysis software. Once the sound pressure level was recorded, the frequency was changed and again the sound pressure level was recorded. This procedure was repeated for the four operational frequencies described above at several axial positions between the fluidized bed aeration plate and the freeboard region.

This procedure was performed first without any material inside the fluidized bed and then with both materials (glass beads and ground walnut shell with a particles size range of 500-600 μm) inside the fluidized bed. In both situations, different superficial gas velocities ($U_g = 0U_{mf}$, $1U_{mf}$ and $3U_{mf}$, where $0U_{mf}$ corresponds to a static bed) were tested in order to determine if the presence of fluidizing gas inside the fluidized bed affected the reading of the microphone; and

thus, the behavior of the sound wave. The minimum fluidization values used were the ones determined by Escudero and Heindel (Escudero and Heindel, 2013).

Once all the measurements for all the conditions were obtained, the sound pressure level data was plotted as a function of microphone axial location relative to the aeration plate. This provided information on how the sound pressure level varied within the fluidized bed, and is used to further understand the effects of the acoustic waves on the minimum fluidization velocity, local gas holdup distribution, and finally the effects on jetting produced by the distributor plate.

7.2.1 One Dimensional Acoustic Model

When a sound wave is confined in a fluidized bed, where two single-phase (gas and solid) elements are presented, the transmission of the sound wave occurs in the following way: the incident wave pressure from the acoustic source (P_i) first travels through air, when P_i reaches the interface between air and the fluidizing material, part of the energy of P_i is reflected (P_r) and the rest of the energy is transmitted downward through the material (P_t). Once the incident wave P_{i1} reaches the distributor plate, another reflected wave P_{r1} appears. These waves have an additive effect creating what is called in acoustics engineering a standing wave. Figure 7.1 shows a schematic of the acoustic pressures at various locations inside the fluidized bed.

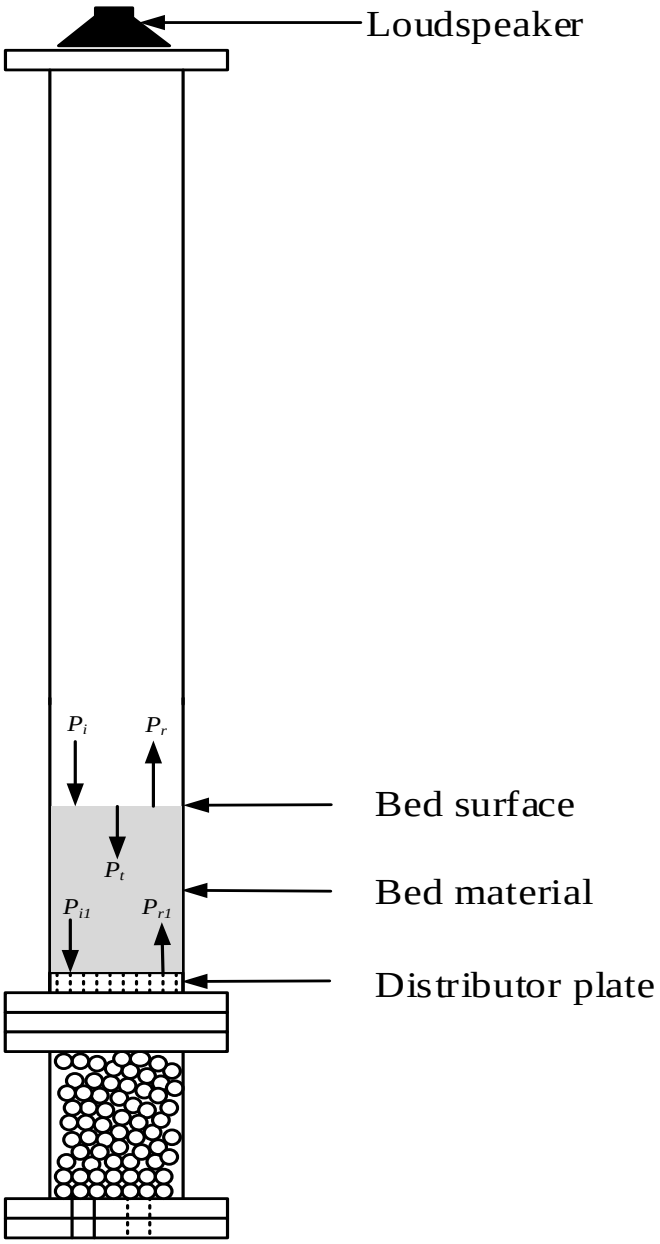

Figure 7.1: Schematic of the sound wave transmission in a fluidized bed.

Using the theory of a standing wave, a simple 1D model of the propagation of the sound wave inside the fluidized bed can be developed. For this particular study, the model equations were developed using Matlab and are based on the model previously developed by Herrera et al. (Herrera et al., 2002).

The sound pressure distribution can be described by:

$$p(x,t)=P_{fs}\sqrt{\frac{\cos^2 kx}{\cos^2 kh}}\cos\omega t \qquad (7.1)$$

where P_{fs} is the source amplitude in dB, k is the wave number which can be expressed as $k = 2\pi f/c$ (f is the frequency and c is the speed of sound) , x is the distance from the distributor plate, h is the height of the static bed material inside the fluidized bed, and ω is the angular velocity ($2\pi f$). Since only positive values are used in this model, the maximum amplitude of Eq. (7.1) is:

$$|p(x,t)|=P_{fs}\sqrt{\frac{\cos^2 kx}{\cos^2 kh}} \qquad (7.2)$$

When bed material is present, the pressure distribution of the sound wave changes due to the fact there is an attenuation of the wave caused by the attenuation coefficient α, which is an acoustic property of the material; therefore the amplitude of the sound pressure distribution with attenuation is described by:

$$|p(x,t)|=2P_{fs}\sqrt{\cosh^2 \alpha x\cos^2 kx+\sinh^2 \alpha x\sin^2 kx} \qquad (7.3)$$

Using these equations in Matlab, a model was developed and validated with the experimental data obtained using the procedures explained in the previous subsection.

7.3 Results and Discussion

7.3.1 Experimental Data

Sound pressure level values were obtained at different positions along the fluidized bed for an empty fluidized bed, and for a fluidized bed filled with glass beads and ground walnut shell. Figure 7.2 shows the sound pressure level for an empty reactor at different frequencies and different superficial gas velocities. As Figure 7.2 shows, as the superficial gas velocity increases there is a slight change (~1-2%) in the sound pressure level for every frequency tested. This change can be attributed to the increase of noise caused by the increase in the amount of air present inside the fluidized bed. It is also important to notice that as frequency increases, the

sound pressure level starts to exhibit standing wave behavior. Similar results were observed by Herrera et al. (Herrera et al., 2002).

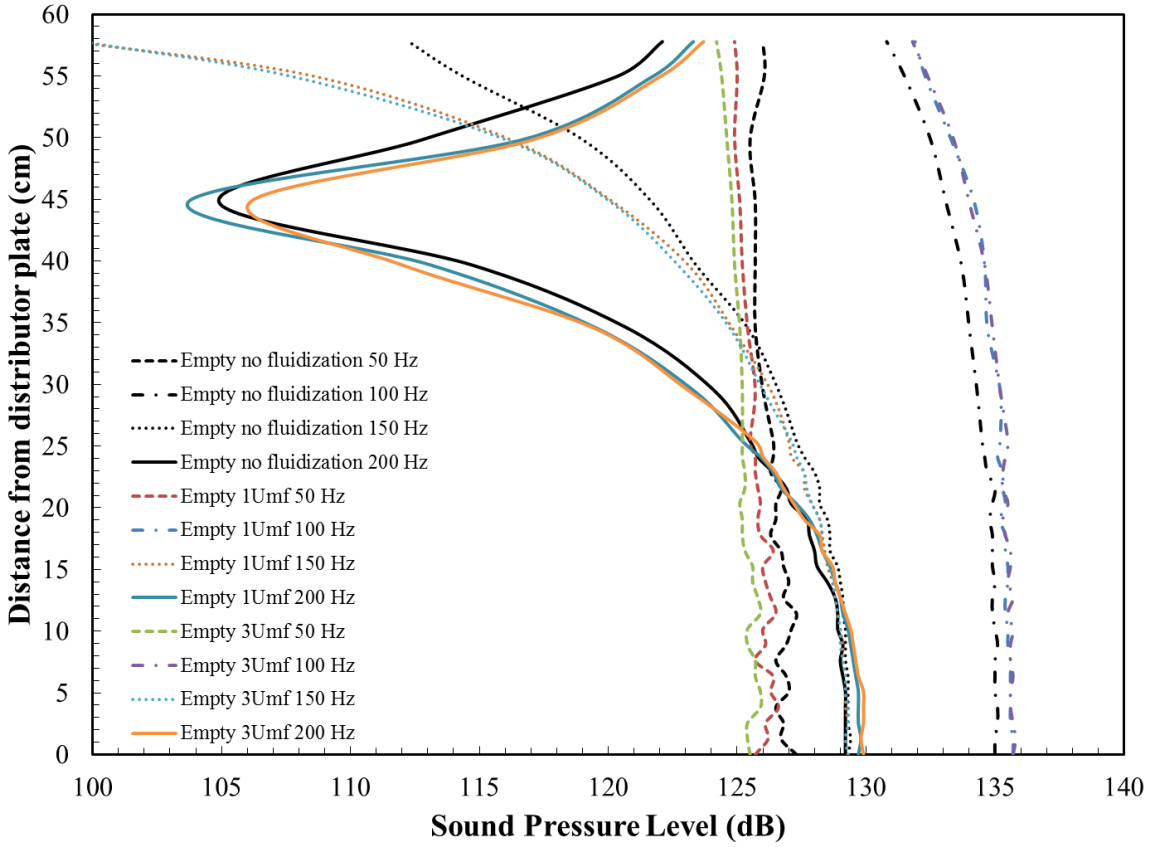

Figure 7.2: Sound pressure level as a function of distance for an empty reactor.

As shown in Figure 7.3, adding particulate material to the reactor modifies the sound pressure level profile. Figure 7.3 shows the sound pressure level as a function of distance from the aeration plate. For this condition, the bed was filled with 500-600 µm glass beads to an initial bed height of H/D = 1.5. As Figure 7.3 shows, when there is no fluidization and when the fluidized bed is just at the minimum fluidization velocity, there is a linear increase of the sound pressure level from the aeration plate to the free surface of the bed. Hence, the presence of the bed material affects the form of the wave. When the sound wave reaches the top of the bed material some of the energy is reflected and some of the energy of the wave is transmitted

through the material, as the sound wave energy travels deeper into the material there is a decrease in the sound pressure level indicating there is an attenuation of the sound wave due to the properties of the material. Conversely, when the sound wave is travelling in the portion where no material is present (freeboard region), the form of the wave maintains a similar trend as the one observed in Figure 7.2 for an empty reactor, although it is shifted up by approximately the static bed height..

When the superficial gas velocity is $U_g = 3U_{mf}$, the sound pressure level trends when the sound wave is travelling inside the material differ from the previous explanation, with the exception of the 100 Hz data. For the rest of the frequencies tested, instead of experiencing an increase in the sound pressure level from the distributor plate to the free surface of the bed material, the sound pressure level suffers a decrease. This phenomenon can be attributed to the fact that at this high velocity, there is more movement of particles; this movement may allow having a higher reflection of the transmitted sound wave which explains the higher sound pressure level at the bottom of the fluidized bed. Similar results are observed in Figure 7.4 for ground walnut shell.

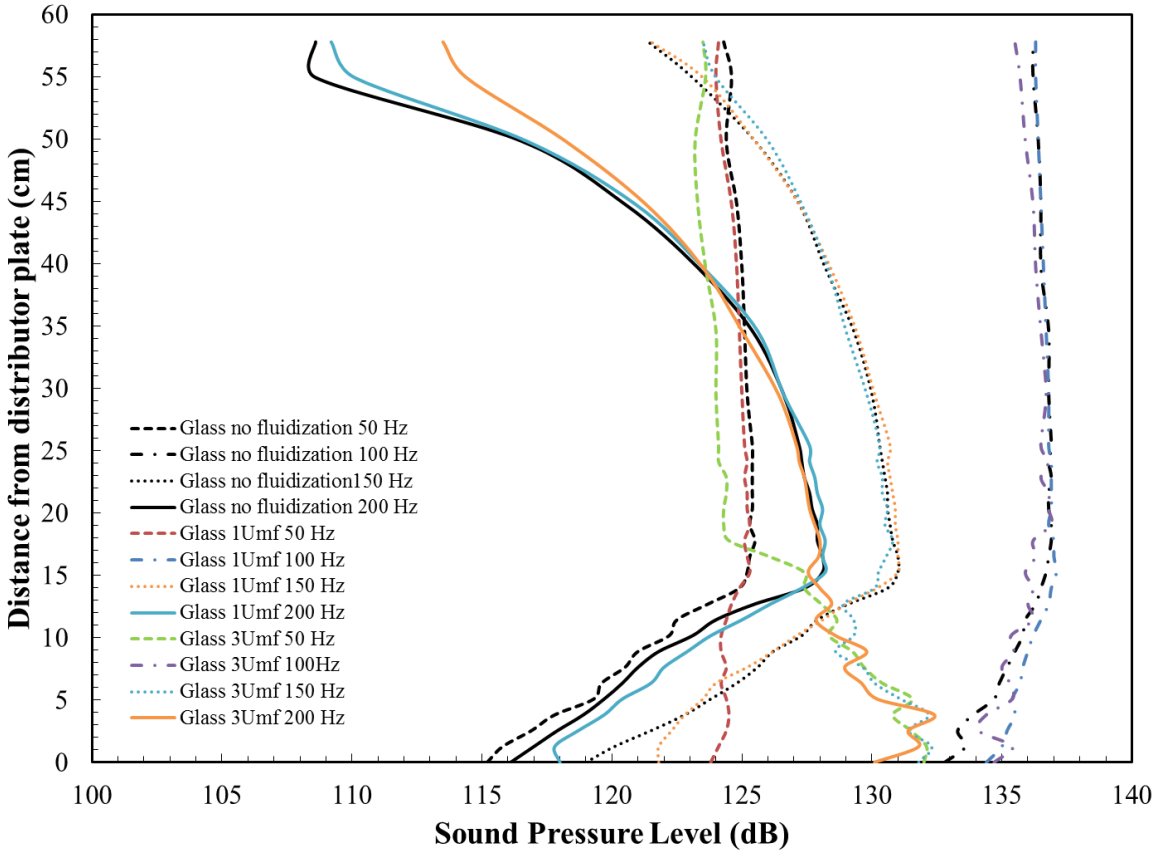

Figure 7.3: Sound pressure level as a function of distance for a fluidized bed filled with 500-600 µm glass beads**.**

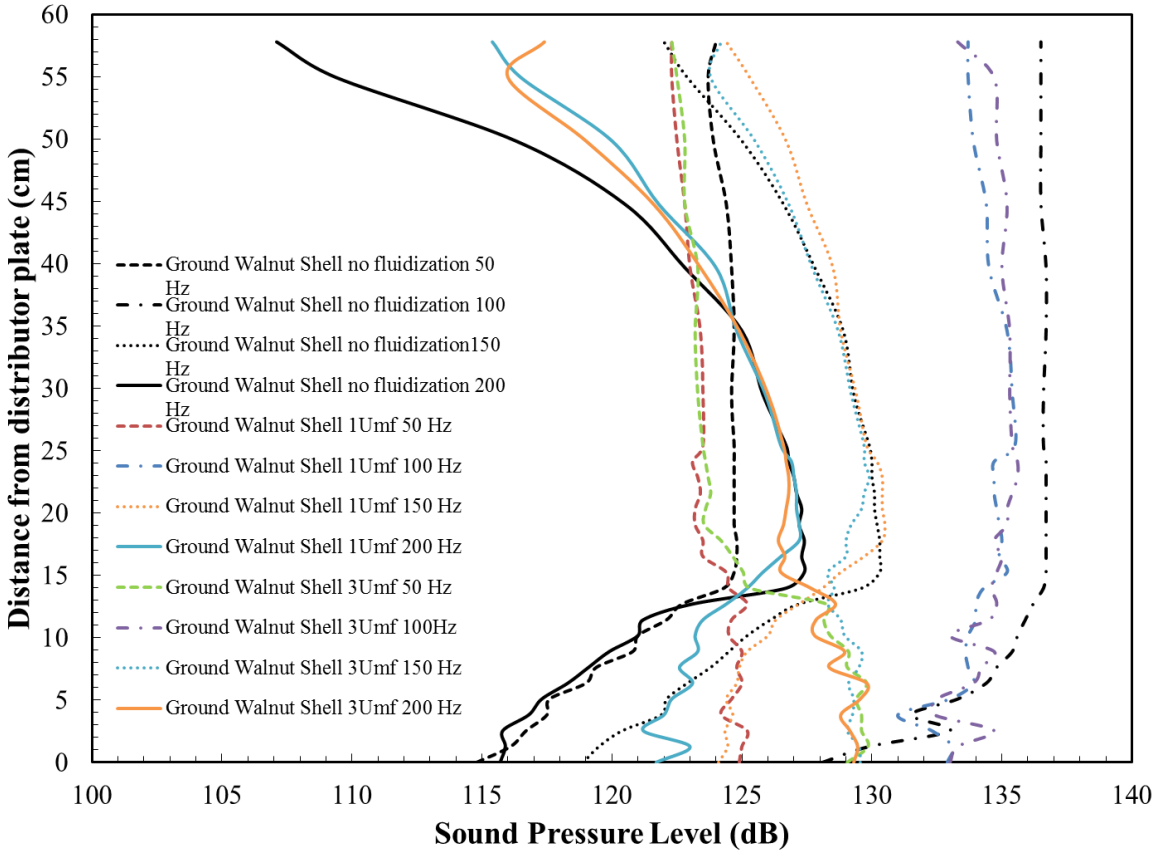

Figure 7.4: Sound pressure level as a function of distance for a fluidized bed filled with 500-600 µm ground walnut shell.

7.3.2 Comparison with the Model

Figure 7.5 shows the sound pressure level as a function of bed height for an empty reactor using the experimental data and the data obtained from the model. As shown, the trends exhibited for both the experiments and the model at the different frequencies are similar. As frequency increases, the sound pressure level starts to show a sinusoidal wave form (200 Hz), corroborating that in fact the acoustic waves inside a fluidized bed follow the standing wave theory, which was assumed in to the model too. The only big discrepancy between the model and the experimental data is the one observed for the 150 Hz curves. The model predicts higher values of the sound pressure level than the experimental values; this discrepancy is due to the

characteristic of the implemented model, which produces very large values of the pressure distribution at certain values of frequency. At the particular frequency of 150 Hz the model reaches a resonant state which creates these larger values of sound pressure level creating the gap between the model and the experimental data. Similar observations were made by Herrera et al. (Herrera et al., 2002).

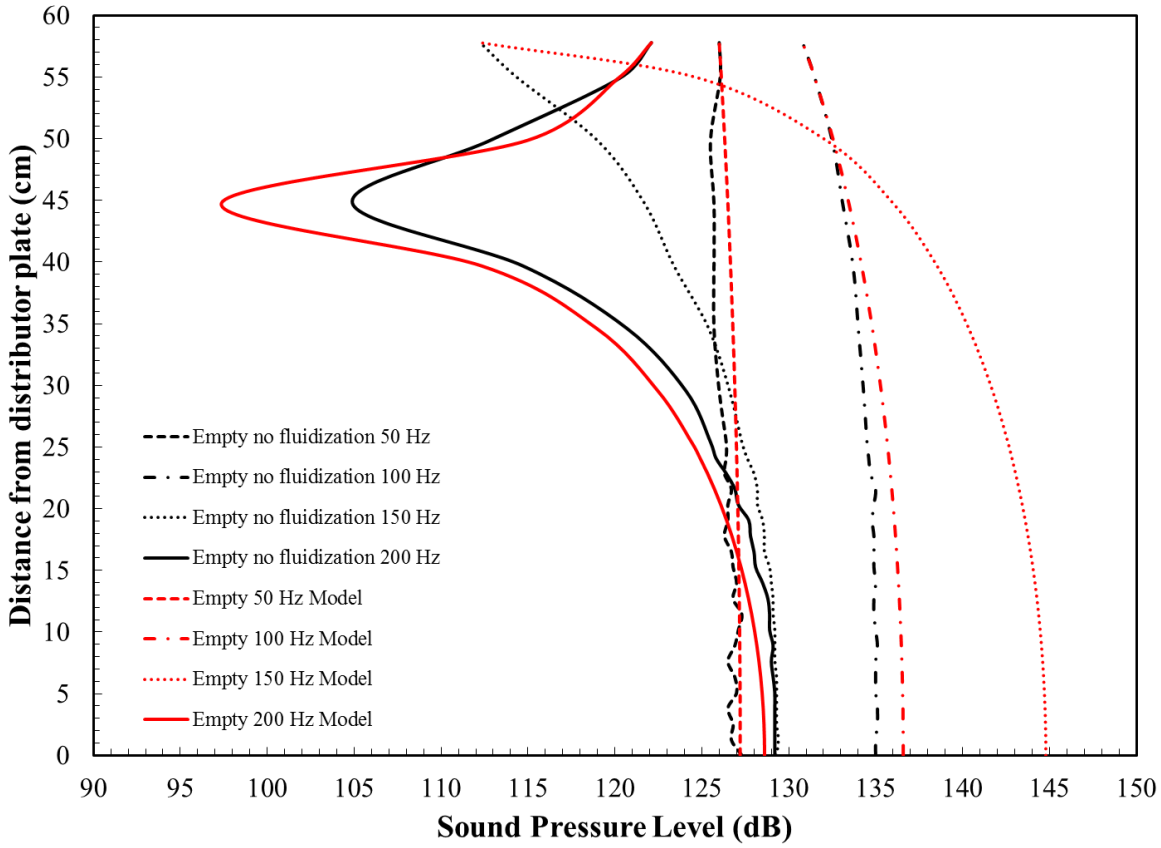

Figure 7.5: Experimental and model data for sound pressure level as a function of distance for an empty reactor.

When the bed is filled with glass beads or ground walnut shell, the experimental sound pressure level exhibits a different behavior than the model when the sound wave is within the bed material. Figure 7.6 compares the experimental and model sound pressure level for a fluidized bed filled with glass beads without fluidization. As Figure 7.6 shows, when the sound wave is

located inside the static bed, the sound pressure level for the model exhibits a sinusoidal pattern with a general increase in the sound pressure level from the bottom of the distributor plate to the free surface of the bed material. This trend is not observed in the experimental sound pressure level data, even though both the model and the experimental data show a general increase in the sound pressure level as height increases within the bed. In the freeboard region, both the model and the experimental sound pressure level exhibit similar trends having a bigger discrepancy between sound pressure level values at a frequency of 200 Hz, which can be considered as a resonant frequency of the bed. Similar results are observed as the superficial gas velocity increases. When the bed material is changed to ground walnut shell similar trends are observed and are presented in Figure 7.7.

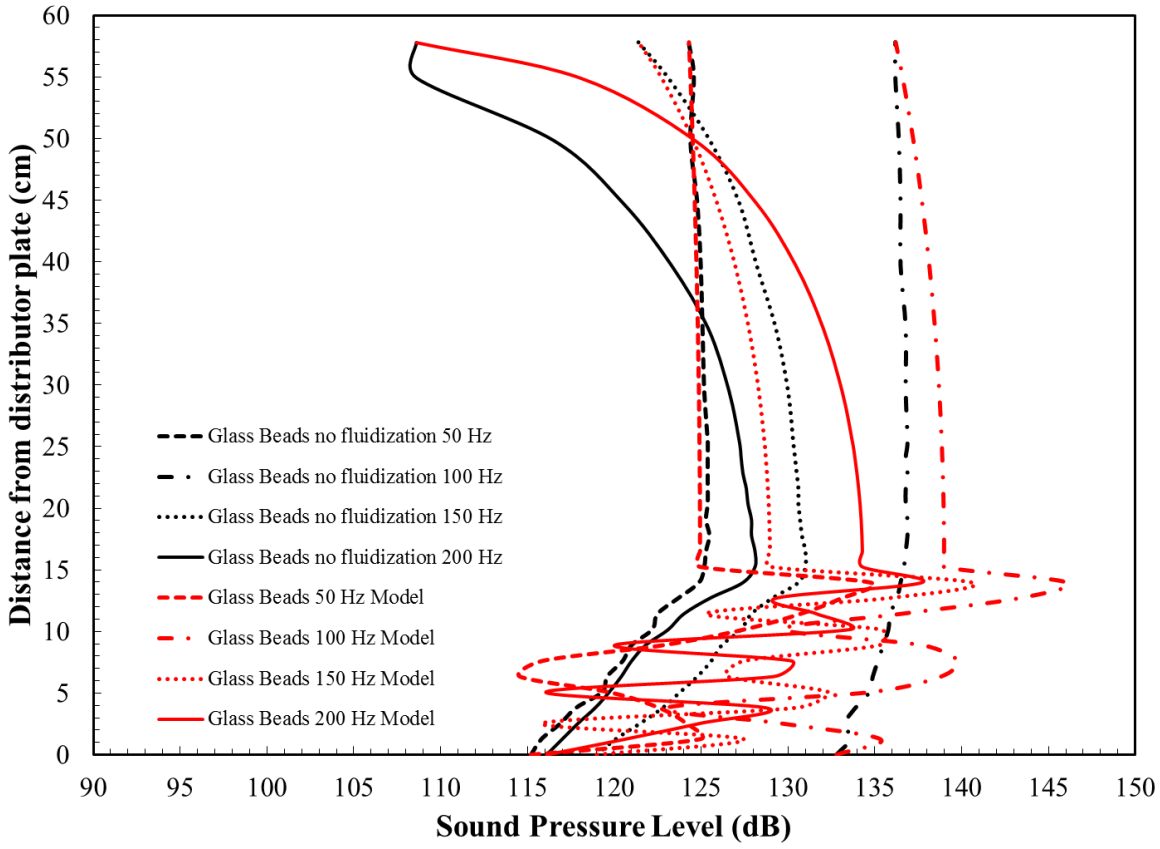

Figure 7.6: Experimental and model data for sound pressure level as a function of distance for 500-600µm glass beads fluidized bed.

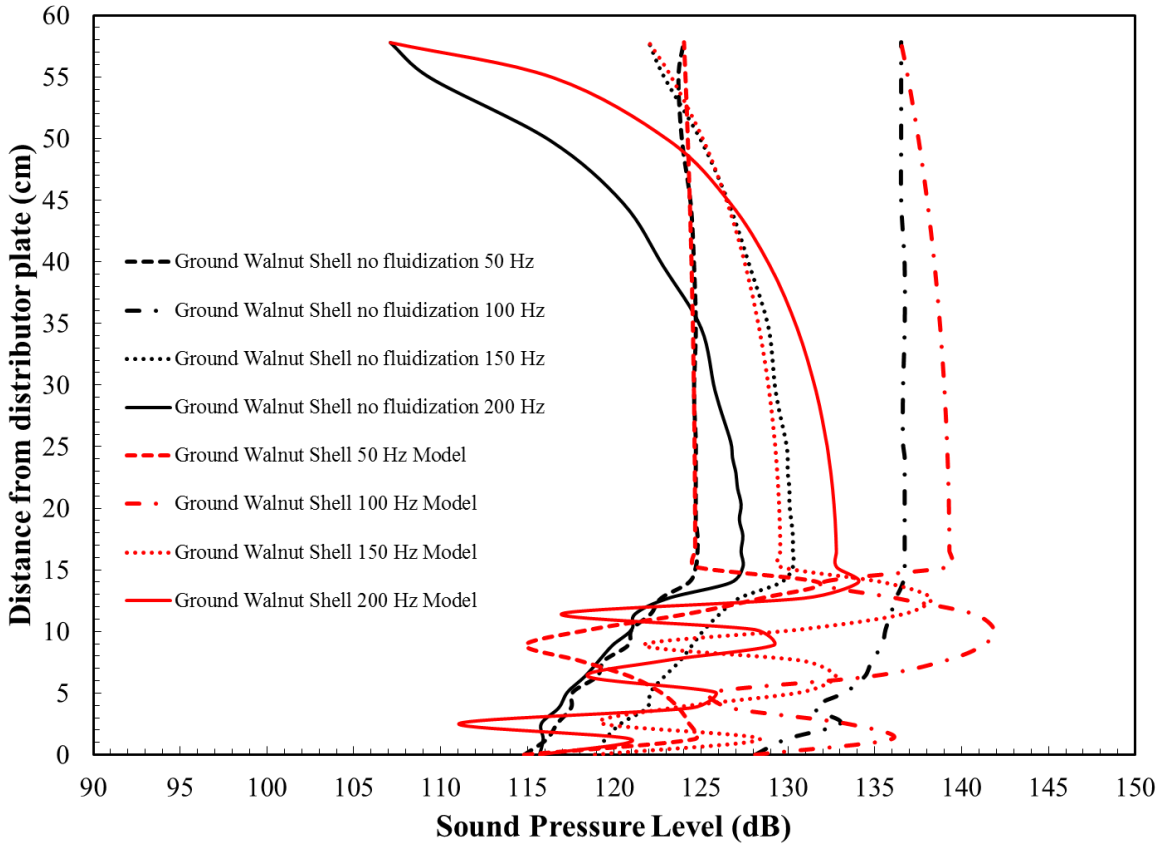

Figure 7.7: Experimental and model data for sound pressure level as a function of distance for 500-600μm ground walnut shell fluidized bed.

7.4 Conclusions

The acoustic pressure distribution inside the freeboard region of a fluidized bed exhibits standing wave behavior. Experiments showed that for an empty fluidized bed, the increase in the superficial gas velocity produced a slight change in the sound pressure level along the length of the fluidized bed.

A fluidized bed filled with material (500-600 μm glass beads or ground walnut shell) affects the sound wave pattern. When the fluidized bed has no fluidization and when it is at the minimum fluidization velocity, the sound pressure level exhibits a linear increase from the bottom of the distributor plate to the free surface of the bed material. When the sound wave

reaches the top of the bed material some of the energy is reflected and some of the energy of the wave is transmitted through the material; as the sound wave energy travels deeper into the material there is a decrease in the sound pressure level indicating there is an attenuation of the sound wave due to the particle properties.

The model presented in this study shows a very good agreement between the experimental data and the model data of the pressure distribution when there is no material inside the fluidized bed. When material is introduced inside the fluidized bed, the sound pressure distribution observed between the model and the experimental data differ: the experimental data shows a linear increase in the sound pressure level inside the material while the model data shows a sinusoidal increase in the sound pressure level when the sound wave is passing the bed material.

CHAPTER 8: CONCLUSION AND RECOMMENDATIONS

8.1 Conclusions

This dissertation provided important findings regarding the hydrodynamic structure of 3D fluidized bed under the influence of acoustic vibrations using X-ray computed tomography imaging techniques. These findings will help to better understand the interaction between gas-solid materials inside a multiphase flow reactor. The conclusive findings obtained from this research study are related to the objectives described in Chapter 1, and are the following:

Objective 1: Determine the effects of frequency and sound pressure level on the minimum fluidization velocity.

Conclusion 1: The minimum fluidization velocity for a non-acoustic fluidized bed and for an acoustic fluidized was obtained using two different materials at different bed heights. Results showed that for every material tested, the acoustic field presence improved the ease of material fluidization (i.e., it lowered U_{mf}).

Results also showed that minimum fluidization velocity decreased with an increase in acoustic frequency until the material reached a point of homogeneous fluidization, beyond that point, U_{mf} started to increase.

An increase in the sound pressure level produced a decrease in the minimum fluidization velocity for both materials tested, for the entire particle size range, and for the different bed height conditions. The increase in SPL provided additional energy that assisted fluidization.

Moreover, acoustic fluidized beds exhibit dependence between bed height and minimum fluidization velocity. As bed height increased at a fixed frequency, the changes in the minimum fluidization velocity were very noticeable; which did not happen when there was no acoustic field present in the bed.

Objective 2: Evaluate the effects of the acoustic field on the time-average local gas holdup.

Conclusion 2: Using X-ray computed tomography; local time-average gas holdup was obtained for the materials tested at different operating conditions.

Results showed that for a fluidized bed filled with glass beads, the presence of an acoustic field produced a more uniform void fraction distribution compared to a fluidized bed without any acoustic intervention.

For glass bead beds with small particles size ranges of 212-500 μm, the presence of the acoustic field did not show any influence. However, for particles in the 500-600 μm range, acoustics did show an influence in the gas holdup distribution, showing a more homogenous void fraction distribution for a fixed U_g relative to U_{mf}.

For a ground walnut shell fluidized bed, the acoustic vibration effects had a strong dependence with the particle size ranges tested. For the particular frequency and sound pressure level tested, two out of the three particle size ranges did not exhibit any significant change in the void fraction distribution of the fluidized bed compared to the no acoustic case. While the 425-500 μm particle size ranges did exhibit differences between the acoustic and no acoustic case in void fraction distribution.

Objective 3: Using the time-average local gas holdup images, determine qualitatively and quantitatively characteristics of the jetting phenomena produced by the distributor plate.

Conclusion 3: Qualitative and quantitative information regarding the jetting phenomena were determined using the gas holdup images obtained from X-ray CT imaging. Results showed that the acoustic field influenced the jetting phenomena present near the aeration plate, where it was observed that the jets in the acoustic fluidized bed merged higher in the bed compared to the no acoustic condition.

The presence of acoustic vibrations allowed larger air bubbles to break into smaller ones, this increased the presence of solid particles; allowing the jets to have a higher average jet length compared with the fluidized bed without acoustics vibrations.

Due to a lower minimum fluidization velocity, a consequence of the presence of the acoustic waves, the acoustic fluidized bed presented less active jets in the bed with a particle size greater than 500 μm, therefore less jetting phenomena near the distributor plate is observed compared to the one observed in the no acoustic fluidized bed. However, the acoustic bed produced a better and more homogenous distribution of the void fraction outside the aeration region.

8.2 Recommendations

Future studies examining the effects that different forms of waves (square, triangle) should be performed using the same fluidized bed to evaluate how the different shapes of the sound waves influenced the fluidization and the hydrodynamics of the bed; these results should be compared to those of this study to establish differences in the improvement of the fluidization of different type of particles.

Future experiments should be performed using material of higher particle sizes, higher sound frequencies, higher sound pressure levels, and different locations of the acoustic source, to evaluate the fluidization and hydrodynamics dependency on material properties and acoustic parameters. Moreover, information regarding local time average gas holdup must be obtained for a range of frequencies and sound pressure levels to understand completely the effects of the acoustic field in the structure of the fluidized bed. Thus, performing these future experiments will expand the work that has been done in this research.

REFERENCES

Barletta, D., Donsì, G., Ferrari, G., Poletto, M. and Russo, P. (2008). "The effect of mechanical vibration on gas fluidization of a fine aeratable powder." *Chemical Engineering Research and Design*. **86**(4): 359-369.

Barletta, D. and Poletto, M. (2012). "Aggregation phenomena in fluidization of cohesive powders assisted by mechanical vibrations." *Powder Technology*. **225**(0): 93-100.

Barletta, D., Russo, P. and Poletto, M. (2013). "Dynamic response of a vibrated fluidized bed of fine and cohesive powders." *Powder Technology*. **237**(0): 276-285.

Baron, T., Briens, C. L., Bergougnou, M. A. and Hazlett, J. D. (1987). "Electrostatic effects on entrainment from a fluidized bed." *Powder Technology*. **53**(1): 55-67.

Blake, T. R., Webb, H. and Sunderland, P. B. (1990). "The nondimensionalization of equations describing fluidization with application to the correlation of jet penetration height." *Chemical Engineering Science*. **45**(2): 365-371.

Cao, C., Dong, S., Zhao, Y. and Guo, Q. (2010). "Experimental and numerical research for fluidization behaviors in a gas-solid acoustic fluidized bed." *AIChE Journal*. **56**(7): 1716-1725.

Chaouki, J., Larachi, F. and Dudukovic, M. P. (1997). "Noninvasive tomographic and velocimetric monitoring of multiphase flows." *Industrial and Engineering Chemistry Research*. **36**(11): 4476-4503.

Chen, J., Lu, X., Liu, H. and Liu, J. (2008). "The effect of solid concentration on the secondary air-jetting penetration in a bubbling fluidized bed." *Powder Technology*. **185**(2): 164-169.

Cranfield, R. R. and Geldart, D. (1974). "Large particle fluidisation." *Chemical Engineering Science*. **29**(4): 935-947.

Crowe, C. T. (2006). Multiphase Flow Handbook. Boca Raton, FL, CRC Press.

Drake, J. B. and Heindel, T. J. (2011). "The repeatability and uniformity of 3D fluidized beds." *Powder Technology*. **213**(1–3): 148-154.

Drake, J. B. and Heindel, T. J. (2012). "Local time-average gas holdup comparisons in cold flow fluidized beds with side-air injection." *Chemical Engineering Science*. **68**(1): 157-165.

Du, B., Warsito, W. and Fan, L.-S. (2003). "Bed nonhomogeneity in turbulent gas-solid fluidization." *AIChE Journal*. **49**(5): 1109-1126.

Du, B., Warsito, W. and Fan, L.-S. (2005). "ECT studies of gas−solid fluidized beds of different diameters." *Industrial & Engineering Chemistry Research*. **44**(14): 5020-5030.

Escudero, D. (2010). "Bed height and material density effects on fluidized beds hydrodynamics". M.S. Thesis MSc, Iowa State University.

Escudero, D. and Heindel, T. J. (2011). "Bed height and material density effects on fluidized bed hydrodynamics." *Chemical Engineering Science*. **66**(16): 3648-3655.

Escudero, D. and Heindel, T. J. (2013). "Minimum fluidization velocity in a 3D fluidized bed modified with an acoustic field." *Chemical Engineering Journal*. **231**(0): 68-75.

Escudero, D. R. and Heindel, T. J. (2012). Acoustic field effects on minimum fluidization velocity in a 3D fluidized bed. ASME 2012 Fluids Engineering Division Summer Meeting, FEDSM 2012 Collocated with the ASME 2012 Heat Transfer Summer Conf. and the ASME 2012 10th International Conference on Nanochannels, Microchannels, and M, FEDSM 2012, July 8, 2012 - July 12, 2012, Rio Grande, Puerto rico, American Society of Mechanical Engineers.

Escudero, D. R. and Heindel, T. J. (2014). "Acoustic fluidized bed hydrodynamics characterization using X-ray computed tomography." *Chemical Engineering Journal*. **243**(0): 411-420.

Ettehadieh, B., Yang, W.-C. and Haldipur, G. B. (1988). "Motion of solids, jetting and bubbling dynamics in a large jetting fluidized bed." *Powder Technology*. **54**(4): 243-254.

Fahy, F. (2001). Foundations of Engineering Acoustics, Academic Press.

Franka, N. P. and Heindel, T. J. (2009). "Local time-averaged gas holdup in a fluidized bed with side air injection using X-ray computed tomography." *Powder Technology*. **193**(1): 69-78.

Franka, N. P., Heindel, T. J. and Battaglia, F. (2007). Visualizing cold-flow fluidized beds with x-rays. ASME International Mechanical Engineering Congress and Exposition. Seattle, Washington, ASME**:** 7.

Geldart, D. (1973). "Types of gas fluidization." *Powder Technology*. **7**(5): 285-292.

Grassler, T. and Wirth, K. E. (2000). "X-ray computer tomography - potential and limitation for the measurement of local solids distribution in circulating fluidized beds." *Chemical Engineering Journal*. **77**(1): 65-72.

Gunn, D. J. and Hilal, N. (1997). "The expansion of gas-fluidised beds in bubbling fluidisation." *Chemical Engineering Science*. **52**(16): 2811-2822.

Guo, Q., Liu, H., Shen, W., Yan, X. and Jia, R. (2006). "Influence of sound wave characteristics on fluidization behaviors of ultrafine particles." *Chemical Engineering Journal*. **119**(1): 1-9.

Guo, Q., Si, C. and Zhang, J. (2010). "Flow Characteristics in a Jetting Fluidized Bed with Acoustic Assistance." *Industrial & Engineering Chemistry Research*. **49**(16): 7638-7645.

Guo, Q., Tang, Z., Yue, G., Liu, Z. and Zhang, J. (2001). "Flow pattern transition in a large jetting fluidized bed with double nozzles." *AIChE Journal*. **47**(6): 1309-1317.

Guo, Q., Yue, G., Zhang, J. and Liu, Z. (2001). "Hydrodynamic characteristics of a two-dimensional jetting fluidized bed with binary mixtures." *Chemical Engineering Science*. **56**(15): 4685-4694.

Guo, Q., Zhang, J. and Hao, J. (2011). "Flow characteristics in an acoustic bubbling fluidized bed at high temperature." *Chemical Engineering and Processing: Process Intensification*. **50**(3): 331-337.

Gupta, C. and Sathiyamoorthy, D. (1999). Fluid bed technology in materials processing. Boca Raton, FL, CRC Press.

Heindel, T. J. (2011). "A review of X-ray flow visualization with applications to multiphase flows." *Journal of Fluids Engineering*. **133**(7): 074001-074001 - 074001-074016.

Heindel, T. J., Gray, J. N. and Jensen, T. C. (2008). "An X-ray system for visualizing fluid flows." *Flow Measurement and Instrumentation*. **19**(2): 67-78.

Herrera, C. A. and Levy, E. K. (2001). "Bubbling characteristics of sound-assisted fluidized beds." *Powder Technology*. **119**(2-3): 229-240.

Herrera, C. A., Levy, E. K. and Ochs, J. (2002). "Characteristics of acoustic standing waves in fluidized beds." *AIChE Journal*. **48**(3): 503-513.

Hilal, N., Ghannam, M. T. and Anabtawi, M. Z. (2001). "Effect of bed diameter, distributor and inserts on minimum fluidization velocity." *Chemical Engineering and Technology*. **24**(2): 161-165.

Kaliyaperumal, S., Barghi, S., Zhu, J., Briens, L. and Rohani, S. (2011). "Effects of acoustic vibration on nano and sub-micron powders fluidization." *Powder Technology*. **210**(2): 143-149.

Kantzas, A., Wright, I. and Kalogerakis, N. (1997). "Quantification of channelling in polyethylene resin fluid beds using X-ray computer assisted tomography (CAT)." *Chemical Engineering Science*. **52**(13): 2023-2035.

Leu, L.-p., Li, J.-t. and Chen, C.-M. (1997). "Fluidization of group B particles in an acoustic field." *Powder Technology*. **94**(1): 23-28.

Levy, E. K. and Celeste, B. (2006). "Combined effects of mechanical and acoustic vibrations on fluidization of cohesive powders." *Powder Technology*. **163**(1–2): 41-50.

Levy, E. K., Shnitzer, I., Masaki, T. and Salmento, J. (1997). "Effect of an acoustic field on bubbling in a gas fluidized bed." *Powder Technology*. **90**(1): 53-57.

Mandal, D., Sharma, V. K., Pant, H. J., Sathiyamoorthy, D. and Vinjamur, M. (2012). "Quality of fluidization in gas–solid unary and packed fluidized beds: An experimental study using gamma ray transmission technique." *Powder Technology*. **226**(0): 91-98.

Marring, E., Hoffmann, A. C. and Janssen, L. P. B. M. (1994). "The effect of vibration on the fluidization behaviour of some cohesive powders." *Powder Technology*. **79**(1): 1-10.

Müller, C. R., Holland, D. J., Davidson, J. F., Dennis, J. S., Gladden, L. F., Hayhurst, A. N., Mantle, M. D. and Sederman, A. J. (2009). "Geometrical and hydrodynamical study of gas jets in packed and fluidized beds using magnetic resonance." *The Canadian Journal of Chemical Engineering*. **87**(4): 517-525.

Parasu Veera, U. (2001). "Gamma ray tomography design for the measurement of hold-up profiles in two-phase bubble columns." *Chemical Engineering Journal*. **81**(1–3): 251-260.

Patel, A. K., Waje, S. S., Thorat, B. N. and Mujumdar, A. S. (2008). "Tomographic diagnosis of gas maldistribution in gas-solid fluidized beds." *Powder Technology*. **185**(3): 239-250.

Pore, M., Holland, D. J., Chandrasekera, T. C., Müller, C. R., Sederman, A. J., Dennis, J. S., Gladden, L. F. and Davidson, J. F. (2010). "Magnetic resonance studies of a gas-solids fluidised bed: Jet-jet and jet-wall interactions." *Particuology*. **8**(6): 617-622.

Ramos Caicedo, G., García Ruiz, M., Prieto Marqués, J. J. and Guardiola Soler, J. (2002). "Minimum fluidization velocities for gas-solid 2D beds." *Chemical Engineering and Processing*. **41**(9): 761-764.

Rees, A. C., Davidson, J. F., Dennis, J. S., S Fennell, P., Gladden, L. F., Hayhurst, A. N., Mantle, M. D., Müller, C. R. and Sederman, A. J. (2006). "The nature of the flow just above the perforated plate distributor of a gas-fluidised bed, as imaged using magnetic resonance." *Chemical Engineering Science*. **61**(18): 6002-6015.

Roy, R., Davidson, J. F. and Tuponogov, V. G. (1990). "The velocity of sound in fluidised beds." *Chemical Engineering Science*. **45**(11): 3233-3245.

Russo, P., Chirone, R., Massimilla, L. and Russo, S. (1995). "The influence of the frequency of acoustic waves on sound-assisted fluidization of beds of fine particles." *Powder Technology*. **82**(3): 219-230.

Sau, D. C., Mohanty, S. and Biswal, K. C. (2007). "Minimum fluidization velocities and maximum bed pressure drops for gas-solid tapered fluidized beds." *Chemical Engineering Journal*. **132**(1-3): 151-157.

Si, C. and Guo, Q. (2008). "Fluidization characteristics of binary mixtures of biomass and quartz sand in an acoustic fluidized bed." *Industrial & Engineering Chemistry Research*. **47**(23): 9773-9782.

Wang, F., Yu, Z., Marashdeh, Q. and Fan, L.-S. (2010). "Horizontal gas and gas/solid jet penetration in a gas-solid fluidized bed." *Chemical Engineering Science*. **65**(11): 3394-3408.

Wen, C. Y., Deole, N. R. and Chen, L. H. (1982). "STUDY OF JETS IN A THREE-DIMENSIONAL GAS FLUIDIZED BED." *Powder Technology*. **31**(2): 175-184.

Yang, W.-C. (1998). "Comparison of jetting phenomena in 30-cm and 3-m diameter semicircular fluidized beds." *Powder Technology*. **100**(2-3): 147-160.

Yang, W.-C. and Keairns, D. L. (1987). "A study of fine particles residence time in a jetting fluidized bed." *Powder Technology*. **53**(3): 169-178.

Yang, W. (2003). Handbook of Fluidization and Fluid Particle Systems. New York, Marcel Dekker Inc.

Yates, J. G., Cheesman, D. J., Lettieri, P. and Newton, D. (2002). "X-Ray analysis of fluidized beds and other multiphase systems." *Kona*. **20**: 10.

Zhang, L., Hou, J., Bi, X. T., Grace, J. R., Janke, T. and Arato, C. (2012). "Fluidization characteristics and charging behavior of fly ash in a vibro-fluidized bed." *Powder Technology*. **215–216**(0): 235-241.

Zhang, Y., Jin, B., Zhong, W., Ren, B. and Xiao, R. (2010). "DEM simulation of particle mixing in flat-bottom spout-fluid bed." *Chemical Engineering Research and Design*. **88**(5-6): 757-771.

Zhong, W., Chen, X. and Zhang, M. (2006). "Hydrodynamic characteristics of spout-fluid bed: Pressure drop and minimum spouting/spout-fluidizing velocity." *Chemical Engineering Journal*. **118**(1-2): 37-46.

Zhou, D., Dong, S., Wang, H. and Bi, H. T. (2008). "Minimum fluidization velocity of a three-phase conical fluidized bed in comparison to a cylindrical fluidized bed." *Industrial & Engineering Chemistry Research*. **48**(1): 27-36.

Zhu, H., Zhu, J., Li, G. and Li, F. (2008). "Detailed measurements of flow structure inside a dense gas-solids fluidized bed." *Powder Technology*. **180**(3): 339-349.